Trends and signals in tree-ring parameters

Dissertation

zur Erlangung des Grades

"Doktor der Naturwissenschaften"

im Promotionsfach Geographie

am Fachbereich Chemie, Pharmazie und Geowissenschaften

der Johannes Gutenberg-Universität

in Mainz

Oliver Konter

geb. in Saarburg

Mainz, den 06. November 2015

Summary

Tree-rings are frequently used to develop annually resolved paleoclimate reconstructions of periods in time when meteorological instrumental measurements are not available. Commonly used proxy records derived from tree-rings are ring width, maximum latewood density, and stable carbon and oxygen isotopes. Calibrating the different tree-ring proxies against available meteorological data is a prerequisite for reconstruction approaches, as results provide the essential statistical relationships to convert proxy data into the targeted climate data. Additionally, the evaluation of potential non-climatic biases is crucial for accurate calibration results. In this dissertation, methods for identifying proxy-specific biases are developed and evaluated for associated impact on various calibration setups. Focus is placed on age-related climate sensitivity trends in growth and density data, insect-induced disturbances in interannual growth patterns, and effects of elevated atmospheric CO_2 concentrations on stable isotopic compositions.

Age-related alternation in the climate sensitivity of tree-ring width data has been previously reported and is here revisited by analyzing a large dataset of 692 *Pinus sylvestris* L. series from northern Fennoscandia. Additionally and for the first time, maximum latewood density measurements of the same trees are included. Results indicate significant decreasing climate sensitivity with increasing age in both tree-ring parameters, while density data are less affected, thus, more suitable for the development of climate reconstructions. Temperature reconstructions for this region can dismiss age-related biases, by using density data from evenly distributed cambial ages, i.e. including young and old trees, as a function of time.

The larch budmoth (*Zeiraphera diniana* Gn.) is characterized by regular population oscillations and cyclic mass outbreaks (8-10 years), causing interannual disturbances in tree-ring width chronologies from host trees and reduced climate signal strength. In contrast to reported historical evidence over 1200 years from the European Alps, cyclic mass outbreaks in the Slovakian High Tatra Mountains are, in this dissertation, found to be absent during the last 300 years. Low stand densities in the spatially limited larch forests in this habitat prevent larch budmoth populations from peaking at mass outbreaks levels. The significantly synchronized *Larix decidua* Mill. (host) and *Pinus cembra* L. (non-host) chronologies, both free of insect-induced pulsed disturbances, exhibit distinct early-summer temperature signals ideal for East-European temperature reconstructions.

Stable isotope data from tree-rings provide extensive information on interactions between tree-physiological processes and external climatic forcing. Annually and decadally resolved stable carbon ($\delta^{13}C$) and oxygen ($\delta^{18}O$) isotope time series from *Pinus uncinata* Ramond ex DC tree-rings from the Spanish Pyrenees exhibit climate sensitivity - $\delta^{18}O$ values are controlled by spring precipitation and other more complex factors, and $\delta^{13}C$ data embeds a significant summer temperature signal. However, different correction methods addressing effects of elevated atmospheric CO_2 on the carbon isotopic composition add low-frequency information to the data, and alter the magnitude of the climate signal strength and its temporal robustness. Selecting the most appropriate correction method remains challenging, as the habitat-specific natural adaptation of tree-intrinsic physiological processes to elevated atmospheric CO_2 could not be clarified, and objective criteria for best-fit corrections are still missing. Using the correction method resembling summer temperature characteristics, a newly developed 750-year decadal summer temperature reconstruction comprises greater amplitude compared to previously reported reconstructions derived from ring width and density data. Additionally, the novel approach in tree-ring stable isotope chronology development of detrending-techniques are applied to the $\delta^{13}C$ isotopic data, providing the background of this temperature reconstruction.

The detection and evaluation methods for potential biases in calibration setups presented in this dissertation can be utilized as conceptual basis to evaluate existing and to advance future reconstruction, thereby, improving our understanding of long-term climate variations.

Zusammenfassung

Die Jahrringe verschiedener Baumarten werden häufig für dendroklimatische Forschung genutzt, vor allem für Rekonstruktionen vergangener Klimaschwankungen. Dabei können unterschiedliche Datengrundlagen gewonnen werden, wie z. B. die Jahrringbreite, die maximale Spätholzdichte und die Zusammensetzung der stabilen Kohlenstoff- und Sauerstoffisotope. Eine Analyse der Klimasignale in Jahrringzeitreihen bildet die Basis für Klimarekonstruktionen, denn die ermittelten statistischen Klimawachstumsbeziehungen ermöglichen die Übertragung der Ergebnisse aus der Kalibrationsperiode auf Jahrringdaten der Rekonstruktionsperiode in vorindustrieller Zeit, für die in der Regel meteorologische instrumentelle Messdaten fehlen. Zusätzlich ist eine Bewertung der potenziell verfälschenden Einflussgrößen in der Kalibrationsanalyse obligatorisch. Diese Dissertation legt den Schwerpunkt auf die Evaluation unterschiedlicher Kalibrationseinstellungen, entwickelt Methoden zur Identifizierung parameterspezifischen Verzerrungen und bestimmt das Ausmaß ihrer Auswirkungen. Im Speziellen sind altersbedingte Trends in der Klimasensitivität, Störungen im jährlichen Wachstumsmuster durch Insektenbefall und die Auswirkungen der erhöhten atmosphärischen CO2-Konzentrationen von Interesse. Ziel dieser Arbeit ist es, in unterschiedlichen Kalibrationsanalysen „nicht-klimatische“ Einflussgrößen zu identifizieren, sowie Lösungsstrategien für deren Vermeidung zu entwickeln.

Die altersbedingten Veränderungen der Klimasensitivität in Ringbreitendaten sind Gegenstand der Untersuchung in mehreren publizierten Studien. In dieser Arbeit wird dieses Thema durch die Analyse von *Pinus sylvestris* L. Jahrringbreiteserien aus dem nördlichen Fennoskandien aufgegriffen und durch die erstmalige Hinzunahme von Dichtedaten der gleichen Bäume erweitert. Die Ergebnisse zeigen eine signifikante altersbedingte Abnahme der Temperatursensitivität mit zunehmendem Alter. Die Dichtedaten erweisen sich hiervon weniger beeinflusst und sind folglich besser geeignet für Klimarekonstruktionen. Temperaturrekonstruktionen dieser Region zeigen keine altersbedingten Verzerrungen, wenn die zugrundeliegenden Daten unter der Prämisse von gleich verteilten Altersgruppen, also von jungen als auch alten Bäume, erhoben wurden.

Der Lärchenwickler (*Zeiraphera diniana* Gn.) wird mit regelmäßigen Populationsschwankungen und zyklischen Massenvermehrungen (alle 8-10 Jahre) in Verbindung gebracht, was zu Veränderungen in der Jahrringbreite und reduzierter Klimasensitivität von Wirtsbäumen führt. Im Gegensatz zu den bekannten 1200-jährigen

historischen Belegen aus den Alpen, lehnen die Ergebnisse dieser Arbeit die Annahme einer zyklischen Massenvermehrung des Lärchenwicklers für die letzten 300 Jahre in der slowakischen Hohen Tatra ab. Niedrige Bestandsdichten in räumlich begrenzten Lärchenwäldern verhindern die massenhafte Vermehrung des Lärchenwicklers. Signifikant gleichläufige *Larix decidua* Mill. (Wirt) und *Pinus cembra* L. Jahrringserien, bestehend aus 323 Proben, zeigen zudem deutliche Klimasignale frühsommerlicher Temperaturschwankungen und liefern somit ideale Voraussetzungen für osteuropäische Temperaturrekonstruktionen.

Die Analyse von stabilen Isotopendaten aus Jahrringen bietet umfangreiche Informationen über Auswirkungen von externen klimatischen Einflussfaktoren auf physiologische Prozesse der Bäume. Kohlenstoff- ($\delta^{13}C$) und Sauerstoff- ($\delta^{18}O$) Isotopendaten von *Pinus uncinata* Jahrringen aus den spanischen Pyrenäen weisen signifikante Klimasensitivität auf. Während die $\delta^{18}O$ Zeitreihen durch Frühjahrsniederschläge und andere komplexere Faktoren gesteuert werden, zeigen die $\delta^{13}C$ Zeitreihen ein eindeutiges Sommertemperatursignal. Aufgrund der erhöhten atmosphärischen CO_2 Konzentration werden in dieser Dissertation unterschiedliche Korrekturverfahren für $\delta^{13}C$ Daten verwendet, welche jedoch die niederfrequenten Trends verändern, was Auswirkungen auf die Klimasignalstärke nach sich zieht. Welches Korrekturverfahren als letzte Instanz ausgewählt werden soll bleibt eine Herausforderung, da die natürliche Anpassung der baumphysiologischen Prozesse an diesem Standort nicht quantifiziert werden konnten und objektive Kriterien für eine optimale CO_2-Korrektur weiterhin fehlen. Mit einem neuartigen Ansatz trendbereinigter $\delta^{13}C$ Daten im juvenilen Baumalter konnte eine 750-jährige Rekonstruktion dekadischer Sommertemperaturen entwickelt werden. Diese Rekonstruktion zeigt im historischen Verlauf größere Temperaturamplituden im Vergleich zu bereits publizierten Rekonstruktionen, welche auf traditionellen Jahrringparametern beruhen.

Vorhandene als auch zukünftige Rekonstruktionen können durch Anwendung der vorgestellten Nachweismethoden auf mögliche Verzerrungen überprüft werden. Die Ergebnisse dieser Dissertation liefern somit einen Beitrag zur Debatte über zuverlässige Schätzungen vergangener Klimaschwankungen und deren Bedeutung als Grundlage für die Vorhersage zukünftiger Trends.

Acknowledgements

Not available online.

Table of contents

1. Introduction

The wide distribution of conifer trees and their longevity over several decades to centuries put tree-ring research in a prominent position within paleoclimate research. Due to wood-anatomical characteristics, conifer tree-rings are characterized by distinct boundaries, as the differentiation between the lighter earlywood with large lumen sizes and the darker latewood with thicker cell walls is often visible even without using optical devices (Schweingruber, 1996, 2007; Speer, 2010). Annual tree-rings are formed in environments with seasonal climate fluctuations, because winter conditions regularly cause dormancy of the cambium and cessation of radial growth (Fritts, 1976; Schweingruber, 1996, 2007; Speer, 2010). Favorable climate conditions in the vegetation periods amplify metabolic processes, such as cambial cell division and cell wall thickening, and alter interannual ring-characteristics (Fritts, 1976; Schweingruber, 1996). Chronologies comprising tree-ring sequences from a high amount of tree individuals can be viewed as a climate archive in annual resolution, spatially representative for the region of origin (Esper and Gärtner, 2001; Fritts, 1976; Speer, 2010). Centennial- to millennial-long chronologies for many regions across the globe can be developed to reconstruct large-scale past climate variations, thereby, contributing to the understanding of natural climate fluctuations, specifically when evaluating the 20th century warming (Fritts, 1976; Speer, 2010).

1.1 Tree-ring parameters and the link to climate

The tree-ring archive captures climate information during ring formation and simultaneously provides high-resolution proxy data to address and test paleoclimatic hypotheses. The climate information can be extracted from physical parameters, tree-ring width (TRW) and maximum latewood density (MXD), and from chemical parameters, stable carbon ($\delta^{13}C$) and oxygen ($\delta^{18}O$) isotopic composition (Farquhar et al., 1982; Fritts, 1976; McCarroll and Loader, 2004; Schweingruber, 2007).

The species-specific wood-anatomical structure and xylogenesis depend on genetic expression and hormonal signals, while external factors modify the interannual characteristics (Deslauriers et al., 2008; Meinzer et al., 2011; Schweingruber, 2007). In environments at high latitudes and altitudes, temperature conditions are generally considered to be the limiting factor for tree-growth. Under favorable climatic conditions in the vegetation period, cambial cell division is elevated, resulting in a higher number of newly formed earlywood cells, which lead to wider rings and increased TRW values (Fritts, 1976; Schweingruber, 1996). Additionally, a higher amount of lignin storage in cell walls of the tracheids and related cell wall thickening is detectable as higher MXD values, which define the proportion of thick-walled tracheids to the lumen area (Schweingruber, 1996, 2007; Speer, 2010).

Carbon uptake, in form of CO_2, follows pathways via stomata into the leaves of trees and is crucial for the production of assimilates required for tree growth (Farquhar et al., 1982; McCarroll and Loader, 2004; Treydte et al., 2004). Open stomata, linked to mild and humid conditions, lead to the incorporation of the lighter ^{12}C isotope, resulting in low $\delta^{13}C$ values. Warm and dry conditions cause closed stomata to prevent transpiration losses, which results in high $\delta^{13}C$ values in tree-rings (Helle and Schleser, 2004; McCarroll and Loader, 2004; Treydte et al., 2007).

The main source of oxygen occurs at root-level: H_2O is absorbed by the roots and transported via the xylem to the leaves, where implementation of oxygen in the photosynthetic cycle occurs. Here, open stomata cause an enrichment of the heavier ^{18}O, since the lighter ^{16}O preferably transpires, impacting the $\delta^{18}O$ leaf-water composition, which is reflected in the tree-ring (Helle and Schleser, 2004; McCarroll and Loader, 2004). However, the isotopic composition of H_2O as source signal plays an important role and is also reflected in the tree-ring, allowing an analysis of the waters provenance (McCarroll and Loader, 2004; Treydte et al., 2004). A careful site selection is obligatory to disentangle both mechanisms as a prerequisite to correctly interpret $\delta^{18}O$ values (Helle and Schleser, 2004; Treydte et al., 2007).

1.2 Trends and Signals: Estimating the climate signal strength

A straightforward method to quantify the tree-ring response to climate variations utilizes the Pearson correlation coefficient *r* and estimates the climate signal strength by exploiting monthly instrumental measurements from nearby meteorological stations within a defined calibration period (Esper and Gärtner, 2001; Fritts, 1976; Speer, 2010). Monthly gridded data based on spatially interpolated measurements and calculations, such as drought-related indices, can add information to the interpretation of growth-climate relationships by

synthesizing information on temperature, precipitation, evapotranspiration and soil characteristics in a single dataset (Dai et al., 2004; van der Schrier et al., 2006; Vicente-Serrano et al., 2010).

The most distinct climate signals are generally found when using mean climate conditions for the species-specific vegetation period. Once coherency in high-frequent year-to-year variations and low-frequent trends, as well as temporal robustness in the calibration and defined verification periods are confirmed, the tree-ring data can be transferred into seasonal climate data by applying various statistical techniques (Esper and Gärtner, 2001; Fritts, 1976; Speer, 2010).

Tree growth, however, is not solely controlled by climate variations. Biological or geomorphological processes may impact tree-intrinsic metabolic features and require careful analyses to minimize non-climatic biases in the estimation of climate signal strength and subsequent paleoclimatic reconstructions (Fritts, 1976; Schweingruber, 1996).

1.3 Research context and objectives

This dissertation utilizes the aforementioned tree-ring parameters of conifer trees from altitudinal and latitudinal treeline sites across Europe to overcome pending questions related to previously published temperature reconstructions from these areas (Büntgen et al., 2008; Büntgen et al., 2013; Büntgen et al., 2011a; Dorado Liñán et al., 2012; Esper et al., 2012). The reliability of these reconstructions is evaluated by in-depth analyses of three non-climatic biases potentially altering the growth-climate relationships.

First, the principle for reconstructions is a temporal consistent climate sensitivity of tree growth, independent of cambial tree age. However, age-related biases have been reported for TRW-based calibration and reconstructions approaches (i.e. Szeicz and MacDonald, 1994), while the evaluation of the best-responding age-categories vary from young (Rossi et al., 2008; Rozas et al., 2009) to old trees (Carrer and Urbinati, 2004; Linares et al., 2013; Yu et al., 2008). Other studies found these climate signal age effects (CSAE) to be negligible (Dorado Liñán et al., 2011; Esper et al., 2008; Linderholm and Linderholm, 2004). A straightforward comparison of these contradicting findings appears to be complicated, as these studies comprise different tree-species from different environments. Additionally, a systematic analysis of CSAE in MXD data has been broadly ignored, although this tree-ring parameter is increasingly used for millennial-long reconstructions (Esper et al., 2012; Schneider et al., 2015).

As a second biasing factor, the occurrence of insect-induced disturbances in interannual growth patterns is examined. Many species of foliage-feeding Lepidoptera exhibit cyclic population dynamics. Larch budmoth populations (LBM; *Zeiraphera diniana* Gn.) are associated with 8-10 year cycles causing extensive forest defoliation and subsequent growth depression in larch TRW, reported for subalpine zones in the European Alps (Baltensweiler, 1993; Baltensweiler et al., 1977; Esper et al., 2007). Outside the greater Alpine region, other subalpine natural stands of larch trees with ecological and climatic similarities are known, but systematic assessments of extensive LBM population outbreaks over the past decades to centuries are still missing. Insect-induced disturbances in larch TRW from such subalpine zones in East-Europe may affect growth-climate relationships and subsequent temperature reconstructions (Büntgen et al., 2013), since foresters report occurrence of LBM populations in the habitats.

The third potential bias predominantly concerns effects of atmospheric CO_2 on tree-rings' stable carbon isotope composition. The anthropogenic burning of fossil fuels and deforestation since the beginning of industrialization at ~1850 lead to depletion of atmospheric ^{13}C in atmospheric CO_2 molecules, which if uncorrected results in decreasing trends in the carbon isotopic composition of tree-rings throughout the 20th century (Farquhar et al., 1982; McCarroll and Loader, 2004). In addition, atmospheric CO_2 concentration is steadily increasing causing changes in internal CO_2 concentrations in leaves and adaptations of stomatal conductance, water-use efficiency, and photosynthesis rate (Farquhar et al., 1982; Frank et al., 2015). These processes require corrections, either considering different fixed amounts of isotope fractionation per unit CO_2 increase (Feng and S., 1995; Kürschner, 1996; Schubert and Jahren, 2012), or more complex, data adaptive approaches (McCarroll et al., 2009; Treydte et al., 2009). By applying these correction methods varying amounts of low-frequency information are added to the $\delta^{13}C$ data, thereby impacting climate signal strength and subsequent reconstructions. Systematically lower $\delta^{13}C$ values in data derived from trees younger than 200 years indicate biological, non-climatic effects on the isotopic composition of the juvenile tree-rings and have to be removed via detrending techniques commonly applied to TRW and MXD data (Esper et al., 2010). Applying different CO_2 corrections and detrending methods to the $\delta^{13}C$ data results in varying low-frequency trends, which are crucial for reliable temperature reconstructions.

1.4 Structure of this dissertation

Section 2, "Climate Signal Age Effects In Boreal Tree-Rings: Lessons To Be Learned For Paleoclimatic Reconstructions", presents an analysis of 692 MXD and TRW series of *Pinus sylvestris* trees from northern Fennoscandia, with the aim to assess climate signal age effects throughout the 1879-2006 calibration period. Individual core measurements and age-related chronologies were developed to detect trends as a function of cambial age. Results are discussed in terms of potential biases on low-frequency variations in published climate reconstructions (Büntgen et al., 2011a; Esper et al., 2012).

In section 3, "Tree-ring evidence for the historical absence of cyclic larch budmoth outbreaks in the Tatra Mountains", growth patterns of 163 *Larix decidua* Mill. (host) and 155 *Pinus sylvestris* L. (non-host) TRW samples from the Slovakian High Tatra Mountains are analyzed to assess species-specific growth-climate relationships. Residuals between the two chronologies, spanning the common period 1725-2012, are used to detect growth depressions in larch host data, indicative of defoliation patterns caused by mass outbreaks of foliage-feeding larch budmoth populations. Additionally, the host data is tested for occurrence of cyclic dynamics over the past 300 years, as recurrent 8-10 year cycles are reported from the European Alps (Esper et al., 2007). Results are discussed relative to insect-induced disturbances potentially affecting the millennium-long temperature reconstruction from the region (Büntgen et al., 2013).

In sections 4-6, the role of elevated atmospheric CO_2 concentration over the past 150 years and its impact on the tree-rings' isotopic composition, incorporated climate signals, and subsequent reconstructions from a Mediterranean high-elevation environment is addressed. A larger network of 26 timeseries (Esper et al., 2010), as well as five newly developed timeseries of tree-ring stable isotope composition extracted from *Pinus uncinata* Ramond ex DC trees from the Spanish Pyrenees were used for calibration trials. Annually resolved and individually measured $\delta^{13}C$ and $\delta^{18}O$ timeseries were used to identify climate signals throughout the 20^{th} century, and to evaluate the coherency among both isotope datasets (section 4, "Climate sensitivity and parameter coherency in annually resolved $\delta^{13}C$ and $\delta^{18}O$ from *Pinus uncinata* tree-ring data in the Spanish Pyrenees"). The elevated atmospheric CO_2 concentration and associated effects on carbon isotope fractionation are examined using three different correction procedures.

Section 5, "Trends And Signals In Decadally Resolved Carbon Isotopes From The Spanish Pyrenees", describes the estimation of climate signals in decadally resolved carbon isotope

data from six trees, thereby allowing the comparison of calibration results derived from data with different temporal resolutions. The impact of varying low-frequency trends associated with applied CO_2 correction procedures is assessed, and spurious trends in the chronology are developed to discuss the significance of replication, which is generally low in tree-ring stable isotope studies.

Finally, a 750-year long decadal June-August temperature reconstruction based on $\delta^{13}C$ data is presented in section 6 “Long-Term Summer Temperature Variations In The Pyrenees From Detrended Stable Carbon Isotopes”. In contrast to the common development of tree-ring stable isotope chronologies, a novel approach of detrending the $\delta^{13}C$ values is executed, due to systemic low values in tree-rings younger than 200 years. Results are compared to MXD-derived reconstructions from the same region (Büntgen et al., 2008; Dorado Liñán et al., 2012), thereby, contributing to the discussion on past temperature variations, particularly considering the late 20th century warming.

2. Climate signal age effects in boreal tree-rings: lessons to be learned for paleoclimatic reconstructions

Oliver Konter[1], Ulf Büntgen[2,3,4], Marco Carrer[5], Mauri Timonen[6,], Jan Esper[1]

[1] *Department of Geography, Johannes Gutenberg University, 55099 Mainz, Germany*

[2] *Swiss Federal Research Institute WSL, Birmensdorf, Switzerland*

[3] *Oeschger Centre for Climate Change Research, Bern, Switzerland*

[4] *Global Change Research Centre AS CR, Brno, Czech Republic*

[5] *Dipartimento TeSAF, Università degli Studi di Padova, Agripolis, Legnaro (PD), Italia*

[6] *Rovaniemi Research Unit, Finnish Forest Research Institute, 96301 Rovaniemi, Finland*

submitted to Quaternery Science Reviews, November 2015

2.1 Introduction

The ability of trees to form annually resolved rings in extra-tropical environments allows paleoclimatologists to develop annually resolved and absolutely dated climate reconstructions over several centuries to sometimes even millennia (Briffa et al., 2008; Büntgen et al., 2013; Büntgen et al., 2011b; Esper et al., 2007; Esper et al., 2012; Graumlich, 1993; Myglan et al., 2012; Schneider et al., 2015; Trouet et al., 2009; Villalba, 1990). The most frequently used tree-ring parameters, TRW and MXD, therefore provide the backbone of high-resolution paleoclimatology (Büntgen et al., 2013; Esper et al., 2007; Graumlich, 1993; Trouet et al., 2009; Villalba, 1990).

The underlying principle for these reconstructions is a temporal consistent climate sensitivity of tree growth (Fritts, 1976; Speer, 2010). This assumption is considered to hold back not only over geological time and geographical space (Büntgen et al., 2009; Esper and Frank, 2009) but also over cambial tree age. While the first two arguments remain under scrutiny for many sites and species (Cook et al., 2004; D'Arrigo et al., 2006; Frank et al., 2007b; Ljungqvist et al., 2012), the later assumption has not even been explored in a systematic manner.

At the same time, age-dependent changes in raw MXD and TRW values are a well-known feature, associated with geometrical constraints of adjoining new rings to an increasing stem-radius/basal increment (Cook et al., 1990). These trends are less pronounced in MXD as cell walls become gradually thinner with increasing tree age (Schweingruber, 1996). In contrast to TRW, MXD has been reported to contain stronger temperature signals and enhanced signal-to-noise ratios in the high-frequency domain, compared to TRW (Briffa et al., 2002; Büntgen et al., 2015a; Büntgen et al., 2015b; Frank et al., 2007a). Due to lower biological memory (i.e. lower autocorrelation), MXD from cold environments typically exhibits higher correlation coefficients with summer temperature deviations (Esper et al., 2015).

In addition, it has been demonstrated that TRW-based climate reconstructions are, to a certain degree, constrained by age-related biases (Szeicz and MacDonald, 1994). Several studies have recently analyzed these climate signal age effects (CSAE) in TRW, revealing a better agreement between climate variation and the growth of old trees (Carrer and Urbinati, 2004; Esper et al., 2008; Linares et al., 2013; Yu et al., 2008). Other studies using different sites and species, however, found growth-climate relationships to be stronger in younger tree-rings (Dorado Liñán et al., 2011; Rozas et al., 2009). An overview on CSAE, including all previously mentioned cases and others (Linderholm and Linderholm, 2004; Rossi et al., 2008)

is provided in Table 1. While sometimes pondered negligible (Dorado Liñán et al., 2011; Esper et al., 2008; Linderholm and Linderholm, 2004), CSAE can significantly impact the climate sensitivity of tree growth (Carrer and Urbinati, 2004; Linares et al., 2013; Rossi et al., 2008; Rozas et al., 2009; Yu et al., 2008). Varying prerequisites in earlier studies (Figure 2-2), nonetheless, aggravate any straightforward comparison of the individual, and often contradicting findings. On top, testing for CSAE in MXD has been broadly ignored.

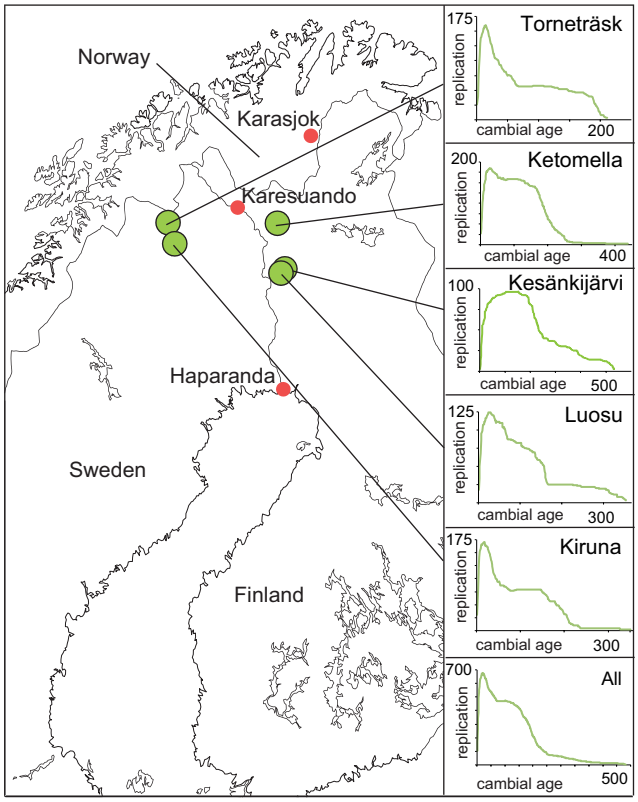

Figure 2-1 Tree-ring sites (green circles), sample replication (panels on the right) and meteorological stations in Karasjok (1876-2011 period), Karesuando (1879-2011), Haparanda (1860-2009; red circles).

Since age is closely related to tree size and height, disentangling this connection is challenging. Increased size can stimulate secondary growth, due to higher light accessibility and reduced competition (Bond, 2000). On the other hand, it can also lead to secondary growth reductions (Ryan and Yoder, 1997), due to hydraulic constraints in water transport and increased respiration (Meinzer et al., 2011; Schweingruber, 1996). Xylogenesis depends on cambial cell division, cell expansion and the growth of secondary cell walls (Schweingruber, 2007), which are intrinsically controlled by gene expression and hormonal signals (Meinzer et al., 2011), and extrinsically by environmental factors, including temperature or precipitation (Deslauriers et al., 2008). Several functional and physiological

processes are affected by tree age, including a reduced foliar efficiency, lower photosynthetic rates, delayed onset of reproduction, and shorter growing seasons (Bond, 2000; Day et al., 2002; Rossi et al., 2008; Thomas, 2011). These age-related changes support the assumptions, that varying physiological processes result in different levels of climate sensitivity throughout a tree's lifespan.

Here, we analyze CSAE in a unique *Pinus sylvestris* L. network from northern Fennoscandia. This dataset of 692 MXD and TRW measurement series from young and old trees provides ideal conditions for the re-organization of data by cambial age, the assessment of CSAE at both, the site and tree level, as well as parameter-specific and age-related comparisons of growth-climate response patterns.

2.2 Material and methods

2.2.1 Tree-ring data

Five well replicated MXD datasets from several sites across northern Sweden and Finland are used (Figure 2-1). This compilation is part of a wider Northern Fennoscandian Network (NFN), previously developed to reconstruct changes in regional summer temperatures (Büntgen et al., 2011a; Esper et al., 2012; Schneider et al., 2014). A total of 692 cores were taken from *Pinus sylvestris* trees, spanning the period 1475-2006 (exceeding ten series in each year). Data include different tree ages ranging from 1-612 years. Sample replication ranges from 99-198 cores per site. TRW was measured with an accuracy of 0.01 mm using a LinTab measurement device and corresponding TSAP software (Rinn, 2007), and all rings were absolutely dated and verified by crossdating using the COFECHA software (Holmes, 1983). Annual MXD values were obtained from high-resolution X-ray densitometry at the Swiss Federal Research Institute WSL in Birmensdorf (Eschbach et al., 1995).

Biologically induced, non-climatic trends associated with juvenile growth/density variations were removed using several detrending techniques. Spline (10 and 100 years), Hugershoff and Negative Exponential functions (without positive slopes), as well as the Regional Curve Standardization (RCS) were applied via the ARSTAN program (Cook, 1985; Cook et al., 1995; Esper et al., 2003; Fritts, 1976). Only TRW data were power-transformed prior to detrending as MXD does not contain any substantial spread-versus-level relationship (Cook and Peters, 1997). Chronologies were calculated using the robust bi-weight mean, and temporal variance changes stabilized considering sample size and varying interseries correlations (Rbar) (Frank et al., 2007b). Chronology signal strength was estimated by

calculating Rbar and the Expressed Population Signal (EPS) statistics over 31-year moving intervals (Wigley et al., 1984).

With respect to previously published age-class grouping categories (Table 2-1), a total of 30 MXD and 30 TRW age-class subset chronologies were calculated by using the software Spotty (Esper et al., 2009). Site chronologies were considered to evaluate the influence of local environmental factors versus age.

2.2.2 Growth-climate relationships and age effects

Monthly data from the three longest nearby meteorological stations with monthly resolution (Haparanda, Karasjok, Karesuando) were utilized to generate seasonal and annual temperature means over the common period 1879-2006. Climate response patterns were estimated using *Pearson's* correlation coefficients (*r*) between the MXD and TRW records (i.e. two main chronologies, ten site chronologies, 60 age-class chronologies, 1384 individual timeseries) and June-August (JJA) temperature means (Büntgen et al., 2011a; D'Arrigo et al., 2008; Esper et al., 2012; Schneider et al., 2014; Schneider et al., 2015). The frequency-dependent reliability of growth-climate relationships were analyzed by applying high- (HP) and low-pass (LP) filters to the proxy and the target data, using 31-year smoothing splines and residuals thereof. Climate correlations of individual core samples were aligned by biological/cambial age (Esper et al., 2003) and we fitted linear regression functions to estimate positive or negative slopes in CSAE trends and associated significance levels (Fritts, 1976).

We evaluated the temporal robustness of CSAE by splitting the common period 1879-2006 into nine equidistant periods of 40 consecutive years with a lag of 11 years. The evaluation of CSAE trends during pre-defined periods of marked warming and cooling, as well as the more trend-free episodes in-between, required calculating 1st differences of the 11-year low-pass filtered JJA temperature. To quantify the linear regression functions and explain the coherency between growth-climate linkages and cambial age, we performed analyses of variance (ANOVA) for a single factor and established significance estimation using the associated p-values.

Table 2-1 Published work associated with Climate Signal Age Effects (CSAE).

Publication	Region	Species	# Age-classes	# Cores (min/ max)	Age-effects	Best responding age-class
Carrer and Urbinati, 2004	Eastern Italian Alps	*Larix decidua Pinus cembra*	4	7/60	Yes	old
Dorado Linan et al., 2012	Spanish Pyrenees South-east Spain	*Pinus uncinata* *Pinus nigra*	2	8/18	No	young
Esper et al., 2008	Swiss Alps	*Pinus cembra*	3	35/128	No	old
Linares et al., 2013	Moroccan Atlas	*Cedrus atlantica*	2	50/60	Yes	old
Linderholm and Linderholm, 2004	Scandinavian Mountains	*Pinus sylvestris*	5	5/10	No	varies with time
Rossi et al., 2008	Eastern Italian Alps	*Larix decidua* *Pinus cembra* *Picea abies*	2	15/15	Yes	middle aged
Rozas et al., 2009	Central Spain	*Juniperus thurifera*	5	18/66	Yes	young
Yu et al., 2008	Qilian Mountains China	*Sabina przewalskii*	5	16/34	Yes	old

2.3 Results

2.3.1 Age- and site-related chronologies

CSAE has been addressed in several studies considering a variety of methods and presenting differing results including decreasing (Dorado Liñán et al., 2011) and increasing (Carrer and Urbinati, 2004) climate signal strength with tree aging (overview in Table 1). These differences are related to several factors aggravating comparability: The studies are based on samples from different ecosystems and species, include changing numbers of age-classes ranging from 2 to 5, and numbers of tree samples averaged in age-class chronologies changes dramatically among (and partly within) studies. Sample replication of some age-classes varies considerably from n_{min}=7 to n_{max}=60 (Carrer and Urbinati, 2004), or generally, include just a few trees ranging from 5 to 10 trees (Linderholm and Linderholm, 2004). Some of the differences among existing studies might therefore be due to these differing setups. The

identified best-responding age-class also varies from youngest (Dorado Liñán et al., 2011; Rozas et al., 2009), to middle-aged (Linderholm and Linderholm, 2004) and oldest (Carrer and Urbinati, 2004; Linares et al., 2013).

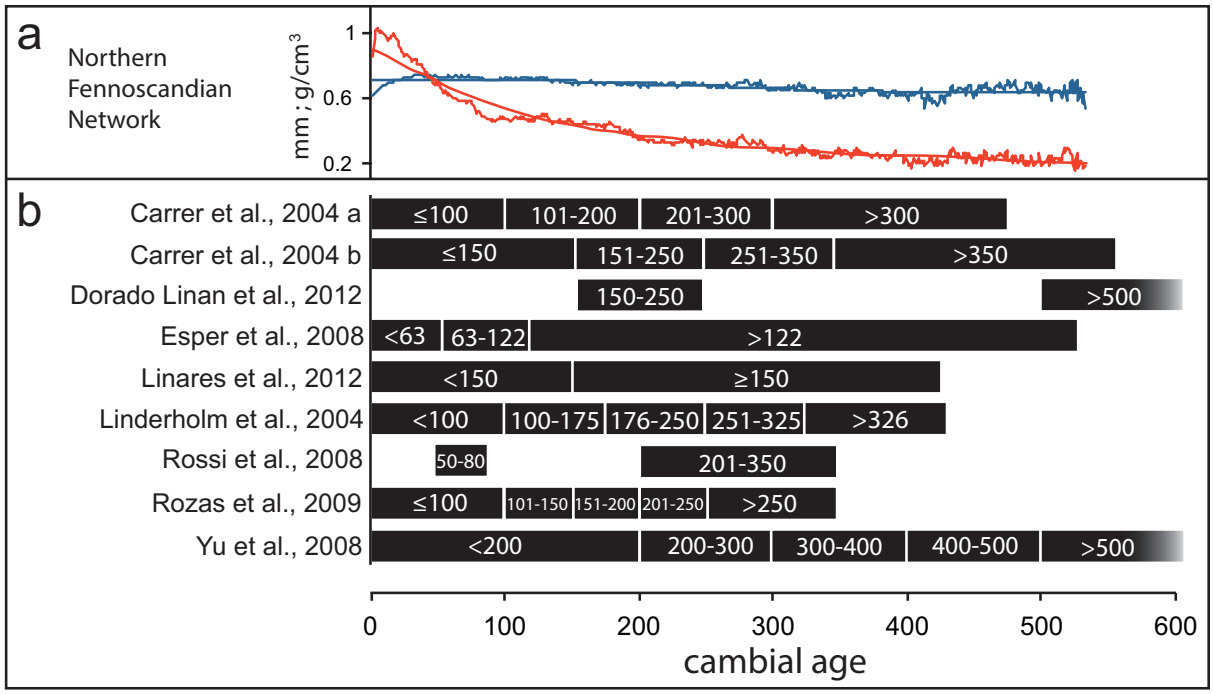

Figure 2-2 Age-class categorizations in previous studies and regional curves. a Regional curves (MXD in blue, TRW in red) of the NFN; b Cambial age-class boundaries as used in studies in CSAE.

The published age-class chronologies consider different thresholds making it difficult to compare existing studies (Figure 2-2). Age-classes range from only 30 years (Linares et al., 2013: age50-80) to 200 years (Yu et al., 2008: age1-200), so that the different age-class chronologies represent different life-stages of trees. Overall, only two out of nine studies considered juvenile age-classes <100 years (Esper et al., 2008; Rossi et al., 2008), while the threshold "100" is used in another three publications (Carrer and Urbinati, 2004; Linderholm and Linderholm, 2004; Rozas et al., 2009). Consideration of these thresholds with age-aligned data (Figure 2-2 upper panel) clearly shows how differing portions of juvenile and adult TRW and MXD data are captured, limiting the comparability of varying, pre-defined age-class systems.

The application of all previously published age-class categorizations to the NFN dataset reveals a general trend of decreasing temperature correlations with increasing cambial age (Figure 2-3). MXD shows a higher coherency with JJA temperatures than TRW. Highest correlations are recorded in the youngest age-classes ($r_{MXD1-150}$=0.78, $r_{TRW1-200}$=0.49), though

these values only slightly exceed the values when using all data (r_{MXDall}=0.76, r_{TRWall}=0.48). Cross-parameter differences appear to be most pronounced in the older age-classes ($r_{MXD500-612}$=0.47, $r_{TRW400-500}$=0.10).

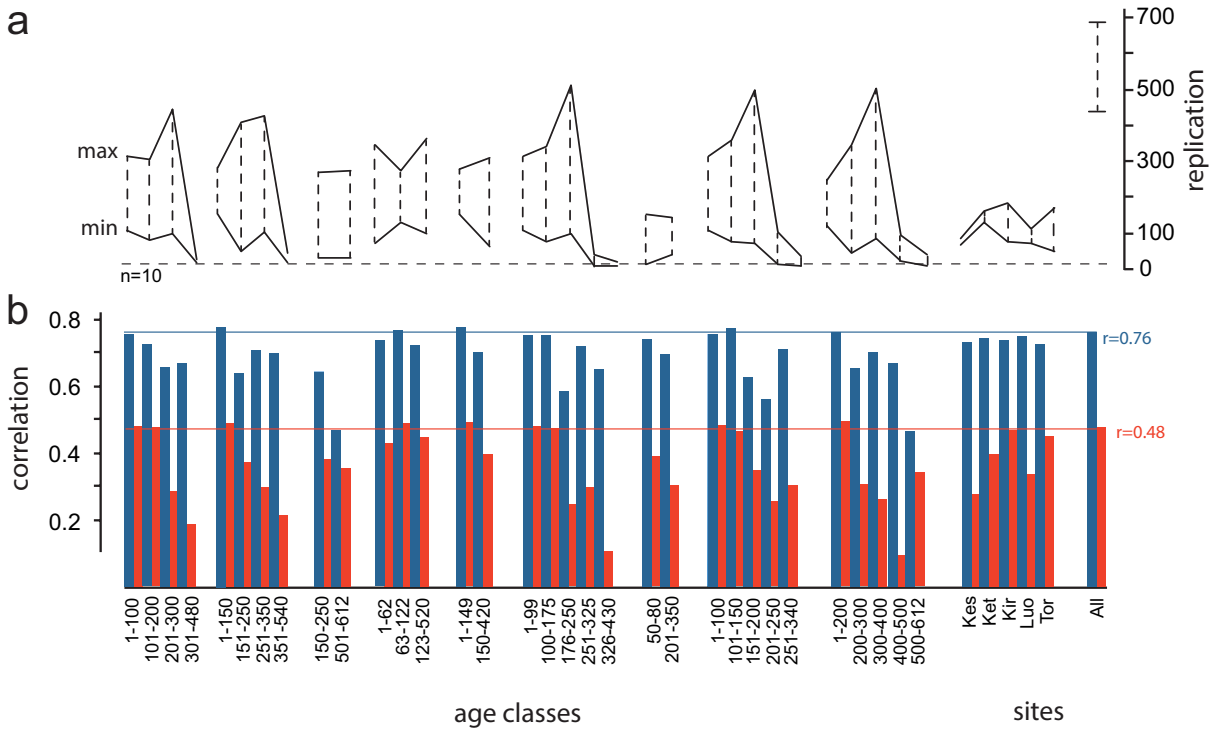

Figure 2-3 Age-class categorizations in previous studies and regional curves. a Regional curves (MXD in blue, TRW in red) of the NFN; b Cambial age-class boundaries as used in studies in CSAE.

These findings are, however, constrained by the changing numbers of MXD and TRW samples averaged in the various age-class chronologies (top panel inFigure 2-3). Some age-class categories divide the data into small sections, thereby reducing minimum replication down to only 12 ($n_{age201-250}$) or 14 samples ($n_{age\ 50-80}$), while other schemes result in much better replicated sub-set chronologies (e.g. $n_{age176-250}$=97, $n_{age63-123}$=129). In four cases ($n_{age251-325}$=8, $n_{age326-430}$=7, $n_{age251-340}$=9, $n_{age500-612}$=10), minimum replication of the age-class chronologies falls below the commonly accepted threshold of >10 samples. In addition, replication within most age-classes varies in increments of ten or up to >400 series (e.g. $\Delta n_{age151-200}$=427, $\Delta n_{age300-400}$=418), due to the amount of 128 consecutive years within the calibration period and simultaneously adapted cambial ages, that lead to the inclusion or exclusion of data within the age-class categories and thresholds. Overall, the comparison of climate signals among age-class and site chronologies (last column in Figure 2-3) reveals a higher variability of correlation values among the different age-classes than between the five

sites. While this indicates the importance of CSAE compared to commonly assessed between-site differences, this conclusion is limited by severe replication changes between the various age-class chronologies.

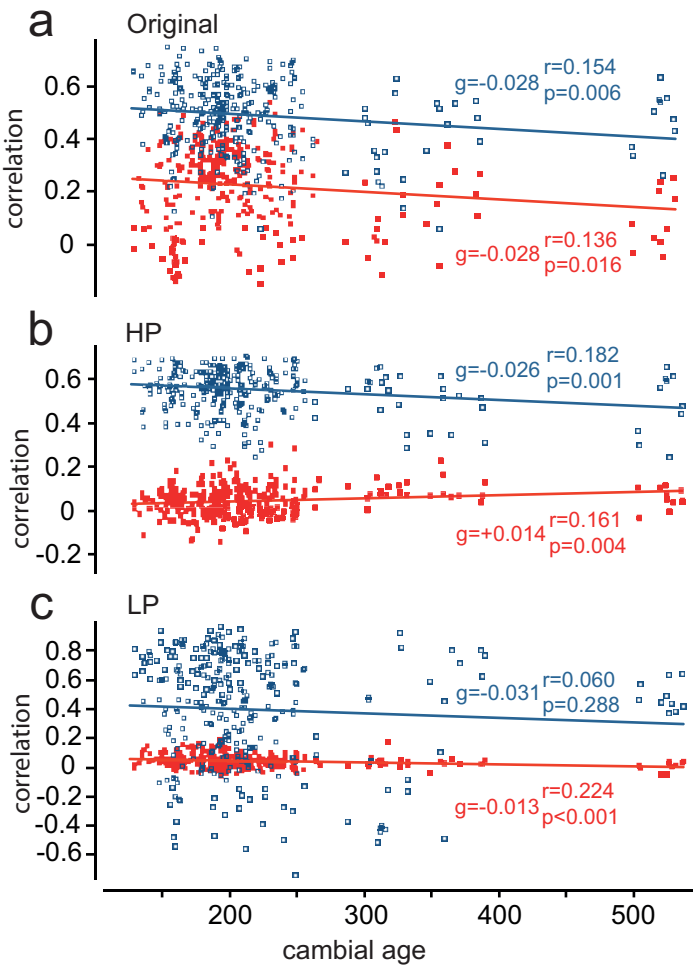

Figure 2-4 Growth-climate relationships of individual trees over the 1879-2006 period. a RCS detrended MXD (blue) and TRW series (red, n=317) correlated against JJA temperatures and linear regressions fitted to the correlation values. With g = regression slope over 100 years, r = correlation coefficient and p = significance level b Same as in a but for high-pass filtered MXD and TRW series c Same as in a but for low-pass filtered data.

2.3.2 Individual series and trends

Using individual core series (rather than age-class chronologies) supports the estimation of CSAE unbiased by changes in replication (Figure 2-4). This assessment reinforces climate signals to be stronger in MXD (than TRW), a finding that holds true in all frequencies, and over various cambial ages and time periods. Linear trend functions demonstrate JJA temperature signal strength to change with individual tree age. The trends are significant in MXD at p=0.006 for the original data and p=0.001 for the high-pass filtered data, showing

robust, decreasing centennial gradients of $g_{MXDOriginal}$=-0.028 and g_{MXDHP}=-0.026 over the 1879-2006 common period. In TRW, climate signal strength depends on cambial age in all frequencies. The linear trends are less pronounced though, and decrease with age in the original ($g_{TRWoriginal}$=-0.028) and low-pass filtered data (g_{TRWLP}=-0.013) but increase in the high-passfiltered data (g_{TRWHP}=+0.014).

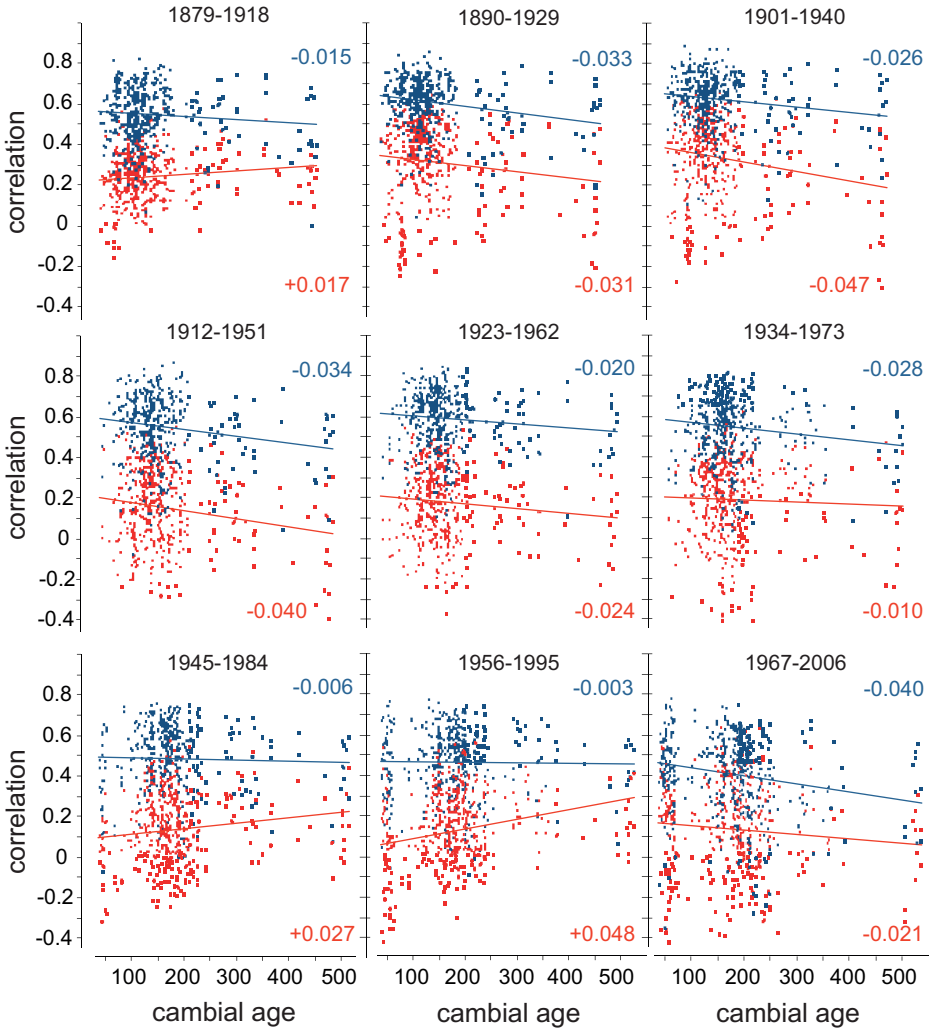

Figure 2-5 Growth-climate relationships of individual trees over equidistant periods (40 years, lag: 11-year lags). RCS detrended MXD (blue) and TRW (red) correlated against JJA temperature and linear trends as in Figure 2-4. The numbers of correlations ranges from n = 418 to n = 456. Values in blue and red indicate the regression line slopes per 100 years.

CSAE in MXD is more robust over time, since correlations in a split calibration approach comprising nine equidistant periods (40 consecutive years with a lag of 11 years) exhibit steadily decreasing values with age throughout the calibration interval (Figure 2-5). Whereas the slopes of the linear trends vary from $g_{MXD1956-1995}$=-0.003 to $g_{MXD1967-2006}$=-0.040, they remain negative in all periods in both the original and the high-pass filtered data Figure 2-6).

In comparison, the TRW data not only correlates weaker with JJA temperature, but also the CSAE slopes also change throughout the calibration interval (Figure 2-5). Only six of the nine calibration periods show negative trends, ranging from $g_{TRW1934\text{-}1973}$=-0.010 and to $g_{TRW1901\text{-}1940}$=-0.047. The three remaining periods yield positive trends with the highest value reached at $g_{TRW1956\text{-}1995}$=+0.048. However, the high-pass filtered TRW data reveals a more coherent pattern, with all periods exhibiting positive, and remarkably trends (Figure 2-6). Whereas for the high frequency data the mean gradient of all sub-periods resembles the common period results, this is not the case in the original data, where the negligible trend from the sub-periods contrasts the significant negative trend over the full calibration period 1879-2006.

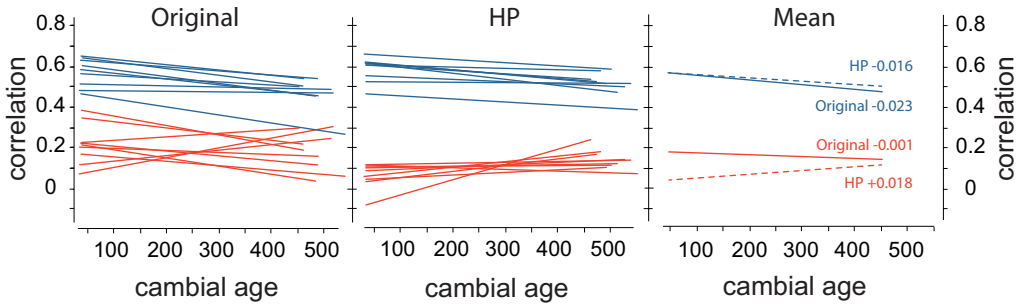

Figure 2-6 CSAE trends. Left: Linear trends of RCS detrended MXD (blue) and TRW data (red) for correlations against JJA temperature in equidistant periods (40 years, 11-year lags). Middle: Linear trends from using high-pass filtered tree-ring and temperature data. Right: Mean trends of the original and high-pass filtered data.

An assessment of the NFN in association with warming and cooling periods over the last 130 years suggests that CSAE is influenced by the temporally changing environmental conditions, a finding that seems to hold true for both TRW and MXD (Figure 2-7). While MXD shows higher correlations and generally decreasing CSAE trends throughout the 1879-2006 calibration period, the TRW signal displays the previously detected oscillation between negative and positive CSAE trends, which can be differentiated in five periods: Two periods of consecutive summer temperature warming (1904-1938 and 1984-2006), two periods of weak trends (1879-1903 and 1961-1983), and one period associated with summer cooling (1939-1960).

The most pronounced CSAE trends, in both tree-ring parameters, are apparent in the recent period 1984-2006 ($g_{1984\text{-}2006}$=-0.075, $p<0.001$), characterized by strong summer temperature warming. Also the second warming period from 1904-1938 is characterized by significant negative trends in both datasets ($g_{MXD1904\text{-}1938}$=-0.034, $g_{TRW1904\text{-}1938}$=-0.060, $p<0.001$) (Figure 2-8). During the period of consecutive summer temperature cooling, CSAE is effectively non-

existent in both, MXD and TRW. Finally, during periods with no clear temperature trend, CSAE is less distinct/homogeneous: During 1879-1903, the MXD trend is significant ($g_{MXD1879\text{-}1903}$=-0.026, p<0.01), whereas the TRW trend is not. During 1961-1983, the TRW trend is significant ($g_{TRW1961\text{-}1983}$=+0.046, p<0.001), but MXD trend is not.

In summary, climate sensitivity of MXD and TRW decline with increasing cambial age. These general tendencies are, however, modified by the differing warming and cooling trends throughout the past 130 years. Gradual summer temperature warming enhances CSAE, whereas decadal scale cooling removes this bias. Since CSAE trends in TRW are overall stronger and frequency-dependent, MXD can be considered as the more reliable proxy that not only correlates stronger with instrumental temperature data, but is also less affected by changes in cambial age throughout the calibration and the reconstruction periods.

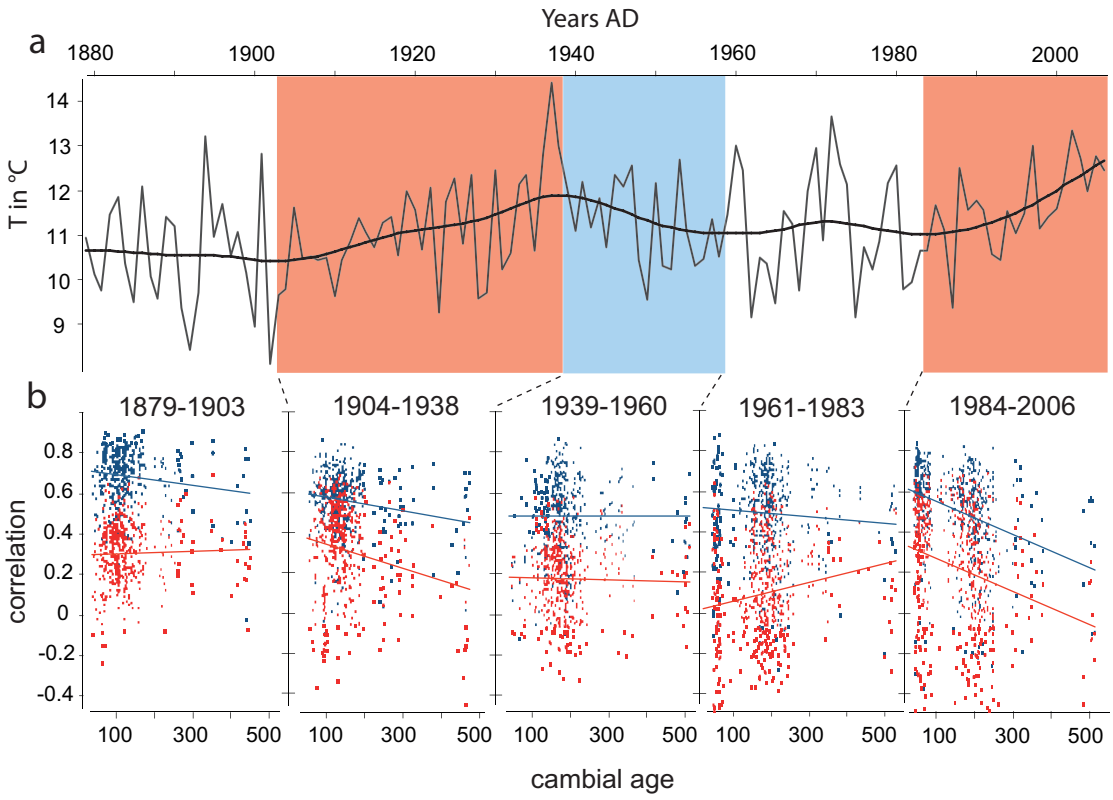

Figure 2-7 CSAE during warming, cooling and trend-free periods. a Mean JJA temperatures from Haparanda, Karasjok and Karesuando over the 1879-2006 period. Bold curve is a 30 year smoothing spline. Colors indicate warming (red), cooling (blue) and trend-free periods (white), calculated from smoothed (11-year spline) and 1st-differenced temperatures of smoothed temperature data (30 year spline) b RCS detrended MXD (blue) and TRW series (red) correlated against JJA temperature during warming, cooling and trend-free periods. Straight lines are linear regression trends.

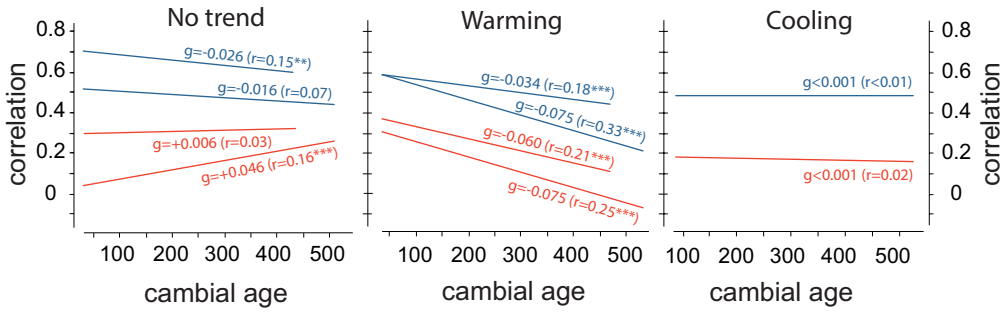

Figure 2-8 CSAE trends during warming, cooling, and trend-free periods of RCS detrended MXD (blue) and TRW series (red) from correlations against regional JJA temperatures. Left panel shows results for the trend-free periods 1879-1903 and 1961-1983. Middle panel shows results for warming periods 1904-1938 and 1984-2006. Right panel shows results for the cooling period 1939-1960, g = regression slope over 100 years, r = correlation coefficient, and significance level: *(p<0.05), ** (p<0.01), ***(p<0.001).

2.4 Discussion

At best, tree-ring chronologies comprise all cambial ages of tree-rings. However, the age distribution as a function of time displays variations, which take place not only in the calibration but also in the reconstruction period. Early reconstruction periods are typically represented by young tree-rings, while cambial ages increase towards older trees in the 20th century calibration period. Here we assessed the influence of changing tree age on climate signals using age-class chronologies and individual series. For this analysis, well-replicated datasets composed of young and old trees are required to minimize replication biases. However, such datasets are rare for TRW as most sampling strategies mostly focused on dominant and old trees (Nehrbass-Ahles et al., 2014). Due to the time-consuming procedure of MXD measurements, the dataset presented her is unique as it includes all cambial ages.

2.4.1 Data structure and characteristics

Splitting the MXD and TRW data into several age-classes considering schemes from previous studies from differing ecological and climatological settings, yielded inconsistent results. By comparing to length of some age-class categories it becomes obvious that a physiological cause in terms of changes in growth or density rates can be excluded. CSAE estimates are sensitive to different age-class thresholds, especially as these thresholds lack a physiological background. Particularly for the juvenile episode of tree-growth, large age-class categorizations of >100 years appear inadequate, since many physiological changes occur during this life-span (Meinzer et al., 2011). Generally, thresholds rather appear estimated as adaptation to the commonly used metric system (e.g. age-class 1-50, 1-100, 1-150, etc.) or to the age span of the samples at hand, thus, raising the question whether some datasets fulfill the requirements of studying CSAE. An evenly distributed mix of young and old trees is

needed to assess differences during the 20th century calibration period. Additionally, replication changes between the age-class chronologies may affect results and cannot easily be distinguished from CSAE. However, for the large dataset including young and old trees studied here, results suggest a gradual decrease of climate sensitivity with increasing age was detected in both TRW and MXD, although replication changes limit this conclusion, particularly for the older age-classes.

Exploring individual core series, instead of age-class chronologies, helped to conquer uncertainties related to replication changes and age-class thresholds, and confirmed the gradual decrease of climate sensitivity with increasing age. The calculation of linear trends also enabled an estimation of CSAE gradients per unit of age and accompanying significance levels. CSAE trends were significant in MXD and TRW (except for low-pass filtered MXD data), although they may not explain large fractions of variance in the data.

In contrast to the robust negative gradients in MXD, TRW climate correlations decrease with age in the low-pass filtered data, while the high-pass filtered data correlate better with increasing cambial age. In the original data, including both high- and low-frequency variance, the trend is again negative containing the strongest gradient. TRW is typically connected with high autocorrelation values and biological memory (Esper, 2015), incorporating a stronger low-frequency component, leading to superimposed negative trend in the original data (Büntgen et al., 2015b; Fritts, 1976). However, this decreasing trend with age is not temporally robust, since results from split calibration approaches do not reflect results over the common period, which was also detected by Linderholm and Linderholm (2004). Cambial age seems to have a frequency-dependent impact on climate signals in TRW, which seems to be absent in MXD. Particularly in the low-frequency domain, MXD contain no significant CSAE trends, thereby reinforcing the strength of this tree-ring parameter for climate reconstruction purposes. This conclusion is supported by the temporal robustness of CSAE trends in MXD, which remain significant and independent of frequency domain.

The significance of CSAE in both tree-ring parameters, MXD and TRW, is related to temporal changes in JJA temperatures over the past 130 years. Whereas warming periods seem to support negative CSAE trends, cooling periods appear to be associated with insignificant CSAE trends. In other words, older trees tend to mirror warming trends in their tree-rings to a smaller extend than younger trees. Particularly the pronounced warming in the most recent period seems to be linked to the strongest CSAE trends. Due to the typical age-structure consisting of oldest living trees and tree-rings in the most recent period together

with the decreasing tree-ages back in time, CSAE can play an important role when establishing climate signals in the late calibration period and may add another factor to ongoing debate about divergence effects in Northern European tree-ring networks (D'Arrigo et al., 2008; Esper and Frank, 2009).

2.4.2 Physiological processes

For the first time we demonstrate that the decrease of temperature sensitivity with increasing cambial age is a significant component in MXD and TRW timeseries from *Pinus sylvestris* in Northern Fennoscandia. Previously reported physiological changes throughout the trees' lifespans seem to affect cambial activity and cell-wall thickness, and their sensitivity to environmental influences. Generally, younger trees tend to prolong the vegetation period at the greater risk of mortality to enhance stem growth in competition for light (Bond, 2000; Day et al., 2002). Contrary, the vegetation period of older trees appear to be shorter, since these trees are well established, access to light is granted by fully formed canopies and competition is of no substantial importance (Rossi et al., 2008).

The interdependency of age-related vegetation period length and seasonal response patterns may contribute to the explanation of CSAE. The JJA period considered here is the best responding season when all trees of this study are included. Our results indicated that by prolonging this season, e.g. to May-September, CSAE appear overall even larger, with young rings correlating better ($r_{MXD1-100}$=0.73, $r_{TRW1-100}$=0.47) than old rings ($r_{MXD500-600}$=0.43, $r_{TRW500-600}$=0.22). A season shortening to only July leads to less pronounced trends in climate correlations: Older age-classes display higher or similar correlations to July temperatures compared to younger classes ($r_{MXD1-100}$=0.56, $r_{MXD500-612}$=0.60, $r_{TRW1-100}$=0.49, $r_{TRW500-600}$=0.48). The JJA season was chosen here, as it showed the strongest correlations among sites and proxies, and was previously considered in the climate reconstructions from the region (Büntgen et al., 2011a; Esper et al., 2012; Schneider et al., 2014). The estimated CSAEs may, however, be a masked expression of the temporal shift of age-related growth seasonality.

Generally, MXD and TRW data are derived from the same tree-rings, but are controlled by differing physiological processes. MXD is closely related to cell-wall thickness, which is primary linked to lignification (Schweingruber, 1996). TRW relates closely to the number of cells and their lumen area (Schweingruber, 1996). In young trees, cells are usually smaller, due to the shorter root-leaves path length and associated hydraulic constraints linked to tree height (Ryan and Yoder, 1997; West et al., 1999). In climatologically favorable periods, the

cambium is prone to produce more cells, thereby enlarging TRW. However, older and taller trees produce only few larger cells per ring and increase to a lesser degree their number under favorable conditions, due to slower and shorter xylogenesis (Rossi et al., 2008). This makes older trees more rigid, especially during warming periods (Carrer et al., 2015). On the opposite, consecutive temperature cooling years seems to affect both, young and old trees. Cell wall thickening (MXD) is usually not that tightly bound with such hydraulic constraints, and age- and height-related changes thereof. CSAE in this parameter probably only results from the shortening of the vegetation period. The phenomenon appears to be temporally more robust, and can probably be more easily avoided by creating datasets with an evenly distributed age-structure, i.e. be including high numbers of samples of all cambial ages.

2.5 Conclusions

Analyzing a northern Fennoscandian MXD and TRW network, we show that climate signal age effects are overall larger than the differences in summer temperature response among different tree sites. However, if we use all data, including all age-classes, the mean chronologies display only marginally lower correlations against temperature data compared to the best responding age-class chronology. On an individual tree level, the relationships between climate and MXD and TRW are age-dependent, except for the low-pass filtered MXD data (though reduced degrees of freedom need to be considered here). Decreasing climate correlations with increasing cambial age appear to be a temporally robust feature in MXD data, while TRW exhibits a more complex behavior including oscillations between positive and negative CSAE trends, depending on climate states (warming or cooling) and frequency domains (high- and low-pass). Changing climate conditions throughout the past 130 years seem to affect both tree-ring parameters: consecutive warming over several years enhanced CSAE in MXD and TRW, while cooling temperatures seems to minimized this bias.

Generally, the calibration results using MXD data are characterized by higher and temporally more robust correlations, even though also these are decreasing with tree age. CSAE is less important in the low-frequency domain, though degrees of freedom were low when testing this, which is likely important for climate reconstruction purposes. Overall warming temperatures seem to foster CSAE, which is a prominent feature of the most recent period of the calibration interval. Our findings show that CSAE bias the estimation of climate signals and subsequent reconstructions from both MXD and TRW data. CSAE should be studied in

climate reconstructions, and can probably be mitigated by a careful selection of sampled trees and inclusion of tree-rings of differing cambial age throughout time.

2.6 Acknowledgements

We thank Anne Verstege and Daniel Nievergelt at the Swiss Federal Research Institute WSL in Birmensdorf for densitometry and ring-width measurements.

2.7 References

Bond, B., 2000. Age-related changes in photosynthesis of woody plants. Trends in Plant Science 5, 349-353.

Briffa, K.R., Osborne, T.J., Schweingruber, F.H., Jones, P.D., Shiyatov, S.G., Vaganov, E.A., 2002. Tree-ring width and density data around the Northern Hemisphere: Part 1, local and regional climate signals. The Holocene 12, 737-757.

Briffa, K.R., Shishov, V.V., Melvin, T.M., Vaganov, E.A., Grudd, H., Hantemirov, R.M., Eronen, M., Naurzbaev, M.M., 2008. Trends in recent temperature and radial tree growth spanning 2000 years across northwest Eurasia. Philosophical transactions of the Royal Society of London. Series B, Biological sciences 363, 2271-2284.

Büntgen, U., Frank, D.C., Carrer, M., Urbinati, C., Esper, J., 2009. Improving Alpine summer temperature reconstructions by increasing sample size. TRACE 7, 36-43.

Büntgen, U., Kyncl, T., Ginzler, C., Jacks, D.S., Esper, J., Tegel, W., Heussner, K.U., Kyncl, J., 2013. Filling the Eastern European gap in millennium-long temperature reconstructions. Proceedings of the National Academy of Science USA 110, 1773-1778.

Büntgen, U., Raible, C.C., Frank, D., Helama, S., Cunningham, L., Hofer, D., Nievergelt, D., Verstege, A., Timonen, M., Stenseth, N.C., Esper, J., 2011a. Causes and Consequences of Past and Projected Scandinavian Summer Temperatures, 500-2100 AD. PLoS ONE 6, e25133.

Büntgen, U., Tegel, W., Nicolussi, K., McCormick, M., Frank, D., Trouet, V., Kaplan, J.O., Heussner, K.-U., Wanner, H., Luterbacher, J., Esper, J., 2011b. 2500 Years of European Climate Variability and Human Susceptibility. Science 331, 578-582.

Büntgen, U., Trnka, M., Krusic, P.J., Kyncl, T., Kyncl, J., Luterbacher, J., Zorita, E., Ljungqvist, F.C., Auer, I., Konter, O., Schneider, L., Tegel, W., Stepanek, P., Brönnimann, S., Hellmann, L., Nievergelt, D., Esper, J., 2015a. Tree-Ring Amplification of the Early Nineteenth-Century Summer Sooling in Central Europe. Journal of Climate 28, 5272-5288.

Büntgen, U., Trnka, M., Krusic, P.J., Kyncl, T., Kyncl, J., Luterbacher, J., Zorita, E., Ljungqvist, F.C., Auer, I., Konter, O., Schneider, L., Tegel, W., Stepanek, P., Brönnimann, S., Hellmann, L., Nievergelt, D., Esper, J., 2015b. Tree-Ring Amplification of the Early-19th Century Summer Cooling in Central Europe. Journal of Climate.

Carrer, M., Urbinati, C., 2004. Age-Dependent Tree-Ring Growth Responses To Climate In Larix Decidua And Pinus Uncinata. Ecology 85, 730-740.

Carrer, M., von Arx, G., Castagneri, D., Petit, G., 2015. Distilling allometric and environmental information from time series of conduit size: the standardization issue and its relationship to tree hydraulic architecture. Tree Physiol 35, 27-33.

Cook, E., Briffa, K., Shiyatov, S., Mazepa, V., 1990. Tree-ring standardization and growth-trend estimation, in: Cook, E.R., Kairiukstis, L.A. (Eds.), Methods of Dendrochronology. Kluwer Academic Publishers, Dordrecht, The Netherlands, pp. 104-123.

Cook, E.R., 1985. A Time Series Analysis Approach To Tree Ring Standardization. University of Arizona, p. 171.

Cook, E.R., Briffa, K.R., Meko, D.M., Graybill, D.A., Funkhouser, G., 1995. The 'segment length curse' in long tree-ring chronology development for palaeoclimatic studies. The Holocene 5, 229-237.

Cook, E.R., Esper, J., D'Arrigo, R.D., 2004. Extra-tropical Northern Hemisphere land temperature variability over the past 1000 years. Quaternary Sci Rev 23, 2063-2074.

Cook, E.R., Peters, K., 1997. Calculating unbiased tree-ring indices for the study of climatic and environmental change. The Holocene 7, 361-370.

D'Arrigo, R., Wilson, R., Jacoby, G., 2006. On the long-term context for late twentieth century warming. Journal of Geophysical Research 111.

D'Arrigo, R., Wilson, R., Liepert, B., Cherubini, P., 2008. On the 'Divergence Problem' in Northern Forests: A review of the tree-ring evidence and possible causes. Global Planet Change 60, 289-305.

Day, M.E., Greenwood, M.S., Diaz-Sala, C., 2002. Age- and size-related trends in woody plant shoot development: regulatory pathways and evidence for genetic control. Tree Physiol 22, 507-513.

Deslauriers, A., Rossi, S., Anfodillo, T., Saracino, A., 2008. Cambial phenology, wood formation and temperature thresholds in two contrasting years at high altitude in southern Italy. Tree Physiol 28, 863-871.

Dorado Liñán, I., Gutiérrez, E., Heinrich, I., Andreu-Hayles, L., Muntán, E., Campelo, F., Helle, G., 2011. Age effects and climate response in trees: a multi-proxy tree-ring test in old-growth life stages. Eur J Forest Res 131, 933-944.

Eschbach, W., Nogler, P., Schär, E., Schweingruber, F.H., 1995. Technical advances in the radiodensitometrical determination of wood density. Dendrochronologia 13, 155-168.

Esper, J., 2015. Memory effects in tree-ring width and maximum latewood density in response to volcanic eruptions: evidence from northern Fennoscandia TRACE 13, 34-41.

Esper, J., Cook, E.R., Krusic, P.J., Peters, K., Schweingruber, F.H., 2003. Tests of the RCS method for preserving low-frequency variability in long tree-ring chronologies. Tree-Ring Res 59, 81-98.

Esper, J., Frank, D., 2009. Divergence pitfalls in tree-ring research. Climatic Change 94, 261-266.

Esper, J., Frank, D., Büntgen, U., Verstege, A., Luterbacher, J., Xoplaki, E., 2007. Long-term drought severity variations in Morocco. Geophys Res Lett 34.

Esper, J., Frank, D.C., Timonen, M., Zorita, E., Wilson, R.J.S., Luterbacher, J., Holzkämper, S., Fischer, N., Wagner, S., Nievergelt, D., Verstege, A., Büntgen, U., 2012. Orbital Forcing of Tree-Ring Data. Nature Climate Change 2, 862-866.

Esper, J., Krusic, P.J., Peters, K., Frank, D., 2009. Exploration of long-term growth changes using the tree-ring detrending program “Spotty”. Dendrochronologia 27, 75-82.

Esper, J., Niederer, R., Bebi, P., Frank, D., 2008. Climate signal age effects—Evidence from young and old trees in the Swiss Engadin. Forest Ecology and Management 255, 3783-3789.

Esper, J., Schneider, L., Smerdon, J., Schöne, B., Büntgen, U., 2015. Signals and memory in tree-ring width and density data. Dendrochronologia.

Frank, D., Büntgen, U., Böhm, R., Maugeri, M., Esper, J., 2007a. Warmer early instrumental measurements versus colder reconstructed temperatures: shooting at a moving target. Quaternary Sci Rev 26, 3298-3310.

Frank, D., Esper, J., Cook, E.R., 2007b. Adjustment for proxy number and coherence in a large-scale temperature reconstruction. Geophys Res Lett 34, n/a-n/a.

Fritts, H.C., 1976. Tree Rings and Climate. Academic Press, London.

Graumlich, L.J., 1993. A 1000-Year Record of Temperature and Precipitation in the Sierra Nevada. Quaternary Research 39, 249-255.

Holmes, R.L., 1983. Computer-assisted quality control in tree ring dating and measurement. Tree Ring Bulletin 43, 69-78.

Linares, J.C., Taïqui, L., Sangüesa-Barreda, G., Seco, J.I., Camarero, J.J., 2013. Age-related drought sensitivity of Atlas cedar (Cedrus atlantica) in the Moroccan Middle Atlas forests. Dendrochronologia 31, 88-96.

Linderholm, H.W., Linderholm, K., 2004. Age-dependent climate sensitivity of Pinus sylvestris L. in the central Scandinavian Mountains. Boreal Environment Research 9, 307-317.

Ljungqvist, F.C., Krusic, P.J., Brattström, G., Sundqvist, H.S., 2012. Northern Hemisphere temperature patterns in the last 12 centuries. Climate of the Past 8, 227-249.

Meinzer, F.C., Lachenbruch, B., Dawson, T.E., 2011. Size- and Age-Related Changes in Tree Structure and Function Springer Science+Business Media, Dordrecht, Heidelberg, London, New York.

Myglan, V.S., Oidupaa, O.C., Vaganov, E.A., 2012. A 2367-Year Tree-Ring Chronology for the Altai–Sayan Region (Mongun-Taiga Mountain Massif). Archaeology, Ethnology and Anthropology of Eurasia 40, 76-83.

Nehrbass-Ahles, C., Babst, F., Klesse, S., Notzli, M., Bouriaud, O., Neukom, R., Dobbertin, M., Frank, D., 2014. The influence of sampling design on tree-ring-based quantification of forest growth. Glob Chang Biol 20, 2867-2885.

Rinn, F., 2007. TSAP Win Professional. Zeitreihenanalysen und Präsentation für Dendrochronologie und verwandte Anwendungen. Benutzerhandbuch. Rinntech, Heidelberg.

Rossi, S., Deslauriers, A., Anfodillo, T., Carrer, M., 2008. Age-dependent xylogenesis in timberline conifers. New Phytologist 177, 199-208.

Rozas, V., DeSoto, L., Olano, J.M., 2009. Sex-specific, age-dependent sensitivity of tree-ring growth to climate in the dioecious tree Juniperus thurifera. The New phytologist 182, 687-697.

Ryan, M.G., Yoder, B.J., 1997. Hydraulic limits to tree height and tree growth. BioScience 47, 235-242.

Schneider, L., Esper, J., Timonen, M., Büntgen, U., 2014. Detection and evaluation of an early divergence problem in northern Fennoscandian tree-ring data. Oikos 123, 559-566.

Schneider, L., Smerdon, J.E., Büntgen, U., Wilson, R.J.S., Myglan, V.S., Kirdyanov, A.V., Esper, J., 2015. Revising midlatitude summer temperatures back to A.D. 600 based on a wood density network. Geophys Res Lett, n/a-n/a.

Schweingruber, F.H., 1996. Tree Rings and Environment. Dendroecology. Swiss Federal Institute for Forest, Snow andLandscape Research, Berne, Stuttgart, Vienna, Haupt.

Schweingruber, F.H., 2007. Wood Structure and Environment. Springer Verlag, Berlin, Heidelberg.

Speer, J.H., 2010. Fundamentals of Tree-Ring Research. The University of Arizona Press, Tucson.

Szeicz, J.M., MacDonald, G.M., 1994. Age-dependent tree-ring responses of subarctic white spruce to climate. Canadian Journal of Forest Research 24, 120-132.

Thomas, S.C., 2011. Age-Related Changes in Tree Growth and Functional Biology: The Role of Reproduction, in: Meinzer, F.C., Lachenbruch, B., Dawson, T.E. (Eds.), Size- and Age-Related Changes in Tree Structure and Function. Springer Science+Business Media, Dordrecht, Heidelberg, London, New York, pp. 33-64.

Trouet, V., Esper, J., Graham, N.E., Baker, A., Scourse, J.D., Frank, D.C., 2009. Persistent Positive North Atlantic Oscilaation Mode Dominated the Medieval Climate Anomaly. Science 324, 78-80.

Villalba, R., 1990. Climatic Fluctuations in Northern Patagonia during the Last 1000 Years as Inferred from Tree-Ring Records. Quaternary Research 34, 346-360.

West, B.G., Brown, J.H., Enquist, B.J., 1999. A general model for the structure and allometry of plant vascular systems. Nature 400, 664-667.

Wigley, T.M.L., Briffa, K.R., Jones, P.D., 1984. On the Average Value of Correlated Time Series, with Applications in Dendroclimatology and Hydrometeorology. Journal of Climate and Applied Meteorology 23, 201-213.

Yu, G., Liu, Y., Wang, X., Ma, K., 2008. Age-dependent tree-ring growth responses to climate in Qilian juniper (Sabina przewalskii Kom.). Trees 22, 197-204.

3. Tree-ring evidence for the historical absence of cyclic larch budmoth outbreaks in the Tatra Mountains

Oliver Konter[1], Jan Esper[1], Andrew Liebhold[2], Tomas Kyncl[3], Lea Schneider[1], Elisabeth Düthorn[1] and Ulf Büntgen[4,5,6]

[1] *Department of Geography, Johannes Gutenberg University, Mainz, Germany*

[2] *Northern Research Station, USDA Forest Service, Morgantown, USA*

[3] *Moravian Dendro-Labor, Brno, Czech Republic*

[4] *Swiss Federal Research Institute WSL, Birmensdorf, Switzerland*

[5] *Oeschger Centre for Climate Change Research, Bern, Switzerland*

[6] *Global Change Research Centre AS CR, Brno, Czech Republic*

published in Trees – Structure and Function 29, 2015

3.1 Introduction

The dynamics of insect populations vary considerably among species with some exhibiting equilibrium dynamics, others having regular cycles, or chaotic patterns (Bjornstad and Grenfell, 2001). Cyclic population behavior has been reported for many species of foliage-feeding Lepidoptera (Berryman, 1996), including the larch budmoth (LBM: *Zeiraphera diniana* Gn.), which exhibits particularly regular cycles of 8-10 years, with recurrent high population densities causing extensive forest defoliation in the subalpine zone of the European Alps (Baltensweiler, 1993a; Baltensweiler et al., 1977). These defoliation episodes alter ring width formation of host larch trees and dendrochronological methods have been used to reconstruct the timing of historical outbreaks over the past 1200 years (Büntgen et al., 2009; Esper et al., 2007; Rolland et al., 2001; Weber, 1997). Surprisingly, the amplitude of regular LBM mass outbreaks has been greatly diminished since the early 1980s (Baltensweiler, 1993b; Ims et al., 2008; Johnson et al., 2010). The fact that this abrupt cessation of outbreak intensity coincides with unprecedented warming, has been noted and hypotheses for causal roles of climate change in the variation of LBM dynamics have been advanced: The temperature-induced optimal altitudinal envelope of LBM outbreak epicenters may have shifted up and down during historical periods of climatic warming and cooling, respectively. In the most recent period of climatic warming, the region favorable for LBM outbreaks appears to have shifted to elevations beyond the upper limits of larch occurrence, thus explaining their cessation (Johnson et al., 2010).

Outside the greater Alpine region, other known natural stands of *Larix decidua* Mill. (larch) are restricted to the lowlands of south Poland and the Carpathian arc including the Slovakian Tatra Mountains (Matras and Pâques, 2008). While local foresters have reported LBM populations to exist in the Tatra (Baltensweiler et al., 1977; Büntgen et al., 2009), it is unclear whether extensive outbreaks have ever occurred sporadically or regularly in larch populations over the past decades to centuries. Dendroecological information about the historical occurrence of LBM mass outbreaks outside the European Alps could potentially shed light on climatic constraints to their frequency and severity, ultimately helping us to better understand the role of climatic changes in the cessation of these well synchronized mass outbreaks across the Alpine arc. Considering the ecological and climatic similarities between the Alps and the Tatra Mountains, the question arises, whether the pattern of recurring LBM outbreaks and associated effects on larch trees widely observed in the Alps, has also occurred in the Tatra Mountains.

Here, we analyze growth patterns in host larch and non-host pine ring width chronologies and detect the influence of temporally variable climate parameters on the growth of both tree species. Growth depressions, indicative of potential defoliation events, are identified in larch hosts and investigated for cyclic dynamics.

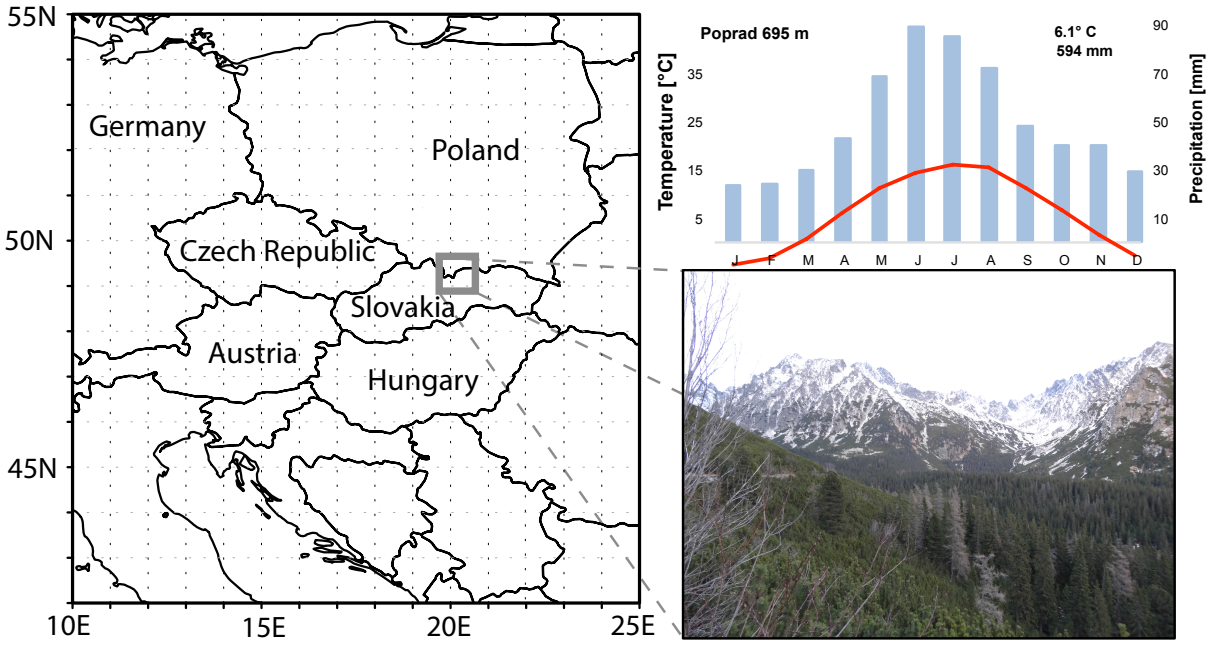

Figure 3-1 Sampling site. Left: Map of Eastern Europe, grey square indicates sampling area, upper right: climate data of nearby meteorological station Poprad, lower right: image of zoomed in sampling site at 1500 m asl.

3.2 Material and methods

We sampled 37 trees (99 cores: three/two cores per tree) from living larch trees at a locally dispersed mixed stand at ~1500 m asl in the Slovakian part of High Tatra Mountains (Fig. 3-1). These new measurements were combined with a previously developed dataset of 43 trees (64 cores: three/two cores per tree) from the same locality (Büntgen et al., 2013), resulting in a well-replicated composite for the period 1671-2012 (> 10 series in each year). Moreover, 62 *Pinus cembra* L. (pine) trees were sampled at the same location (155 cores: three/two cores per tree), spanning the period 1725-2012 (replication >10 series/year). All cores were absolutely cross-dated at annual resolution and well-known juvenile growth trends were removed using commonly applied detrending techniques: Spline (30 and 200 years) and negative exponential functions (NegExp) (Cook, 1985; Cook et al., 1995; Fritts, 1976) after implementation of power transformation (Cook and Peters, 1997), and variance stabilization over a 31-year moving windows (Büntgen et al., 2011; Esper et al., 2012; Frank et al., 2007;

Frank et al., 2010). The resulting chronologies were computed using a robust (biweight) mean, while the signal strength was estimated using 31-year moving intervals of interseries correlation (Rbar) and the Expressed Population Signal (EPS) (Wigley et al., 1984). Frequency-dependent consistency between the larch and pine chronologies was analyzed by high- (HP) and low-pass (LP) filtering the data.

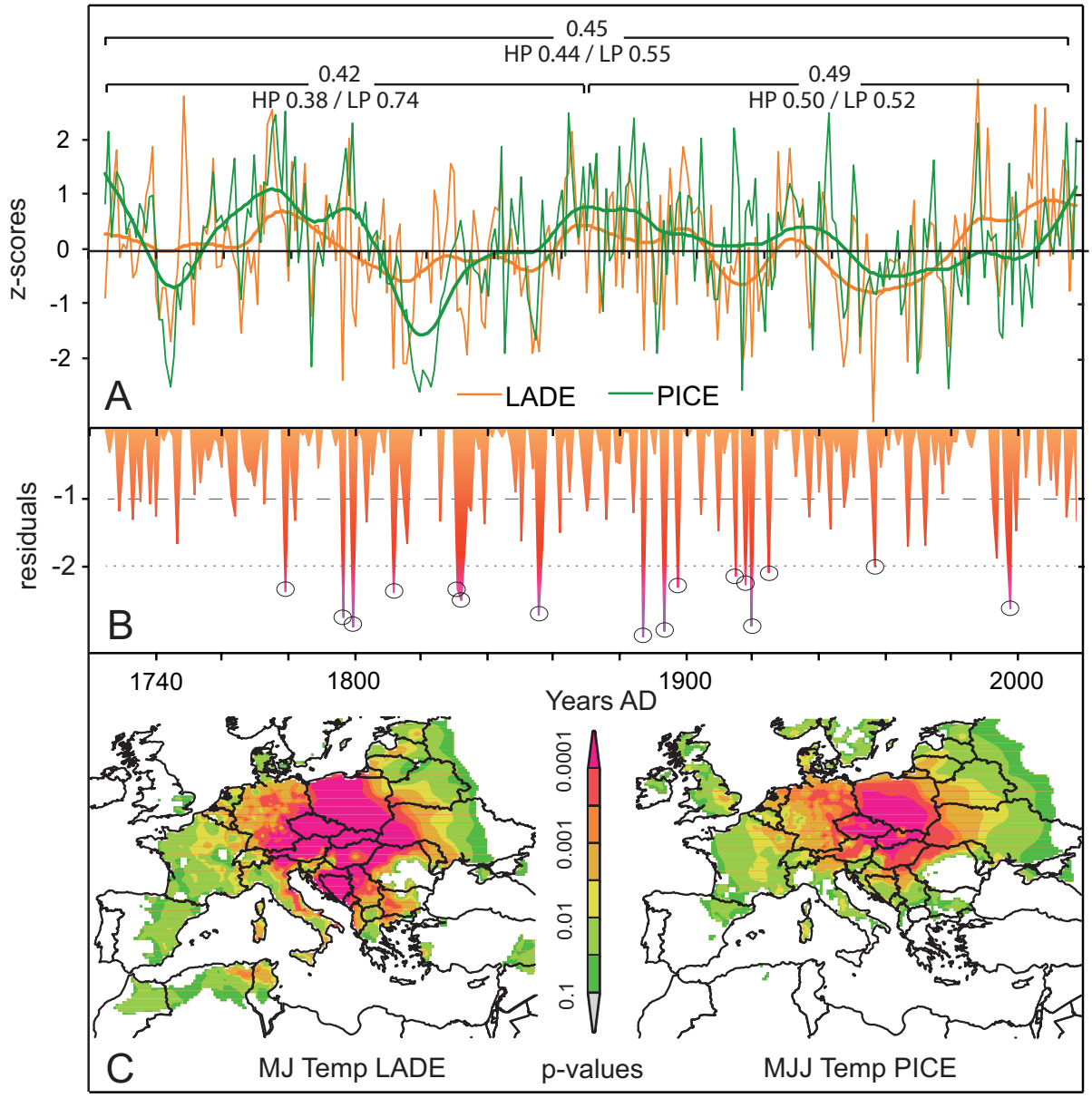

Figure 3-2 Growth coherency and climate sensitivity. (A) Larch (orange) and pine (green) chronologies (bold lines indicate 31yr smoothing splines) using a negative exponential detrending, (B) residuals between both species using 31yr spline detrending, circles denote results > double standard deviation, (C) Spatial field correlations of larch (C), pine (D) and best-fit seasonal temperatures. Maps are compiled using the KNMI Climate Explorer at http://climexp.knmi.nl.

Growth-climate relationships are reported as *Pearson* correlation coefficients (*r*) between the TRW chronologies and instrumental temperature measurements from a nearby (~25km) meteorological station (Poprad; 1951-2012), whereas gridded temperature indices (EOBS; 0.25°) were considered for spatial correlation trials (1950-2012). Species-specific chronology residuals were calculated to detect outbreak-induced growth depressions: Extreme years with negative residual-values exceeding double standard deviation (stdv) display years of high interspecies deviations. Among these extreme years only those were considered indicative of growth depressions caused by defoliation, if corresponding TRW values of the host chronology displayed negative deviations stronger than single stdv. Autocorrelation functions with varying time lags, wavelet analyses and power spectra were further applied to assess a possible cyclic behavior of these events.

3.3 Results

Species-specific coherency among all individual larch (host) and pine (non-host) TRW measurements series is distinct ($Rbar_{larch}$= 0.76 and $Rbar_{pine}$=0.71), and also temporally robust as expressed by running correlations and EPS values (Fig. 3-2 and 3-S1). The abiotic driver of the larch growth pattern can be attributed to early summer temperatures (Fig. 3-S3). Positive correlation coefficients between TRW_{larch} and May (M)/June (J) temperatures reveal a strong relationship, with the highest value detected for seasonal mean temperatures of MJ ($r=0.65$, $p<0.001$) for the 1951-2012 period. Coherently, the pine growth pattern is mainly linked to temperatures in the summer period, covering a longer seasonality, including May, June and July (J). The highest correlation value is found between TRW_{pine} and MJJ temperatures ($r=0.50$, $p<0.001$). Mapping correlations of seasonal temperatures with larch and pine data indicates a widespread association, covering large parts of Eastern Europe (Fig. 3-2).

Since both TRW datasets incorporate distinct temperature signals, a species-comparison of both reveals pronounced agreement in growth trends for the common period 1725-2012 ($r=0.45$), not only in the low- but also in the high-frequency domain ($r=0.55$ and 0.44) (Fig. 3-2). Following separation of the chronologies into two equivalent time periods of 144 consecutive years indicates temporal consistency of this association ($r_{1725-1868}$=0.42; $r_{1869-2012}$=0.49) again covering both, low- and high-frequency.

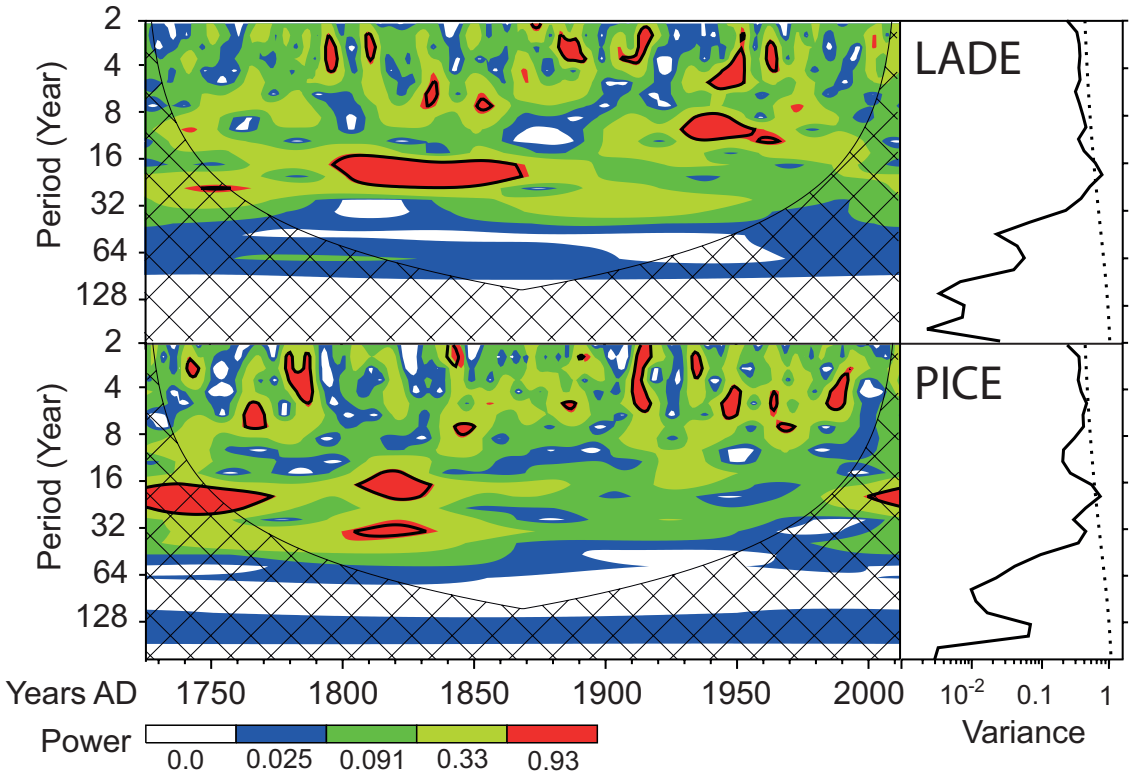

Figure 3-3 Wavelet power spectra of the host and non-host (larch and pine: upper and lower panels) chronologies. Black contour indicates 10% significance level, using a white-noise background spectrum and flexible spline detrended data. Corresponding global wavelet power spectra (black line) and significance levels (dashed line) are shown for both species on the right side.

Comparison of inter-annual differences between host and non-host TRW data in the high-frequency domain reveals conspicuous deviations in several years. Examination of residuals of the two chronologies indicates that data from 16 years deviate stronger than twice the standard deviation (stdv) (Fig. 3-2) and are listed in table 1. However, only 10 out of these 16 extreme deviations could possibly be caused by LBM outbreaks (Fig. 3-S2), and none of these 10 years coincide with reported LBM mass outbreaks in the greater Alpine Region (Esper et al., 2007).

The wavelet power spectrum exhibits no evidence of regular cyclic events (Fig. 3-3). Significant cyclicity with wavelengths of 16-32 years occurs only between 1800-1870, a period too short for robust interpretation. A similar result is detected when analyzing TRW_{pine}, which is as a non-host unaffected by LBM outbreaks. The autocorrelation function for TRW_{larch} over the 1725-2012 period reveals no significant autocorrelation in the 8-10 lag year range as expected should recurrent LBM outbreaks exist (Fig. 3-S4). Lag 9 displays large incoherencies, varying between $r_{1725\text{-}1800}$=0.20 and $r_{1801\text{-}1900}$=-0.34, whereas lag 8 shows negative connections, although evidence from the Alpine Region suggests the opposite (Esper

et al., 2007). In addition, autocorrelation functions of the non-host show similar patterns, thereby, supporting the absence of LBM induced cyclic growth depressions within the host data (Fig. 3-S4).

3.4 Discussion

Both larch (host) and pine (non-host) TRW datasets exceed commonly accepted criteria in terms of temporal robustness and interseries homogeneity. The growth of host and non-host trees is to a great extent controlled by MJ/MJJ temperatures, though TRW deviations exist in specific years. These deviations most likely arise from species-specific dissimilarities in physiological processes rather than from LBM outbreaks. The absence of regular growth depressions in host TRW indicates that if LBM populations in this region are cyclic, the amplitude of such cycles is not high enough to reach defoliating levels that affect tree growth.

Outbreaks of Zeiraphera sp. in the Tatra Mountains are known to have historically occurred on *Picea abies*, and have been reported for the periods 1924-1934, 1956-1959, 1965-1969 and 1977-1982 (Baltensweiler et al., 1977; Modrzyński, 2003). These outbreaks generally do not correspond with growth depressions detected here in larch TRW (s. table 1) and thus there is no evidence that these outbreak populations on spruce transgressed onto larch. Furthermore *Zeiraphera* spp. has also been observed on *Pinus cembra* in the Alps where these populations occasionally reach high levels though never as wide spread as outbreaks on larch (Dormont et al., 2006). Populations of *Zeiraphera* spp. feeding on different conifer genera appear to represent distinct gene-pools that occasionally hybridize (Emelianov et al., 2003).

Infrequent growth depressions were observed on larch trees in our data (s. table 3-1) and it is possible that they coincided with localized LBM outbreaks. However, there are other insects known from this area that are also capable of defoliating larch (eg. Lymantria monacha) and thus definitive conclusions about the specific causes of growth declines in observed larch cannot be drawn. In any case, it is certain that the pattern of recurrent LBM outbreaks, common in the Alps, has not historically occurred in our study region of the Tatras.

In the Alps, the majority of the LBM outbreak area is limited between 1500 and 2000 m asl, even though the range of larch extends from 500-2200 m asl (Baltensweiler and Rubli, 1999). By contrast in the Tatra, larch has a much more restricted distribution between 850 and 1500 m asl. The fact that hosts occur at lower elevations and thus warmer conditions than the dominant LBM outbreak zone in the Alps might explain the absence of recurrent LBM outbreaks in the Tatra.

In addition, spatially continuous larch forests with high densities typical of the LBM outbreak zone in the Alpine Arc rarely occur in the Tatra Mountains. Connectivity of large continuous areas of larch appear to play a role in the formation of LBM outbreaks in the Alps (Johnson et al., 2004). The lack of these large, continuous, pure larch forests in the Tatra may thus inhibit recurrent LBM population cycles prior to reaching mass outbreak levels.

Table 3-1 Potential defoliation events. Residuals: x denotes negative deviations between non-host and host TRW chronologies exceeding double standard deviation; TRW host: x denotes negative deviations of the host chronology exceeding single standard deviation

	1778	1795	1798	1810	1829	1830	1853	1884	1890	1894	1911	1914	1916	1921	1952	1992
Resi-duals	x	x	x	x	x	x	x	x	x	x	x	x	x	x	x	x
TRW (host)		x	x	x	x		x	x	x	x			x		x	

Larch as light-demanding species requires higher direct insolation in the vegetation period. The sampling site at 1500 m asl can be classified as subalpine where trees grow under treeline conditions. Highest monthly precipitation amounts in the Tatra coincide with the period of strongest growth-climate relationship of both species, but associated cloud cover hinders tree growth of larch to a greater extent than pine (Ellenberg, 2009; Hartl-Meier et al., 2014).

Our results refute the occurrence of regular LBM outbreaks and subsequent growth depressions in larch TRW series from the Slovakian Tatra Mountains. The robust chronology coherency and distinct MJ temperature signal is indicative of the potential utility of these high-elevation forest stands for the reconstruction of annually resolved and absolutely dated summer temperature variability over the previous centuries, in the absence of biological disruptions that may weaken similar approaches from the European Alps. The widespread representativeness covering almost all regions of Eastern Europe is particularly important considering the scarcity of historical data and reconstructions for this region.

3.5 Acknowledgements

Ulf Büntgen was supported by the Operational Programme of Education for Competetiveness of Ministry of Education, Youth and Sports of the Czech Republic (Project: Building up a multidisciplinary scientific team focused on drought, No. CZ.1.07/2.3.00/20.0248). Dr. Peter Fleischer from the State forests of TANAP kindly organized and contributed to fieldwork. We thank Marek Turcani for information about historical occurrence of insect outbreaks in the Tatra Mountains.

3.6 References

Baltensweiler, W., 1993a. A contribution to the explanation of the larch bud moth cycle, the polymorphic fitness hypothesis. Oecologia 93, 251-255.

Baltensweiler, W., 1993b. Why the larch bud-moth cycle collapsed in the subalpine larch-cembran pine forest in the year 1990 for the first time since 1850. Oecologia 94, 62-66.

Baltensweiler, W., Benz, G., Bovey, P., Delucchi, V., 1977. Dynamics Of Larch Bud Moth Populations. Annual Review of Entomology 22, 79-100.

Baltensweiler, W., Rubli, D., 1999. Dispersal: an important driving force of the cyclic population dynamics of the larch budmoth, Zeiraperadiniana Gn. Forest Snow and Landscape Research 74, 3-153.

Berryman, A.A., 1996. What causes population cycles of forest Lepidoptera? Trends in ecology & evolution 11, 28-32.

Bjornstad, O.N., Grenfell, B.T., 2001. Noisy clockwork: time series analysis of population fluctuations in animals. Science 293, 638-643.

Büntgen, U., Frank, D., Liebhold, A., Johnson, D., Carrer, M., Urbinati, C., Grabner, M., Nicolussi, K., Levanic, T., Esper, J., 2009. Three centuries of insect outbreaks across the European Alps. The New phytologist 182, 929-941.

Büntgen, U., Kyncl, T., Ginzler, C., Jacks, D.S., Esper, J., Tegel, W., Heussner, K.U., Kyncl, J., 2013. Filling the Eastern European gap in millennium-long temperature reconstructions. Proceedings of the National Academy of Science USA 110, 1773-1778.

Büntgen, U., Tegel, W., Nicolussi, K., McCormick, M., Frank, D., Trouet, V., Kaplan, J.O., Heussner, K.-U., Wanner, H., Luterbacher, J., Esper, J., 2011. 2500 Years of European Climate Variability and Human Susceptibility. Science 331, 578-582.

Cook, E.R., 1985. A Time Series Analysis Approach To Tree Ring Standardization. University of Arizona, p. 171.

Cook, E.R., Briffa, K.R., Meko, D.M., Graybill, D.A., Funkhouser, G., 1995. The 'segment length curse' in long tree-ring chronology development for palaeoclimatic studies. The Holocene 5, 229-237.

Cook, E.R., Peters, K., 1997. Calculating unbiased tree-ring indices for the study of climatic and environmental change. The Holocene 7, 361-370.

Dormont, L., Baltensweiler, W., Choquet, R., Roques, A., 2006. Larch- and pine-feeding host races of the larch bud moth (Zeiraphera diniana) have cyclic and synchronous population fluctuations. Oikos 115, 299-307.

Ellenberg, H., 2009. Vegetation ecology of Central Europe. Cambridge University Press, Cambridge.

Emelianov, I., Simpson, F., Narang, P., Mallet, J., 2003. Host choice promotes reproductive isolation between host races of the larch budmoth *Zeiraphera diniana*. Journal of Evolutionary Biology 16, 208-218.

Esper, J., Buntgen, U., Frank, D.C., Nievergelt, D., Liebhold, A., 2007. 1200 years of regular outbreaks in alpine insects. Proceedings. Biological sciences / The Royal Society 274, 671-679.

Esper, J., Frank, D.C., Timonen, M., Zorita, E., Wilson, R.J.S., Luterbacher, J., Holzkämper, S., Fischer, N., Wagner, S., Nievergelt, D., Verstege, A., Büntgen, U., 2012. Orbital Forcing of Tree-Ring Data. Nature Climate Change 2, 862-866.

Frank, D., Esper, J., Cook, E.R., 2007. Adjustment for proxy number and coherence in a large-scale temperature reconstruction. Geophys Res Lett 34, n/a-n/a.

Frank, D.C., Esper, J., Raible, C.C., Buntgen, U., Trouet, V., Stocker, B., Joos, F., 2010. Ensemble reconstruction constraints on the global carbon cycle sensitivity to climate. Nature 463, 527-530.

Fritts, H.C., 1976. Tree Rings and Climate. Academic Press, London.

Hartl-Meier, C., Dittmar, C., Zang, C., Rothe, A., 2014. Mountain forest growth response to climate change in the Northern Limestone Alps. Trees 28, 819-829.

Ims, R.A., Henden, J.A., Killengreen, S.T., 2008. Collapsing population cycles. Trends in ecology & evolution 23, 79-86.

Johnson, D.M., Bjornstad, O.N., Liebhold, A.M., 2004. Landscape geometry and traveling waves in the larch budmoth. Ecology Letters 7, 967-974.

Johnson, D.M., Büntgen, U., Frank, D.C., Kausrud, K., Haynes, K.J., Liebhold, A.M., Esper, J., Stenseth, N.C., 2010. Climatic warming disrupts recurrent Alpine insect outbreaks. P Natl Acad Sci USA 107, 20576-20581.

Matras, J., Pâques, L., 2008. EUFORGEN Technical Guidelines for genetic conservation and use for European Larch (Larix decidua). Bioversity International, 6.

Modrzyński, J., 2003. Defoliation of older Norway spruce (Picea abies /L./ Karst.) stands in the Polish Sudety and Carpathian mountains. Forest Ecology and Management 181, 289-299.

Rolland, C., Baltensweiler, W., Petitcolas, V., 2001. The potential for using Larix decidua ring widths in reconstructions of larch budmoth (Zeiraphera diniana) outbreak history: dendrochronological estimates compared with insect surveys. Trees 15, 414-424.

Weber, U.M., 1997. Dendroecological reconstruction and interpretation of larch budmoth (Zeiraphera diniana) outbreaks in two central alpine valleys of Switzerland from 1470 - 1990. Trees 11, 277-290.

Wigley, T.M.L., Briffa, K.R., Jones, P.D., 1984. On the Average Value of Correlated Time Series, with Applications in Dendroclimatology and Hydrometeorology. Journal of Climate and Applied Meteorology 23, 201-213.

3.7 Appendix: supplementary figures

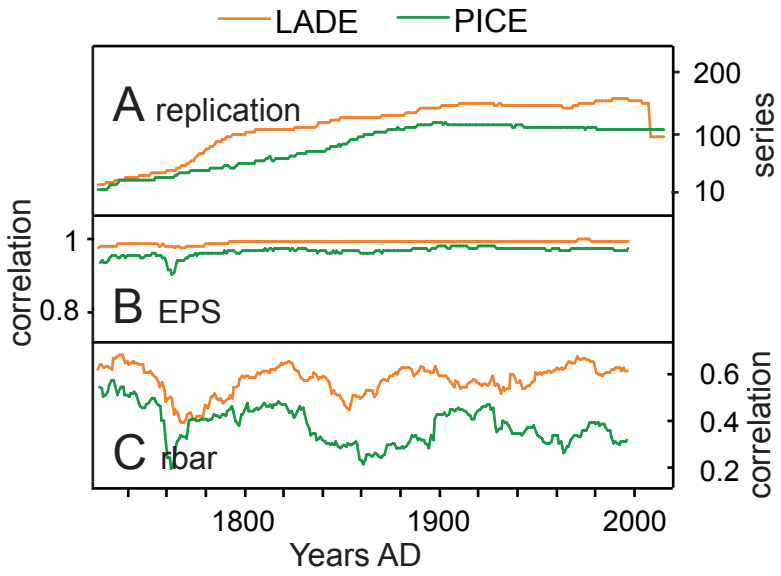

Figure 3-S1 Chronology properties. (A) Replication, (B) expressed population signal (EPS), (C) 31-year running correlation of larch and pine data; host data (larch) in orange and non-host data (pine) in green.

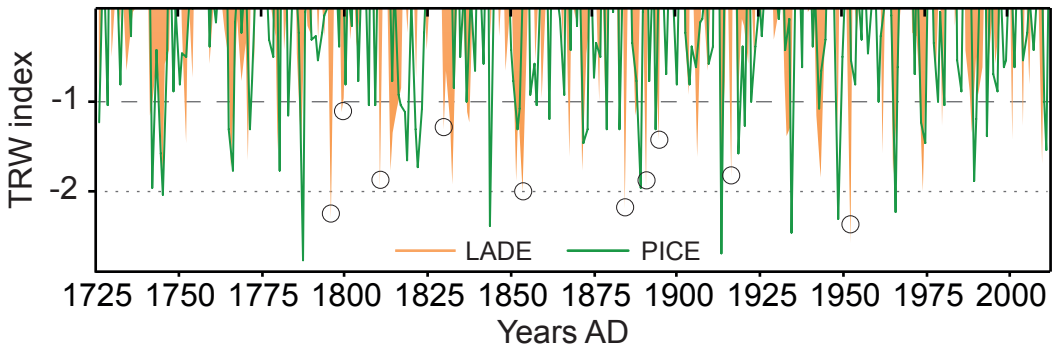

Figure 3-S2 Species-specific growth depressions. Negative values of host data (larch) in filled orange areas and non-host data (pine) in green lines; circles indicate negative outliers > standard deviation only with corresponding years of residuals > double standard deviation (Fig. 1).

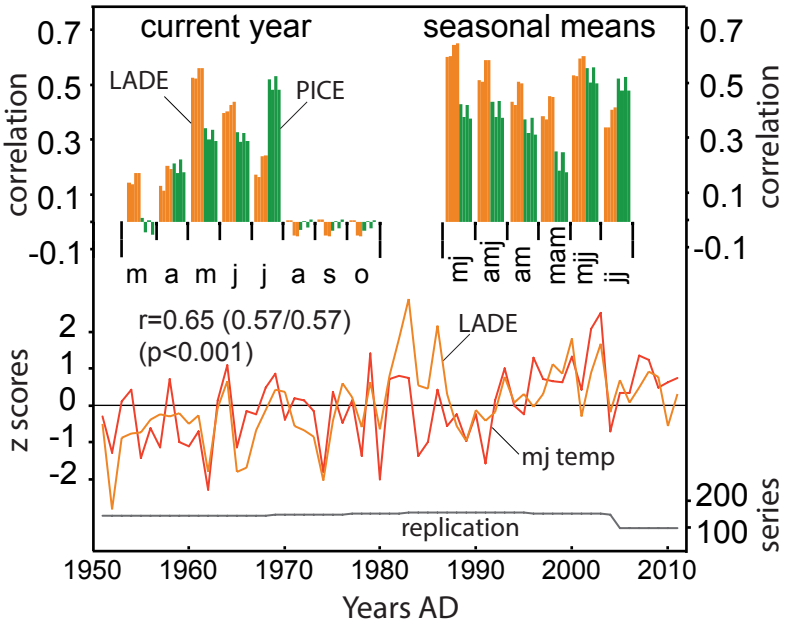

Figure 3-S3 Temperature-growth coherences. Upper panel: calibration of host (larch) and non-host (pine) data against temperature data from the Poprad meteorological station expressed as monthly and seasonal correlations; each bar contains four vertical lines representing four different detrending options of tree-ring data. Lower panel: Best-fit target data (MJ temperatures) and host chronology spanning the period from 1951-2011, including replication (grey line): correlation values in brackets indicate a split calibration period approach. Due to autocorrelation inherent to the data the degrees of freedom were consecutively reduced to mirror realistic significance levels (Büntgen et al. 2011; Esper et al. 2012; Frank et al. 2010).

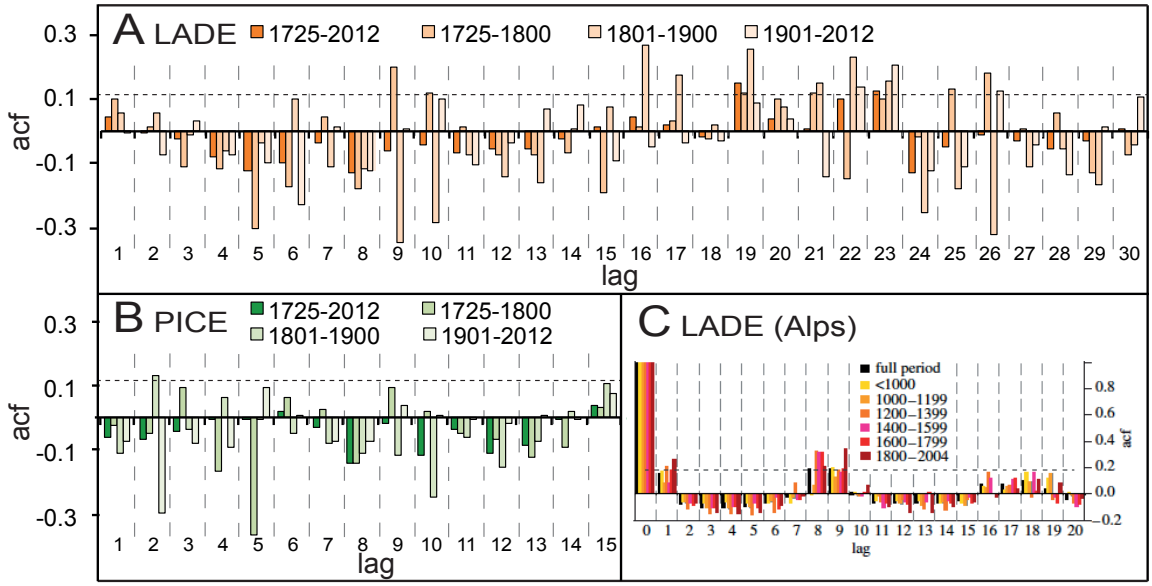

Figure 3-S4 Autocorrelation function (acf). (A) Acf for host (larch), (B) acf for non-host (pine); (C) acf for LBM affected host trees from the Alpine Arc (Esper et al. 2007).

4. Climate sensitivity and parameter coherency in annually resolved $\delta^{13}C$ and $\delta^{18}O$ from *Pinus uncinata* tree-ring data in the Spanish Pyrenees

Oliver Konter[a], Steffen Holzkämper[a,b], Gerhard Helle[c], Ulf Büntgen[d], Matthias Saurer[e], Jan Esper[a]

[a] *Department of Geography, Johannes Gutenberg University, Becherweg 21, 55099 Mainz, Germany*

[b] *Department of Physical Geography and Quaternary Geology, Stockholm University, 10691 Stockholm, Sweden*

[c] *German Centre for Geosciences- GFZ, Section 5.2 Climate Dynamics and Landscape Evolution, Potsdam, Germany*

[d] *Swiss Federal Research Institute for Forest Snow and Landscape (WSL), 8903 Birmensdorf, Switzerland*

[e] *Paul Scherrer Institut, Villigen PSI, Switzerland*

published in Chemical Geology 377, 2014

4.1 Introduction

The influence of temperature on the formation of tree-ring width (TRW) and maximum latewood density (MXD) is well known towards altitudinal and latitudinal treelines, where annually resolved measurements from living trees and relict material allow millennium-long reconstructions to be developed (Büntgen et al., 2011, 2008; Esper et al., 2012). Dendroclimatological studies in the European Mediterranean region reveal temperature-induced growth variations at high-elevation treeline sites (Camarero et al., 1998; Gutiérrez, 1991; Tardif et al., 2003), with MXD generally providing more reliable results in comparison to a reduced sensitivity in TRW (Büntgen et al., 2012, 2010, 2008).

Stable isotope ratios preserved in xylem cells contain information on past environmental conditions and became an important proxy in palaeoclimate studies (Helle and Schleser, 2004; Planells et al., 2009; Schollän et al., 2013a; Treydte et al., 2007). However, the climate-isotope relationships for trees growing in high elevation Mediterranean environments are much less explored than in the European Alps, arid regions in the US, or sites in the northern high latitudes, for example (Heinrich et al., 2013; McCarrol and Loader, 2004). The $^{13}C/^{12}C$ ratio of pine trees from different sites in the Spanish Pyrenees revealed positive correlations with June-October temperatures and negative correlations with June-July precipitation (Andreu et al., 2008; Dorado-Liñan et al., 2011b), but the associations are relatively weak compared to evidence from other regions (Dorado-Liñan et al., 2011a).

Dorado-Liñan et al. (2011a) also demonstrated that calibration studies based on pooled isotope time series (that is the combination of wood samples before isotopic analysis) may be biased by non-climatic low-frequency trends. Other work revealed such limitations to be particularly significant, if the number of pooled trees is <5 (Konter et al., 2013).

We here address these issues, and present 20th century, annually resolved, time series of individually measured $\delta^{13}C$ and $\delta^{18}O$ from five *Pinus uncinata* trees from high elevation environments in the Spanish Pyrenees. The measurement series are used to explore the coherency among trees, and to assess their common climatic signal. $\delta^{13}C$ and $\delta^{18}O$ climate signals are evaluated using instrumental temperature, precipitation and drought data to achieve a deeper understanding of the drivers of tree's isotope fractionation in high elevation environments. Larger scale spatial patterns of climate as well as the effects of $\delta^{13}C$ correction procedures are assessed to evaluate the utilization of tree-ring stable isotope data for reconstruction purposes.

4.2 Material and methods

4.2.1 Study site and sample design

The sampling site is situated at ~2400 m asl near Lake Gerber at the northern border of the 'D'Aigüestortes Estany de Sant Maurici National Park' in the Spanish central Pyrenees, west of Andorra (Fig. 4-1). The prevailing tree species is *Pinus uncinata*, which aggregates as a shade-intolerant conifer in an open forest ecotone (Camarero et al., 1998). Tree heights vary between 3 and 6 m, and stem circumference at breast height ranges from 0.80-3.38 m. The poorly developed soils accumulate in shallow basins and can be identified as skeletal leptosols with no access to ground water (Esper et al., 2010). Between-tree distances vary from 2-12 m and the canopy is sparse (about 10%). Annual mean temperature fluctuates around ~4°C, with maxima in July (~13°C) and minima in January (~-3°C) (Büntgen et al., 2008). Monthly precipitation totals (mean annual sum at ~1200 mm) are highest in May (12 %) and lowest in July (~6 %). Since soils are poorly developed at the sampling site, only a small amount of snowmelt is stored in reservoirs accessible to the trees.

A total of 23 *Pinus uncinata* trees, growing under similar ecological and climatological conditions, were sampled for initial TRW measurements. Four cores per tree were extracted in a radial configuration at breast height, two parallel and two perpendicular to the slope.

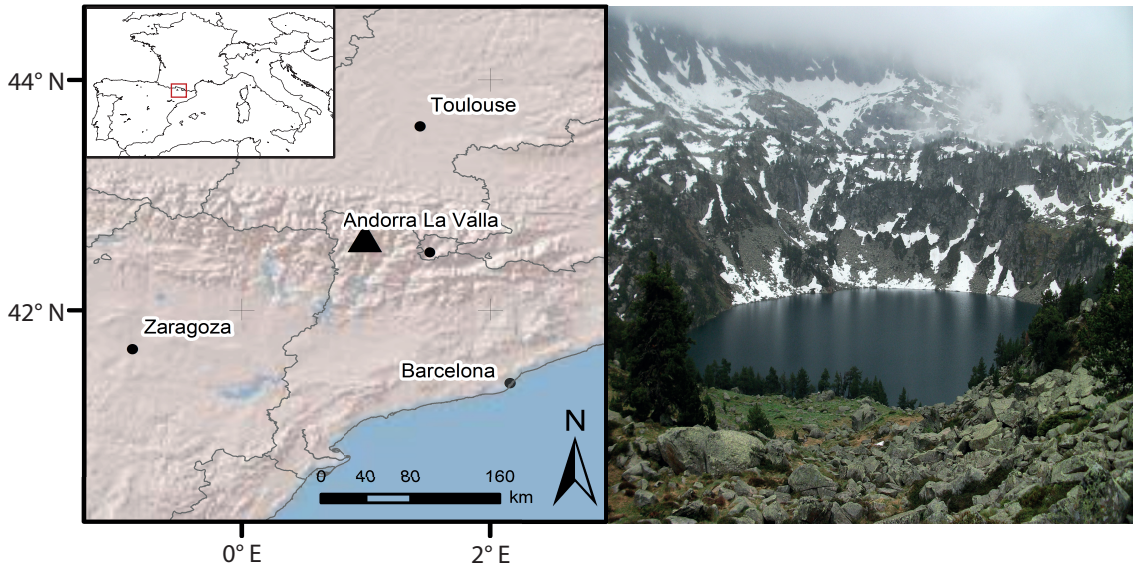

Figure 4-1 *Pinus uncinata* study site at lake Gerber (right) located in the Spanish Pyrenees (left, triangle).

4.2.2 Stable isotope ratio measurements

For stable isotope measurements, a subset of five trees was selected and each tree-ring from 1901-2009 dissected using a scalpel (Leavitt and Long, 1984). Two cores per tree were used and combined to develop five annually resolved wholewood time series spanning the 1901-2009 period. The α-cellulose was extracted from the wholewood samples following procedures detailed in Wieloch et al. (2011). The α-cellulose samples were homogenized using an ultrasonic device (Laumer et al. 2009), freeze dried prior to analyzing (1) $^{13}C/^{12}C$ ratios using an IsoPrime Isotope Ratio Mass Spectrometer (IRMS) with an interfaced elemental analyzer, and (2) $^{18}O/^{16}O$ ratios using a TC/EA pyrolysis furnace (Thermo Finnigan) coupled online to a Delta V Advantage IRMS. Both devices were operated in continuous flow mode, allowing combusting (carbon) or pyrolizing (oxygen), purifying and transporting the sample on a continuous carrier gas flow at the GFZ in Potsdam. The isotope ratios are expressed in the conventional δ notation and in parts per thousand (‰), relative to the VPDB (Vienna Pee Dee Belemnite) standard for carbon ($\delta^{13}C$) and the VSMOW (Vienna Standard Mean Ocean Water) standard for oxygen ($\delta^{18}O$) (Craig 1957). Sample replication resulted in a reproducibility of ±0.1‰ for $\delta^{13}C$ and ±0.25‰ for $\delta^{18}O$.

4.2.3 Time series analyses and corrections

All tree-rings were crossdated and assigned to calendar years, starting with the most recent, fully developed increment in 2009 (trees were sampled in summer 2010). TRW was measured with an accuracy of 0.01 mm using a LinTab measurement device and TSAP software (Rinn, 2007). TRW crossdating was verified using COFECHA (Holmes, 1983), and different detrending methods (Regional Curve Standardization RCS, 100-year spline) applied using the ARSTAN program (Cook et al., 1985; Esper et al., 2003).

4.2.3.1 Tree-ring carbon isotopes

Photosynthetic discrimination of $^{13}CO_2$ against $^{12}CO_2$ is related to the ratio of leaf internal to external CO_2 partial pressure (C_i/C_a), jointly controlled by the stomatal conductance and rate of CO_2 assimilation (Farquhar et al. 1982). Since changes in the atmospheric carbon isotopic source signal are reflected in the tree-ring cellulose, these trends need to be removed in climate studies (Farquhar et al., 1982; Treydte et al., 2009). Accordingly, all tree-ring $\delta^{13}C$ values were corrected to account for the depletion of ^{13}C in the atmosphere's CO_2, due to the burning of fossil fuels and deforestation since ~ AD 1850, and resulting values termed $\delta^{13}C_{atm}$.

Exposure to increasing atmospheric CO_2 also leads to changes in internal CO_2 concentrations of the needles, resulting in adaptations of stomatal conductance, water-use-efficiency, and photosynthetic assimilation rate (Farquhar et al., 1982). These processes require consideration before assessing climate-isotope relationships (McCarroll et al., 2009; Schubert and Jahren, 2012, Treydte et al., 2009), and are here corrected considering fixed amounts of isotope fractionation per unit CO_2 increase, following procedures detailed by Feng and Epstein (1995) based on oak tree greenhouse studies, and Kürschner (1996) based on juniper, pine and oak studies in SW-USA and Egypt. Application of the Feng and Epstein (1995) correction alters the $\delta^{13}C_{atm}$ time series by a factor of 0.02‰ per ppm CO_2 change (resulting time series termed $\delta^{13}C_{FE}$), which is quite sizeable compared to the Kürschner (1996) correction of 0.0073/ppm CO_2 (hereafter $\delta^{13}C_K$). These corrections, however, nicely match the envelop of CO_2-effects in C3-plants for CO_2 concentrations from 280-400 ppm detailed Schubert and Jahren (2012). The so-called pin-correction (McCarroll et al., 2009) was applied, but did not significantly modify the data (because of a slight upward trend in the $\delta^{13}C_{atm}$ data) and therefore is not discussed further. We high- and low-pass filtered the $\delta^{13}C_{atm}$, $\delta^{13}C_K$, and $\delta^{13}C_{FE}$ time series using 20-year cubic smoothing splines for the assessment of coherence among tree-ring parameters.

4.2.4 Meteorological data and climate signal detection

All tree-ring time series, TRW, $\delta^{18}O$, $\delta^{13}C_{atm}$, $\delta^{13}C_K$, and $\delta^{13}C_{FE}$, were correlated against monthly temperature, precipitation, and Palmer Drought Severity Index (PDSI) data. We used temperature readings from the *Pic du Midi* mountain observatory (2,862 m, 43°04'N, 0°09'E), gridded precipitation totals from the Climate Research Unit (TS 3.1; Mitchell and Jones, 2005), and gridded PDSI data from the University Corporation for Atmospheric Research (Dai et al., 2004). In addition to this widely applied drought index, we also considered a self-calibrated PDSI dataset (scPDSI), which according to van der Schrier et al. (2006) provides a more realistic estimation of the occurrence of extremes at a higher spatial resolution. When computing correlation coefficients between proxy and instrumental target data, we adjusted the degrees of freedom considering the varying autocorrelations inherent to the time series using:

$$DF = N \Big/ \frac{1+a1*a2}{1-a1*a2}$$

with N representing the number of values (time series length), a1 the autocorrelation of series 1 (proxy data) at lag 1, and a2 the autocorrelation of series 2 (target data) at lag 1.

4.3 Results

4.3.1 Carbon isotope ratios

The $\delta^{13}C_{raw}$ measurement series include an offset of 2.24‰ (mean values range from -24.02‰ to -21.78‰) and display a decreasing trend over the 20th century visible in all five samples (Fig. 4-2). This decline is related to the non-climatic $\delta^{13}C$ trend in atmospheric CO_2 and removed in the $\delta^{13}C_{atm}$ data (Fig. 4-3). The $\delta^{13}C_K$ and $\delta^{13}C_{FE}$ chronologies, considering additional effects of the increasing CO_2 concentration on the tree's metabolism, show overall increasing trends towards present. The strongest such trend is retained in the $\delta^{13}C_{FE}$ data as a result of potentially severe influences on the carbon isotope fractionation during photosynthetic uptake.

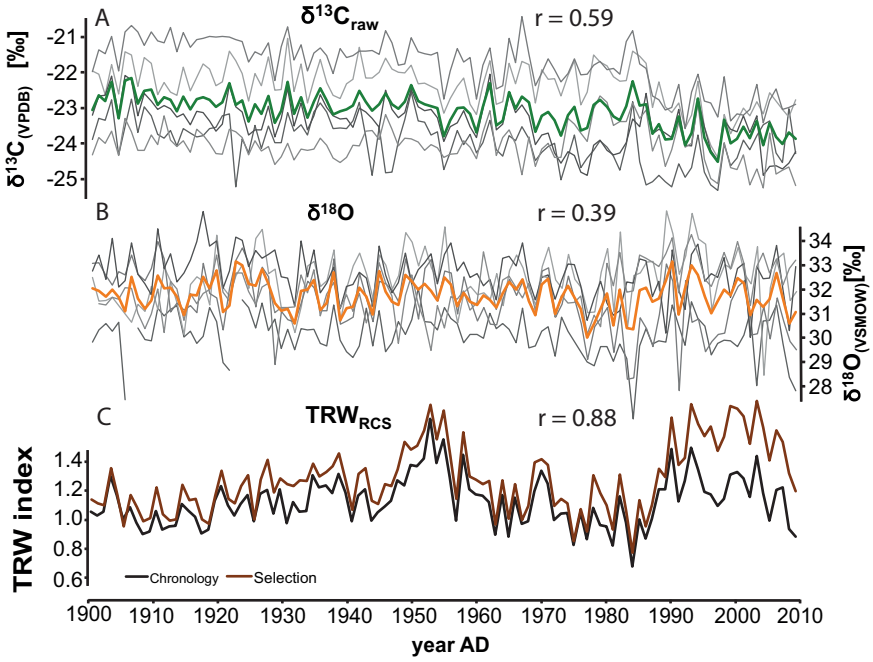

Figure 4-2 Stable isotope and ring width data. (A) Uncorrected $\delta^{13}C_{raw}$ measurement series (grey) and their mean (green). (B) $\delta^{18}O$ measurement series (grey) and mean (orange), and (C) detrended TRW_{RCS} chronology (black) and selection for isotopic measurements (brown). r-values are the interseries correlations.

The estimation of climate signals considers all three $\delta^{13}C$ datasets ($\delta^{13}C_{atm}$, $\delta^{13}C_K$ and $\delta^{13}C_{FE}$), thereby emphasizing potential differences due to the correction procedures (Fig. 4-4). $\delta^{13}C$ climatic signals are most distinct during the summer season, with the June-August season (JJA) displaying the highest positive correlation ($p<0.001$) for temperature, and negative correlation for precipitation. The maximum seasonal response to drought varies from July-September (JAS) for PDSI, to August-September (AS) for scPDSI. The differences between

these various seasons appear rather small, and can perhaps be summarized as a broader summer season signal. Highest correlations are found between summer temperature and $\delta^{13}C_{FE}$ (r=0.57), followed by $\delta^{13}C_K$ (r=0.50) and $\delta^{13}C_{atm}$ (r=0.39). While the same order from stronger to weaker correlations ($\delta^{13}C_{FE}>\delta^{13}C_K>\delta^{13}C_{atm}$) is obtained when calibrating against PDSI, this pattern changes when calibrating against summer precipitation: $\delta^{13}C_{atm}$ (r=-0.50), followed by $\delta^{13}C_K$ (r=-0.45) and $\delta^{13}C_{FE}$ (r=-0.34).

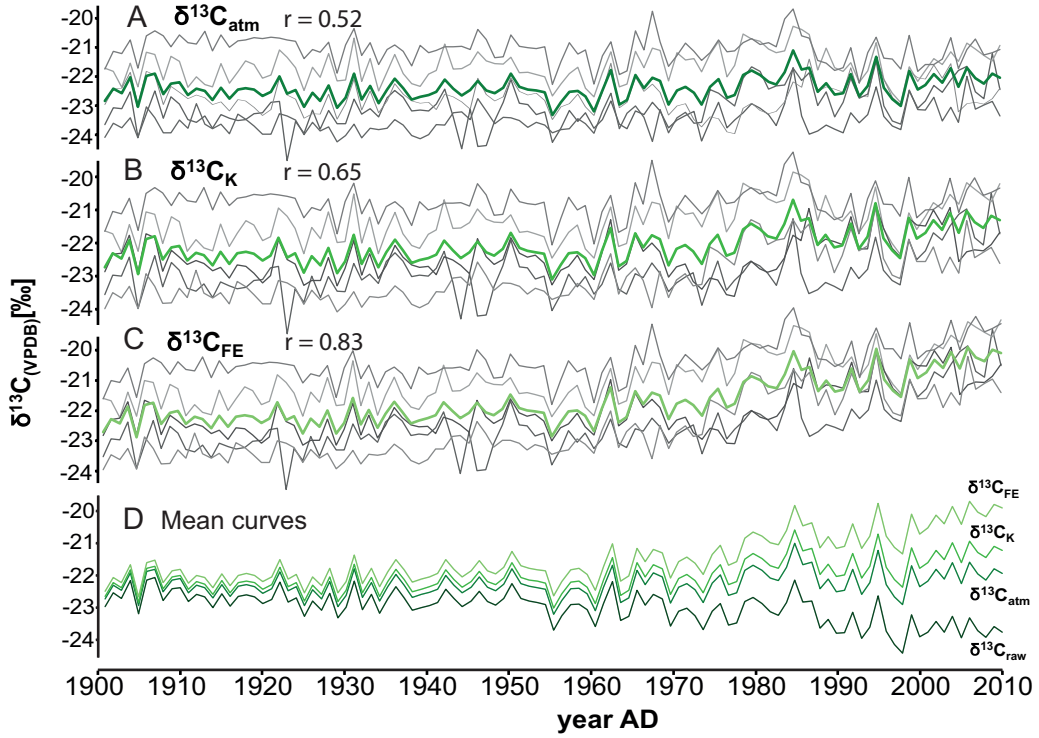

Figure 4-3 Carbon isotope corrections. Single $\delta^{13}C$ time series (grey) and their means (green) after correction for decreasing values due to fossil fuel burning (A: $\delta^{13}C_{raw}$), additional correction following Kürschner (1996) (B: $\delta^{13}C_K$), and Feng & Epstein (1999) (C: $\delta^{13}C_{FE}$). (D) shows the mean curves of all carbon isotopic ratios.

These results are supported by the southern European correlation fields indicating close associations with the western Mediterranean coastal areas, from Italy to France, Spain and Northern Africa, during the summer months. Calibration against previous year instrumental data revealed more heterogeneous and less strong correlations. Previous year precipitation correlates significantly only during September with $\delta^{13}C_{atm}$ and $\delta^{13}C_K$. Previous year temperature, scPDSI and particularly PDSI, all show significant correlations during various months and seasons (Fig. 4-4), thereby indicating possibly associated autocorrelation and low-frequency trends inherent to the data, presumably caused by storage of assimilates during the winter seasons and incorporation into subsequent rings.

The correlations with target climate data increase when shortening the calibration period (starting at 1941, Fig. 4-6), a feature related the sparser and less reliable early 20th century meteorological network (Wijngaard et al., 2003). We here focus on the relationship with temperature and precipitation, since the incorporation of soil moisture in the drought indices leads to high autocorrelations, causing severe reductions of degrees of freedom. Highest correlation is found between temperature and $\delta^{13}C_{FE}$ (r=0.63), since both time series include similar low-frequency variations ($\delta^{13}C_{FE}>\delta^{13}C_K>\delta^{13}C_{atm}$). Although both the proxy and instrumental time series include fairly high autocorrelations (0.38 in temperature and 0.75 in $\delta^{13}C_{FE}$, at lag-1), the values remain significant ($p<0.001$) after reduction of the degrees of freedom for serial correlation effects. The absence of low-frequency trends in $\delta^{13}C_{atm}$ leads to lower but still significant values ($p<0.01$) when correlated with temperature. In contrast, since the precipitation data are effectively free of low-frequency trends (lag-1 autocorrelation is 0.09), $\delta^{13}C_{atm}$ shows the strongest coherence (r=-0.64, $p<0.001$).

4.3.2 Oxygen isotope ratios

The $\delta^{18}O$ mean values of the individual time series range by 2.52‰, from 30.12‰ to 32.65‰, which is even exceeding the offset recorded in $\delta^{13}C_{raw}$. Also the variance is higher (sd=0.65 compared sd=0.39) indicating the influence of fluctuating source water isotopic compositions together with fractionation processes at the leaf level.

The season of strongest response to temperature and precipitation is shifted towards spring (Fig. 4-4), a finding deviating from the commonly reported JJA signal in European tree sites (Saurer et al., 2008; Treydte et al., 2007). Particularly the climatic conditions in May appear influential, reaching r=0.33 for temperature and r=-0.24 for precipitation. The season from January to June displays the strongest negative correlation with precipitation (r=-0.39). Except for the earliest months of the year, the association between $\delta^{18}O$ and climate is generally weaker compared to $\delta^{13}C$, a finding supported by the spatial correlation patterns over the Mediterranean area (Fig. 4-5).

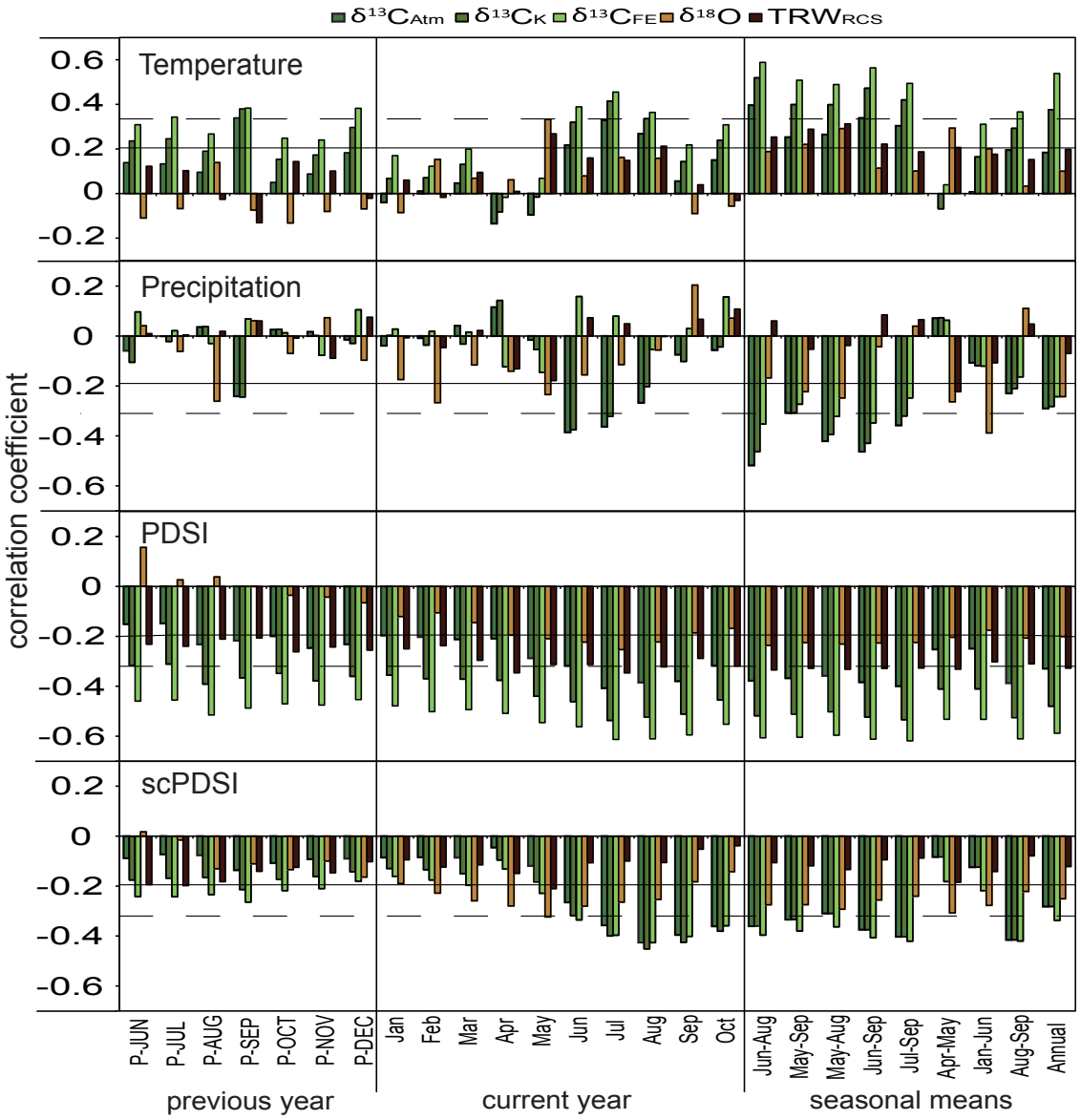

Figure 4-4 Climate-isotope relationships of $\delta^{13}C$ (green: $\delta^{13}C_{atm}$, $\delta^{13}C_{CK}$, $\delta^{13}C_{FE}$), $\delta^{18}O$ (orange) and TRW_{RCS} chronologies (black) with instrumental temperature, precipitation, PDSI, scPDSI data. Correlations are computed over the period 1901-2009 (except scPDSI: 1901-2004) considering previous year June to December (left), current year January to October (middle), and current year seasonal means (right). Horizontal black lines indicate 95% significance levels and dashed lines 99.9% significance levels. Significance levels are calculated without consideration of reductions of degrees of freedom.

The reduced calibration period 1941-2009 (Fig. 3-6) exhibits a strengthened correlation with temperature ($r=0.43$, $p<0.001$), only slightly larger than the relationship with precipitation ($r=-0.35$, $p<0.01$). Autocorrelation is overall lower (0.21 at lag-1) compared to the $\delta^{13}C$ data, and it is clearly evident that high temperature and low precipitation result in increased $\delta^{18}O$ values. A spring-summer drought signal is recorded in both the monthly correlations (Fig. 4-4) and spatial fields (Fig. 4-5).

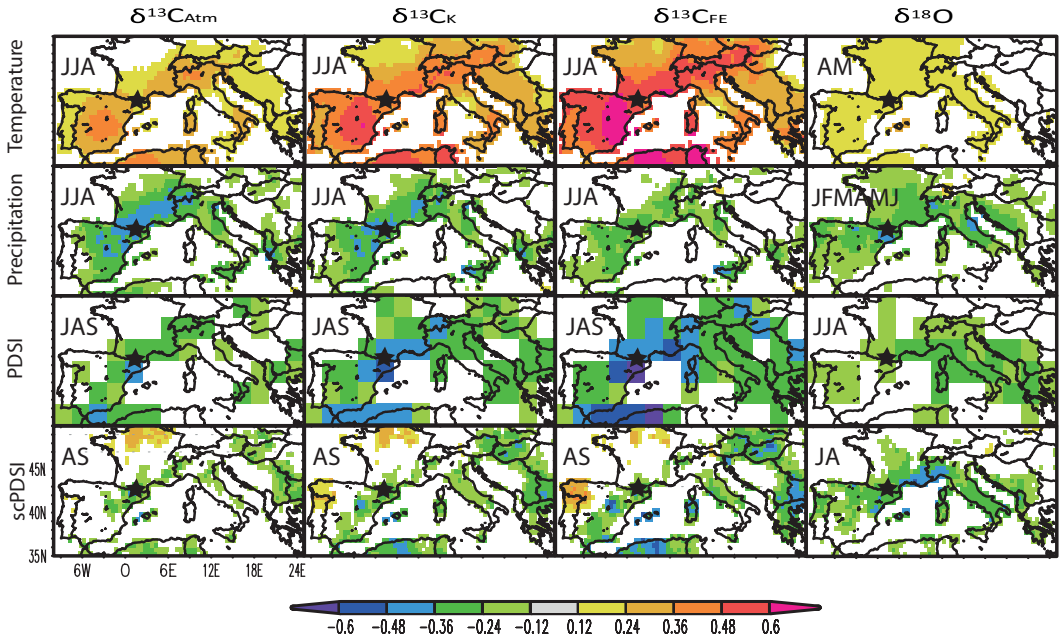

Figure 4-5 Spatial field correlations between $\delta^{13}C$ and $\delta^{18}O$ chronologies and best-fit climate variables. Columns from left to right: $\delta^{13}C_{atm}$, $\delta^{13}C_K$, $\delta^{13}C_{FE}$, $\delta^{18}O$. Rows: CRUTEM 3 temperature, CRU TS 3.1 precipitation, PDSI, and scPDSI. Maps are computed using the KNMI climate explorer at http://climexp.knmi.nl. Colored areas are significant at $p<0.10$. The sampling site is marked with a black star.

4.4 Discussion

4.4.1 Carbon isotope ratios

Comparison with regional instrumental data revealed that all investigated climate parameters display higher coherences with $\delta^{13}C$ than with TRW (e.g. Büntgen et al., 2008; Dorado-Liñán et al., 2011b). These results were achieved, even though the Expressed Population Signal (EPS; Wigley et al., 1984; see Fig. 4-S1) is higher and more stable in TRW than in the isotope datasets. The main climate signal reflected in the TRW can be attributed to water availability, here expressed as PDSI (r=0.34, 1901-2009 period).

The positive correlation with summer temperature and negative correlation with precipitation revealed for $\delta^{13}C$ support previous findings based on fewer data and other species (Andreu et al., 2008; Dorado-Liñan et al., 2011b; Saurer et al., 2008; Treydte et al., 2007), and theoretical background (Helle and Schleser, 2004; Schollän et al., 2013b). The timing of cell formation is influenced by several intrinsic factors including gene expression (Schrader et al., 2004) and hormonal signals (Schrader et al., 2003), as well as environmental factors. While in the Mediterranean area cambial activity is temporally less constrained and frequently even characterized "double-stress" during summer and winter (Cherubini et al., 2003), xylem formation in our high elevation site takes place during the warm and snow-free season

including all summer months. Although greenhouse studies indicated negative temperature coefficients (Schleser et al., 1999), the higher temperatures recorded in natural environments result in positive correlations. Particularly in the Mediterranean, high temperatures are usually accompanied with high vapor-pressure deficits, and the resulting stomatal closure therefore leads to an enrichment of ^{13}C and increasing $\delta^{13}C$ (Linares et al., 2009). In contrast, precipitation events lead to reduced water vapor pressure deficits between the needles and ambient air, enabling trees to open their stomata more widely. The lower temperatures, typically accompanying summer season rain events, result in additionally reduced CO_2 assimilation rates.

As a consequence, increased leaf-internal CO_2 concentrations and depleted ^{13}C of assimilates drive the significant negative correlations between tree-ring $\delta^{13}C$ and moisture conditions during boreal summer. As summer temperature and precipitation are anti-correlated, both elements show a strong and distinct coherence with $\delta^{13}C$, though separation of these two factors remains challenging (Edwards et al., 2000; Schleser et al., 1999). This dilemma might best be compensated by considering the drought indices, PDSI and scPDSI, integrating temperature and precipitation (and soil water capacity).

To account for the Suess effect, McCarrol and Loader (2004) proposed a simple correction method, using the residuals of annually resolved $\delta^{13}C$ values of CO_2, and applying these differences to the tree-ring $\delta^{13}C_{raw}$ data (Fig. 4-3). As a consequence, the interseries correlation of the corrected $\delta^{13}C_{atm}$ data drops from r=0.59 to r=0.52, due to the removal of the common, decreasing low-frequency trend in the single measurement series. The correction procedures accounting for increasing atmospheric CO_2 concentrations ($\delta^{13}C_K$ and $\delta^{13}C_{FE}$) add additional low-frequency trend to the data, and, consequently, between-tree correlation values increase from r=0.65 for $\delta^{13}C_K$ to r=0.83 for $\delta^{13}C_{FE}$.

To date the procedure of correcting trends in tree-ring δ^{13} is a matter of debate within the isotope community, and there is no consensus on which of the methods reflect the fractionation processes within trees most effectively (Saurer et al., 2008; Schubert and Jahren, 2012; Treydte et al., 2007, 2001). Our results show that the varying low-frequency trends added to the data not only alter the interseries correlation among trees, but also affect the correlations between carbon isotope records and climate variables. The derived correlation patterns ($\delta^{13}C_{FE}>\delta^{13}C_K>\delta^{13}C_{atm}$) suggest a relatively strong CO_2 effect on trees growing high elevation sites in the Spanish Pyrenees.

The varying correction procedures are also reflected in changing lag-1 autocorrelations, increasing from 0.27 in $\delta^{13}C_{atm}$ to 0.49 in $\delta^{13}C_K$ and 0.76 in $\delta^{13}C_{FE}$, and in line with the 20th century temperature trend recorded in the study region (Fig. 4-6). The seemingly negative effects of increased autocorrelations on the degrees of freedom, when associating proxy with temperature data, make a clear distinction of the most appropriate correction procedure challenging.

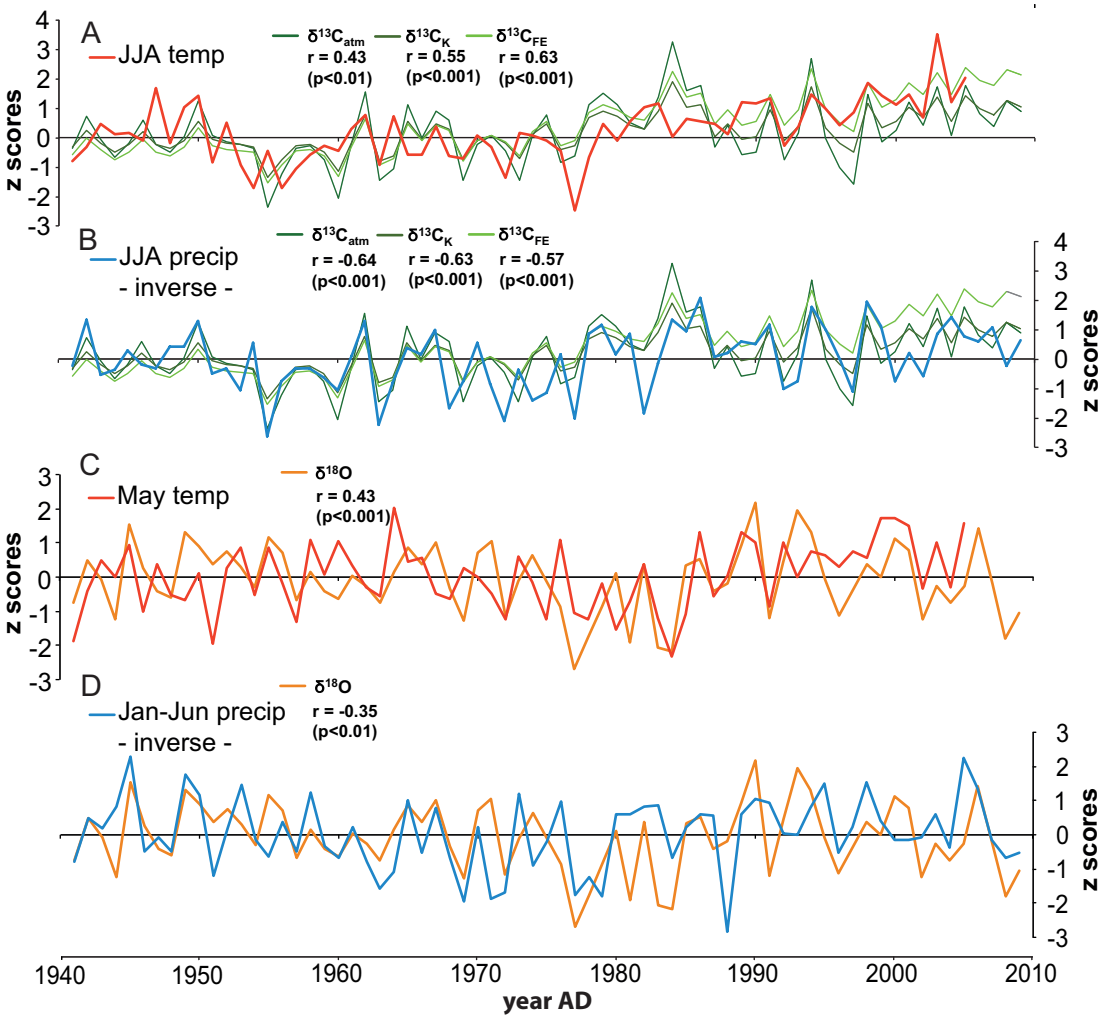

Figure 4-6 Common period climate signals. (A) $\delta^{13}C$ (green) and JJA temperature (red), (B) $\delta^{13}C$ (green) and JJA precipitation (blue), (C) $\delta^{18}O$ (orange) and May temperature (red), and (D) $\delta^{18}O$ (orange) and Jan-Jun precipitation (blue).

The offset between individual $\delta^{13}C$ tree-ring series remains unaltered by the correction procedures, since each tree is treated equally. The substantial offset among trees (>2‰) is largely persistent throughout the 20th century. The high interseries correlation among the individual trees ($\delta^{13}C_{raw}$=0.59) and the coherent growing conditions suggest that potentially

varying climate signals cannot account for the recorded $\delta^{13}C$ offset among trees. The offset is rather caused by genetic differences in water-use efficiency and/or differing soil properties and rooting depths at the micro-site scale. The offset reported here also reinforces the importance of developing individual instead of pooling proxy series, as well as considering detrending techniques (Dorado Liñán, 2011a; Esper et al., 2010; Schollän et al., 2013b; Treydte et al., 2009).

4.4.2 Oxygen isotope ratios

The oxygen isotopic composition in tree-rings is controlled by the isotopic composition of the water taken up via the roots, originating from precipitation in sites with no access to ground water, as well as the subsequent enrichment processes and biochemical fractionations in the needles and stem (Roden et al., 2000; Saurer et al., 2008). While the composition of meteoric H_2O is mainly driven by temperature in the Mediterranean region (Rozanski et al., 1993), leaf water enrichment is controlled by air humidity, and it is therefore expected that tree-ring $\delta^{18}O$ reflects a combination of these influences. A fraction of the leaf water enrichment is lost again when sucrose, transported from the needles to the stem, is broken up into trioses during cellulose formation and exchange of oxygen with xylem water (Roden et al., 2000). Based on these processes, positive correlations to temperatures and negative correlations air humidity, precipitation, and drought are expected, and were indeed observed in this study. In the absence of distinct low-frequency trends in the $\delta^{18}O$ time series, highest correlations were found with May temperature and Jan-Jun precipitation.

Accordingly, the climatic conditions during spring and early summer appear to be key for the oxygen isotopic composition at the study site. Winter temperatures in our treeline site are persistently below 0°C. Precipitation during this season generally falls as snow, while temperatures in May often exceed 0°C providing liquid water from snow melts. These conditions can cause an apparent lag between the months of greatest influence on $\delta^{18}O$, and the months when tree growth occurs (Ehleringer and Dawson, 1992; Holzkämper et al., 2008).

The Pyrenees receive highest precipitation totals in spring, while the subsequent months are dryer. Consequently, the availability of liquid water at a higher temperature level enhances photosynthesis and stimulates cambial activity, resulting in the formation of primary early-wood cells (Rossi et al., 2008). Since water storage inside the stem during winter, at temperatures below 0°C, bears the risk of cell destruction due to volume expansion of frozen

water, trees in this area likely absorb as much liquid water as possible in the early spring season. Consequently, the isotopic composition of spring precipitation is of major importance for the signal incorporated in the cellulose.

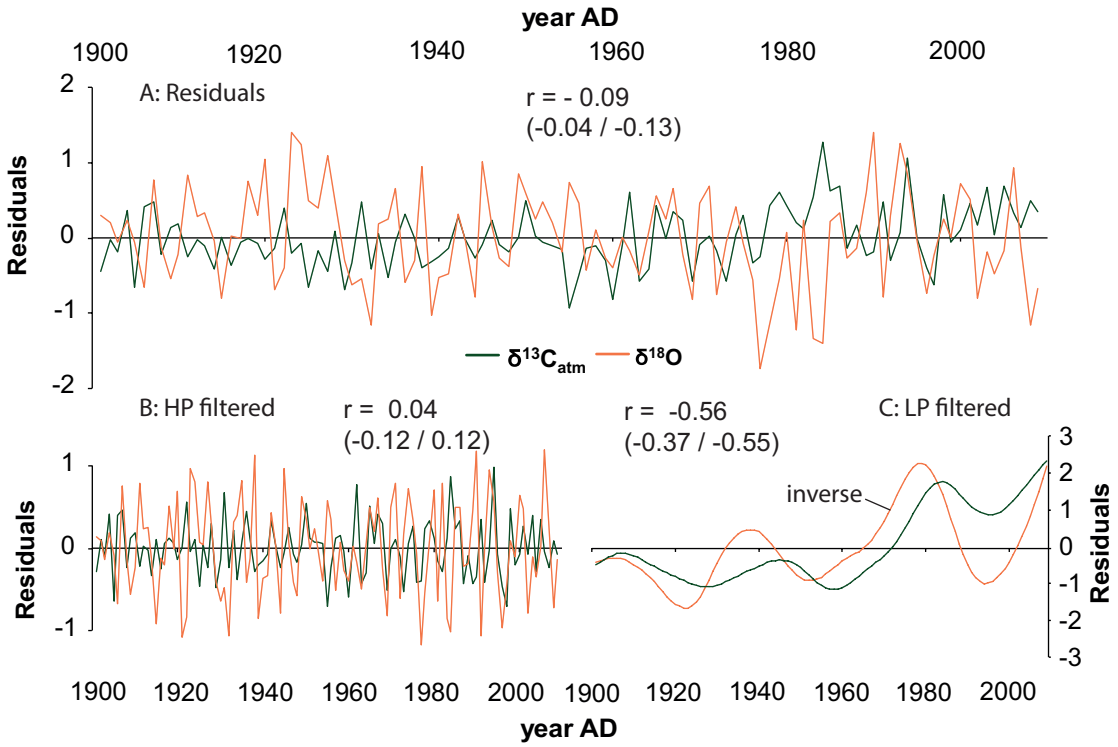

Figure 4-7 Coherency between $\delta^{13}C_{atm}$ (green) and $\delta^{18}O$ (orange) over the 1901-2009 period. Correlation values in brackets refer to early (1901-1940) and late (1941-2009) calibration periods. (A) Residual time series of the 1901-2009 means. (B) High-pass filtered $\delta^{13}C_{atm}$ and $\delta^{18}O$ (residuals from 20-year cubic smoothing splines). (C) 20-year low-pass filtered $\delta^{13}C_{atm}$ and $\delta^{18}O$ time series.

Although the observed relationships are therefore reasonable, the $\delta^{18}O$ interseries correlation (r=0.39) is weaker compared to $\delta^{13}C_{raw}$ (r=0.59), a circumstance that could be related to the more complex operational sequences influencing tree-ring $\delta^{18}O$, including source water effects, leaf-level fractionations, and equilibrium reactions during assimilate transport (Saurer et al., 2008; Treydte et al., 2007). In addition, the mixed seasonal influences as discussed above may be a reason for lower correlations observed in the Mediterranean compared to more temperate, wetter regions.

4.4.3 Parameter coherency

Coherency between the two isotopic datasets is low, in contrast to results reported by Treydte et al. (2007) for a number of European forest sites. The $\delta^{13}C_{atm}$ and $\delta^{18}O$ time series are non-correlated (r=-0.09), and no association is recorded when high-pass filtering the data (r=0.02) (Fig. 4-7). Using a 20-year low-pass filter, however, results in a negative though not significant correlation (r=-0.44) revealing the *Pinus uncinata* $\delta^{13}C_{atm}$ and $\delta^{18}O$ chronologies share common variance at decadal to multi-decadal time scales.

4.5 Conclusions

Carbon isotope ratios from five high-elevation *Pinus uncinata* trees in the Pyrenees reflect a significant summer temperature signal over the 1941-2005 period. This signal enables the reconstruction of JJA temperatures over the western Mediterranean region. Correcting carbon isotope values for effects caused by increasing atmospheric CO_2 concentrations, adds low-frequency trend to the proxy data, which has an impact on estimating the climate signals. In subsequent climate reconstructions, the under/overestimation of adaptation processes within trees could lead to deceptive results. Consequently, correction methods have to be carried out with caution, since it is unclear, which procedure best reflects the natural adaptation of the treeline pines in the Spanish Pyrenees (Saurer et al., 2008; Treydte et al., 2009; Treydte et al., 2001).

The oxygen isotope fractionation in these trees is shown to be sensitive to spring precipitation and drought, indicating good potential for the reconstruction of hydroclimate in the Pyrenees. However, the oxygen isotope signal is not just determined by one single factor, and different seasonalities introduced by the soil water on the one hand and evaporative enrichment on the other hand, result in more complicated information encoded in this parameter (Dorado-Liñán et al., 2011a, Saurer et al., 2008; Treydte et al., 2007). Nevertheless, measurements of both $\delta^{13}C$ and $\delta^{18}O$ from *Pinus uncinata* in the Spanish Pyrenees offer good complementary proxy data to evaluate and reconstruct past climatic variations representative for the western Mediterranean region.

4.6 Acknowledgements

We thank Steffen Luft for assistance in the field, and Carmen Bürger and Heiko Baschek (supported by ICLEA, Helmholtz Association) for laboratory support.

4.7 References

Andreu, L., Planells, O., Gutierrez, E., Helle, G., Schleser, G.H., 2008. Climatic significance of tree-ring width and $\delta^{13}C$ in a Spanish pine forest network. Tellus B 60, 771-781.

Büntgen, U., Frank, D., Grudd, H., Esper, J., 2008. Long-term summer temperature variations in the Pyrenees. Clim. Dyn. 31, 615-631.

Büntgen, U., Frank, D.C., Trouet, V., Esper, J., 2010. Diverse climate sensitivity of Mediterranean tree-ring width and density. Trees 24, 261-273.

Büntgen, U., Tegel, W., Nicolussi, K., McCormick, M., Frank, D., Trouet, V., Kaplan, J.O., Herzig, F., Heussner, K.-U., Wanner, H., Luterbacher, J., Esper, J., 2011. European climate variability and human susceptibility over the past 2500 years. Science 331, 578-582.

Büntgen, U., Frank, D., Neuenschwander, T., Esper, J., 2012. Fading temperature sensitivity of Alpine tree growth at its Mediterranean margin and associated effects on large-scale climate reconstructions. Clim. Change 114, 651-666.

Camarero, J.J., Guerrero-Campo, J., Gutiérrez, E., 1998. Tree-ring growth and structure of *Pinus uncinata* and *Pinus sylvestris* in the Central Spanish Pyrenees. Arct. Alp. Res. 30, 1-10.

Cherubini, P., Gartner, B.L., Tognetti, R., Bräker, O.U., Schoch, W., Innes, J.L., 2003. Identification, measurement and interpretation of tree rings in woody species from Mediterranean climates. Biologic. Rev. 78, 119-148.

Cook, E.R., 1985. A time series analysis approach to tree-ring standardization, Univ. of Ariz., Tucson.

Craig, H., 1957. Isotopic standards for carbon and oxygen and correction factors for mass-spectrometric 467 analysis of carbon dioxide. Geochim. Cosmochim. Acta 12, 133-149.

Craig, H., 1961. Isotopic variations in meteoric waters. Science 133, 1702-1703.

Dai, A., Trenberth, K.E., Qian, T., 2004. A global dataset of Palmer Drought Severity Index for 1870–2002: Relationship with soil moisture and effects of surface warming. J. Hydrometeorol. 5, 1117-1130.

Dansgaard, W., 1964. Stable isotopes in precipitation. Tellus B 16, 436-468.

Dorado-Liñán, I., Gutiérrez, E., Helle, G., Heinrich, I., Andreu-Hayles, L., Planells, O., Leuenberger, M., Bürger, C., Schleser, G., 2011a. Pooled versus separate measurements of tree-ring stable isotopes. Sci. Total Environ. 409, 2244-2251.

Dorado-Liñán, I., Gutiérrez, E., Heinrich, I., Andreu-Hayles, L., Muntán, E., Campelo, F., Helle, G., 2011b. Age effects and climate response in trees: a multi-proxy tree-ring test in old-growth life stages. Eur. J. For. Res. 131, 933-944.

Edwards, T.W.D., Graf, W., Trimborn, P., Stichler, W., Lipp, J., Payer, H.D., 2000. $\delta^{13}C$ response surface resolves humidity and temperature signals in trees. Geochim. Cosmochim. Acta 64, 161-167.

Ehleringer, J.R., Dawson, T.E., 1992. Water-Uptake by Plants - Perspectives from Stable Isotope Composition. Plant Cell and Environ. 15, 1073-1082.

Esper, J., Cook, E.R., Schweingruber, F.H., 2002. Low-frequency signals in long tree-ring chronologies and the reconstruction of past temperature variability. Science 295, 2250-2253.

Esper, J., Cook, E.R., Krusic, P.J., Peters, K., Schweingruber, F.H., 2003. Tests of the RCS method for preserving low-frequency variability in long tree-ring chronologies. Tree-Ring Res. 59, 81-98.

Esper, J., Frank, D.C., Battipaglia, G., Büntgen, U., Holert, C., Treydte, K., Siegwolf, R., Saurer, M., 2010. Low-frequency noise in $\delta^{13}C$ and $\delta^{18}O$ tree-ring data: A case study of Pinus uncinata in the Spanish Pyrenees. Global Biochem. Cycles 24: doi: 10.1029/2010GB0037772.

Esper, J., Frank, D.C., Timonen, M., Zorita, E., Wilson, R.J.S., Luterbacher, J., Holzkämper, S., Fischer, N., Wagner, S., Nievergelt, D., Büntgen, U., 2012. Orbital forcing of tree-ring data. Nat. Clim. Chang. 2, 862-866.

Farquhar, G.D., O'Leary, M.H., Berry, J.A., 1982. On the relationship between carbon isotope discrimination and the intercellular carbon dioxide concentration in leaves. Aust. J. Plant Physiol. 9, 121-137.

Feng, X., Epstein, S., 1995. Carbon isotopes of trees from arid environments and implications for reconstructing atmospheric CO2 concentration. Geochim. Cosmochim. Acta 59, 2599-2608.

Fritts, H.C., 1976. Tree Rings and Climate, New Jersey.

Green, J.W., 1963. Wood Cellulose. In Whistler, R.L. (Ed.), Methods of Carbohydrate Chemistry III. New York, pp. 9-21.

Gutiérrez, E., 1991. Climatic tree growth relationships for *Pinus uncinata* Ram in the Spanish pre-Pyrenees. Acta Oecol. 12, 213-225.

Heinrich, I., Touchan, R., Dorado Liñán, I., Vos, H., Helle, G., 2013. Winter-to-spring temperature dynamics in Turkey derived from tree rings since AD 1125. Clim. Dyn. DOI 10.1007/s00382-013-1702-3.

Helle, G., Schleser, G.H., 2004. Interpreting climate proxies from tree rings, in: Fischer, H., Floeser, G., Kumke, T., Lohmann, G., Miller, H., Negendank, J.F.W., von Storch, H. (Eds.), The climate in Historical Times, Towards a synthesis of Holocene proxy data and climate models. Berlin, pp. 129-148.

Holmes, R.L., 1983. Computer-assisted quality control in tree-ring dating and measurement. Tree-ring Bull. 43, 69-78.

Holzkämper, S., Kuhry, P., Kultti, S., Gunnarson, B., Sonninen, E., 2008. Stable isotopes in tree rings as proxies for winter precipitation changes in the Russian Arctic over the past 150 years. Geochronometria 32, 37-46.

Kürschner, K., 1996. Leaf stomata as biosensors of paleoatmospheric CO_2 levels. PhD Thesis, Utrecht University, LPP Contributions Series No.5, 153pp.

Konter, O., Holzkämper, S., Helle, G., Büntgen, U., Esper, J. (2013): Trends and signals in decadally resolved carbon isotopes from the Spanish Pyrenees. In: Helle,G., et al., TRACE Tree Rings in Archaeology, Climatology and Ecology. Volume 11; Deutsches GeoForschungsZentrum GFZ, Potsdam, Scientific Technical Report STR13/05; DOI:10.2312/GFZ.b103-13058.

Laumer, W., Andreu, L., Helle, G., Schleser, G. H., Wieloch, T., Wissel, H., 2009. A novel approach for the homogenization of cellulose to use micro-amounts for stable isotope analyses. Rapid Commun. Mass Spectrom. 23, 1934-1940.

Leavitt, S.W., Long, A, 1984. Sampling strategy for stable isotope analysis of tree rings in pine. Nature 311, 145-147.

Linares, J.-C., Delgado-Huertas, A., Camarero, J., Merino, J., Carreira, J.A., 2009. Competition and drought limit the response of water-use efficiency to rising atmospheric carbon dioxide in the Mediterranean fir Abies pinsapo. Oecologia 161, 611-624.

Loader, N.J., Robertson, I., Barker, A.C., Switsur, V.R., Waterhouse, J.S., 1997. An improved technique for the batch processing of small wholewood samples to α-cellulose. Chem. Geol. 136, 313-317.

McCarroll, D., Loader, N.J., 2004. Stable isotopes in tree rings. Quat. Sci. Rev. 23, 771-801.

McCarrol, D., Gagen, M., Loader, N., Robertson, I., Anchukaitis, K., Los, L., Young, G., Jalkanen, R., Kirchhefer, A., Waterhouse, J. 2009. Correction of tree ring stable carbon isotope chronologies for changes in the carbon dioxide content of the atmosphere. Geochim. Cosmochim. Acta 73, 1539-1547.

Mitchell, T.D., Jones, P.D. 2005. An improved method of constructing a database of monthly climate observations and associated high-resolution grids. Int. J. Climatol. 25, 693-712.

Planells, O., Gutiérrez, E., Helle, G., Schleser, G.H., 2009. A forced response to twentieth century climate conditions of two Spanish forests inferred from widths and stable isotopes of tree rings. Clim. Chang. 97, 229-252.

Rinn, F., 2007. TSAP - WinTM Professional. Zeitreihenanalyse und Präsentation für Dendrochronologie und verwandte Anwendungen. Benutzerhandbuch, Heidelberg.

Roden, J.S., Lin, G.G., Ehleringer, J.R., 2000. A mechanistic model for interpretiation of hydrogen and oxygen isotope ratios in tree-ring cellulose. Geochim. Cosmochim. Acta 64, 21-35.

Rossi, S., Deslauriers, A., Anfodillo, T., Carrer, M., 2008. Age-dependent xylogenesis in timberline conifers. New Phytol. 177**,** 199-208.

Rozanski, K., Araguas-Araguas, L., Gonfiantini, R., 1993. Isotopic patterns in modern global precipitation, in: Swart, P.K., Lohmann, K.C., McKenzie, J.A., Savin, S., (Eds.), Climate change in continental isotopic records. Washington D.C., pp. 1-36.

Saurer, M., Robertson, I., Siegwolf, R., Leuenberger, M., 1998. Oxygen isotope analysis of cellulose: An interlaboratory comparison. Anal. Chem. 70, 2074-2080.

Saurer, M., Cherubini, P., Reynolds-Henne, C.E., Treydte, K.S., Anderson, W.T., Siegwolf, R.T.W., 2008. An investigation of the common signal in tree ring stable isotope chronologies at temperate sites. J. Geophys. Res. 113, doi: 10.1029/2008JG000689.

Schleser, G.H., Helle, G., Lücke, A., Vos, H., 1999. Isotope signals as climate proxies: the role of transfer functions in the study of terrestrial archives. Quat. Sci. Rev. 18, 927-943.

Schollän, K., Heinrich, I., Neuwirth, B., Krusic, P. J., D'Arrigo, R. D., Karyanto, O., Helle, G., 2013a. Multiple tree-ring chronologies (ring width, $\delta^{13}C$ and $\delta^{18}O$) reveal dry and rainy season signals of rainfall in Indonesia. Quat. Sci. Rev. 73, 170-181.

Schollän, K., Heinrich, I., Helle, G., 2013b. UV-laser-based microscopic dissection of tree rings – a novel sampling tool for $\delta^{13}C$ and $\delta^{18}O$ studies. New Phytol., doi:10.1111/nph.12587.

Schrader, J., Baba, K., May, S.T., Palme, K., Bennet, M., Bhalerao, R.P., Sandberg, G., 2003. Poplar auxin transport in the wood-forming tissues of hybrid aspen is under simultaneous control of developmental and environmental signals. PNAS 130, 10096-10101.

Schrader, J., Moyle, R., Bhalerao, R., Hertzberg, M., Lundeberg, J., Nilsson, P., Bhalerao, R.P., 2004. Cambial meristem dormancy in trees involves extensive remodelling of the transcriptome. Plant J. 40, 173-187.

Schubert, B.A., Jahren, A.H., 2012. The effect of atmospheric CO_2 concentration on carbon isotope fractionation in C3 land plants. Geochim. Cosmochim. Acta 96, 29-43.

Tardif, J., Camarero, J.J., Ribas, M., Gutiérrez, E., 2003. Spatiotemporal variability in tree growth in the Central Pyrenees: Climatic and site influences. Ecol. Monogr. 73, 241-257.

Treydte, K., Schleser, G. H., Schweingruber, F. H, Winiger, M., 2001. The climatic significance of $\delta^{13}C$ in subalpine spruces (Lötschental, Swiss Alps): A case study with respect to altitude, exposure and soil moisture. Tellus B 53, 593-611.

Treydte, K., et al., 2007. Signal strength and climate calibration of a European tree ring isotope network, Geophys. Res. Lett. 34, doi: 10.1029/2007GL031106.

Treydte, K., Frank, D.C., Saurer, M., Helle, G., Schleser, G.H., Esper, J., 2009. Impact of climate and CO_2 on a millennium-long tree-ring carbon isotope record. Geochim. Cosmochim. Acta 71, 4635-4647.

Van der Schrier, G., Briffa, K.R., Jones, P.D., and Osborn, T.J., 2006. Summer moisture variability across Europe. J. Clim. 19, 2818–2834.

Wieloch, T., Helle, G., Heinrich, I., Voigt, M., Schyma, P., 2011. A novel device for batch-wise isolation of α-cellulose from small-amount wholewood samples. Dendrochronologia 29, 115-117.

Wigley, T.M.L., Briffa, K.R., Jones, P.D., 1984. On the Average Value of Correlated Time Series, with Applications in Dendroclimatology and Hydrometerology. J. Clim. Appl. Meteorol. 23, 201-213.

Wijngaard, J.B., Klein Tank, A.M.G., Können, G.P., 2003. Homogeneity of 20th century European daily temperature and precipitation series. Int. J. Climatol. 23, 679-692.

4.8 Appendix: supplementary figure

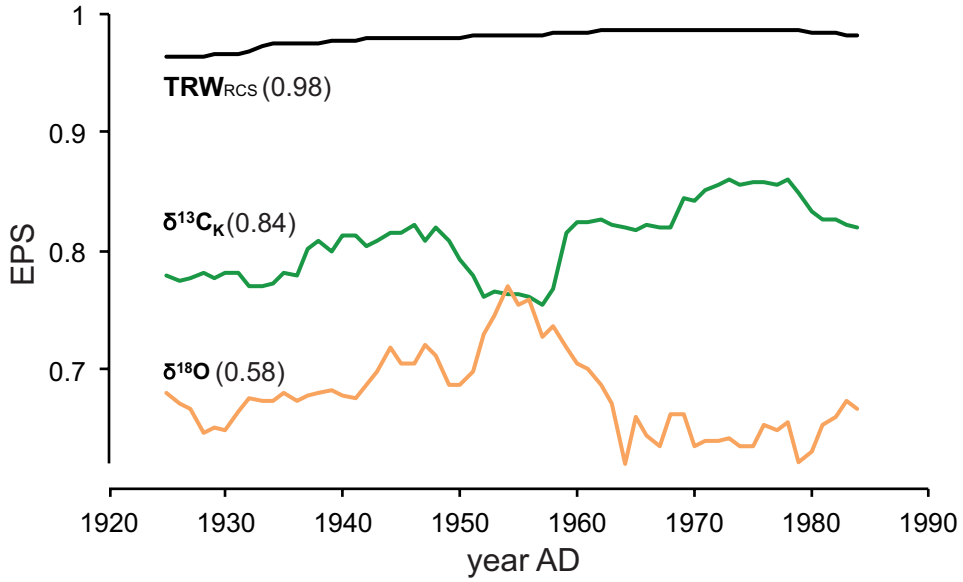

Figure 4-S1 The expressed population signal (EPS) calculated for TRW (black), $\delta^{13}C_K$ (green) and $\delta^{18}O$ (orange) calculated over 50 year windows shifted along the time series. Values in brackets indicate EPS over the 1901-2009 period.

5. Trends and signals in decadally resolved carbon isotopes from the Spanish Pyrenees

O. Konter[1], S. Holzkämper[1,2], G. Helle[3], U. Büntgen[4], J. Esper[1]

[1] *Department of Geography, Johannes Gutenberg University, Becherweg 21, 55099 Mainz, Germany*

[2] *Department of Physical Geography and Quaternary Geology, Stockholm University, 10691 Stockholm, Sweden*

[3] *German Centre for Geosciences, Climate Dynamics and Landscape Evolution, Dendro Laboratory, Potsdam, Germany*

[4] *Swiss Federal Research Institute WSL, 8903 Birmensdorf, Switzerland*

published in Helle, G., Gärtner, H., Beck, W., Heinrich, I., Heußner, K.-U., Müller, A., Sanders, T. (Eds.), 2013

5.1 Introduction

The Mediterranean Basin is considered to be a hotspot of global warming, associated with severe impacts on both bio-ecological and socio-economical systems (IPCC 2007). Several dendroclimatological studies have been carried out in the Pyrenees, where robust temperature signals are predominantly retained from nearby altitudinal treeline ecotones (Büntgen et al. 2010). Büntgen et al. (2008) analyzed maximum latewood densities (MXD) from a high-elevation sampling site in the Spanish Pyrenees and reconstructed May-September temperatures back to medieval times. Despite the commonly used tree ring width (TRW) and MXD parameters (Büntgen et al. 2010, Dorado Liñán et al. 2012), carbon isotopic ratios also showed promising results in different locations and became an important proxy of past climate variability (overview in Treydte et al. 2007). In the Pyrenees, climatic signals retained in stable carbon isotopes include both summer precipitation and temperature (Andreu et al. 2008, Dorado Liñán et al. 2011). Carbon fractionation procedures within trees and their impact on low-frequency trends are not well understood, as variations in the amount and isotopic composition of atmospheric CO_2 as well as climate variations are simultaneously incorporated in tree rings (Farquhar et al. 1982, Feng & Epstein 1995, Kürschner 1996, Treydte et al. 2004, McCarroll & Loader 2004, Helle & Schleser 2004). Analyses of low-frequency changes in tree ring stable isotopes are constrained by the work load required to produce annually resolved $\delta^{13}C$ and $\delta^{18}O$ time series from single trees. Esper et al. (2010) established decadally resolved, millennial-length $\delta^{13}C$ and $\delta^{18}O$ records to analyze long-term trends in tree ring isotope data. These data have, however, not being calibrated against instrumental time series, a procedure explored here.

We present six decadally resolved carbon isotope records spanning the 1901-2009 period, derived from *Pinus uncinata* trees originating from the same sampling site as used in Esper et al. (2010). These single-tree $\delta^{13}C_{raw}$ time series are transformed considering various correction methods (Feng & Epstein 1995, Kürschner 1996, McCarroll & Loader 2004) and calibrated against climate data to assess the reconstruction potential of the millennial-length carbon isotope data from the region.

5.2 Material and methods

5.2.1 Study site and sampling strategy

The altitude of the selected treeline site, located near Gerber Lake at the northern border of the "D'Aigüestortes Estany de Sant Maurici" Spanish National Park in the Central Pyrenees,

west of Andorra, ranges from 2314 to 2380 m asl. The prevailing tree species is *Pinus uncinata*, a shade-intolerant conifer tree in the open forest ecotone. Tree height varies between 3-6 m, and diameter at breast height ranges from 0.25-1.08 m.

In June 2010 twenty-three *Pinus uncinata* trees were selected at the aforementioned treeline site. The selection of the pine individuals was based on the estimated tree ages, to establish a dataset including only trees of similar or comparable age throughout the calibration period. Since dry-dead material was rare, the selection focused on material from living trees. The sampled trees have no access to ground water. Four cores (0.5 cm diameter) were sampled from each tree in a radial configuration at breast height, two diametrically parallel and two diametrically perpendicular to the slope, whenever possible.

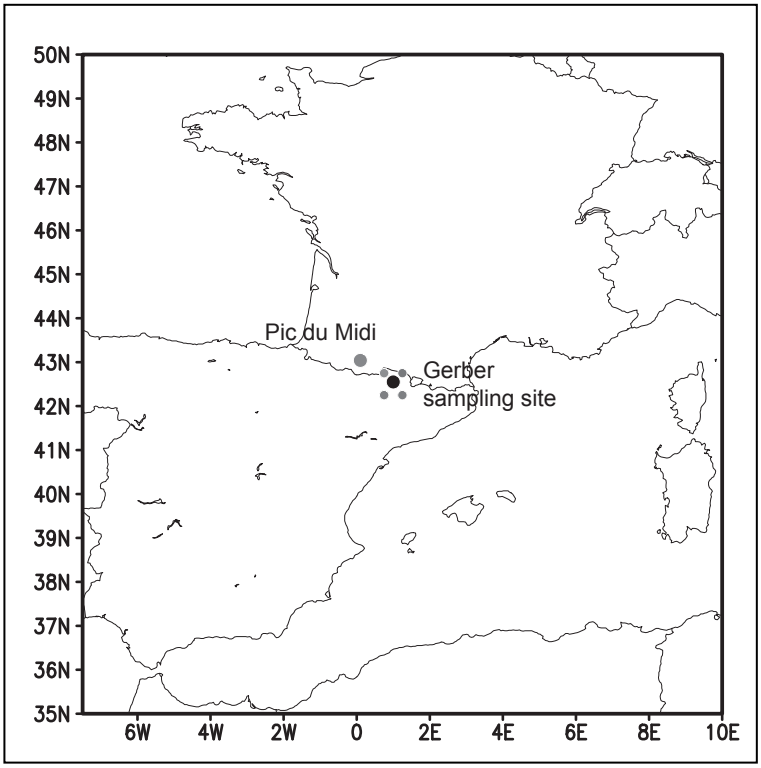

Figure 5-1 Study area; Gerber sampling site shown in black, gridded climate data in grey, and Pic du Midi station in grey (large dot).

5.2.2 Tree-ring width and stable isotope measurements

Core samples were cut lengthwise and vertically to the wood fiber to maintain plain surfaces. Tree ring widths were measured using TSAP-WinTM Professional (Rinn et al. 2007), cross-dated using CoFecha (Holmes 1983), and detrended using the Regional Curve Standardization technique (RCS, Esper et al. 2003) within ARSTAN (Cook 1985).

A subset of six trees was selected and each tree ring, from 1901-2009, sectioned with a scalpel. For isotopic measurements, two core samples were merged to represent a single tree, i.e. two cut samples (from the same year) were joined. From this basic wood material α-cellulose was extracted following procedures established by Green (1963) and advanced by Loader (1996). Homogenization of the α-cellulose samples was achieved by using an ultrasonic technique (Laumer et al. 2009). Samples were freeze-dried prior to analyzing carbon isotope ratios using an IsoPrime (GV Instruments, Manchester, UK) Isotope Ratio Mass Spectrometer (IRMS) with an interfaced elemental analyzer (Fisons NA 1500 NC) on a continuous carrier gas flow, operated at the *GeoForschungsZentrum (GFZ) Potsdam*.

The resulting annual values, expressed relative to the international VPDB standard in per mill (‰), were transformed to decadal, no mass weighted values by calculating 10-year-means (1901-1910,..., 1991-2000; except 2001-2009 representing only 9 values) to transform the explored climate signal to the millennial long, decadally resolved time series displayed in Esper et al. (2010). Six $\delta^{13}C$ time series representing individual trees (two radii per tree) and consisting of eleven decadal values from 1901 to 2009 are used in this assessment.

5.2.3 Tree-ring width and stable isotope measurements

Core samples were cut lengthwise and vertically to the wood fiber to maintain plain surfaces. Tree ring widths were measured using TSAP-WinTM Professional (Rinn et al. 2007), cross-dated using CoFecha (Holmes 1983), and detrended using the Regional Curve Standardization technique (RCS, Esper et al. 2003) within ARSTAN (Cook 1985).

A subset of six trees was selected and each tree ring, from 1901-2009, sectioned with a scalpel. For isotopic measurements, two core samples were merged to represent a single tree, i.e. two cut samples (from the same year) were joined. From this basic wood material α-cellulose was extracted following procedures established by Green (1963) and advanced by Loader (1996). Homogenization of the α-cellulose samples was achieved by using an ultrasonic technique (Laumer et al. 2009). Samples were freeze-dried prior to analyzing carbon isotope ratios using an IsoPrime (GV Instruments, Manchester, UK) Isotope Ratio Mass Spectrometer (IRMS) with an interfaced elemental analyzer (Fisons NA 1500 NC) on a continuous carrier gas flow, operated at the *GeoForschungsZentrum (GFZ) Potsdam*.

The resulting annual values, expressed relative to the international VPDB standard in per mill (‰), were transformed to decadal, no mass weighted values by calculating 10-year-means (1901-1910, …, 1991-2000; except 2001-2009 representing only 9 values) to transform the explored climate signal to the millennial long, decadally resolved time series displayed in

Esper et al. (2010). Six $\delta^{13}C$ time series representing individual trees (two radii per tree) and consisting of eleven decadal values from 1901 to 2009 are used in this assessment.

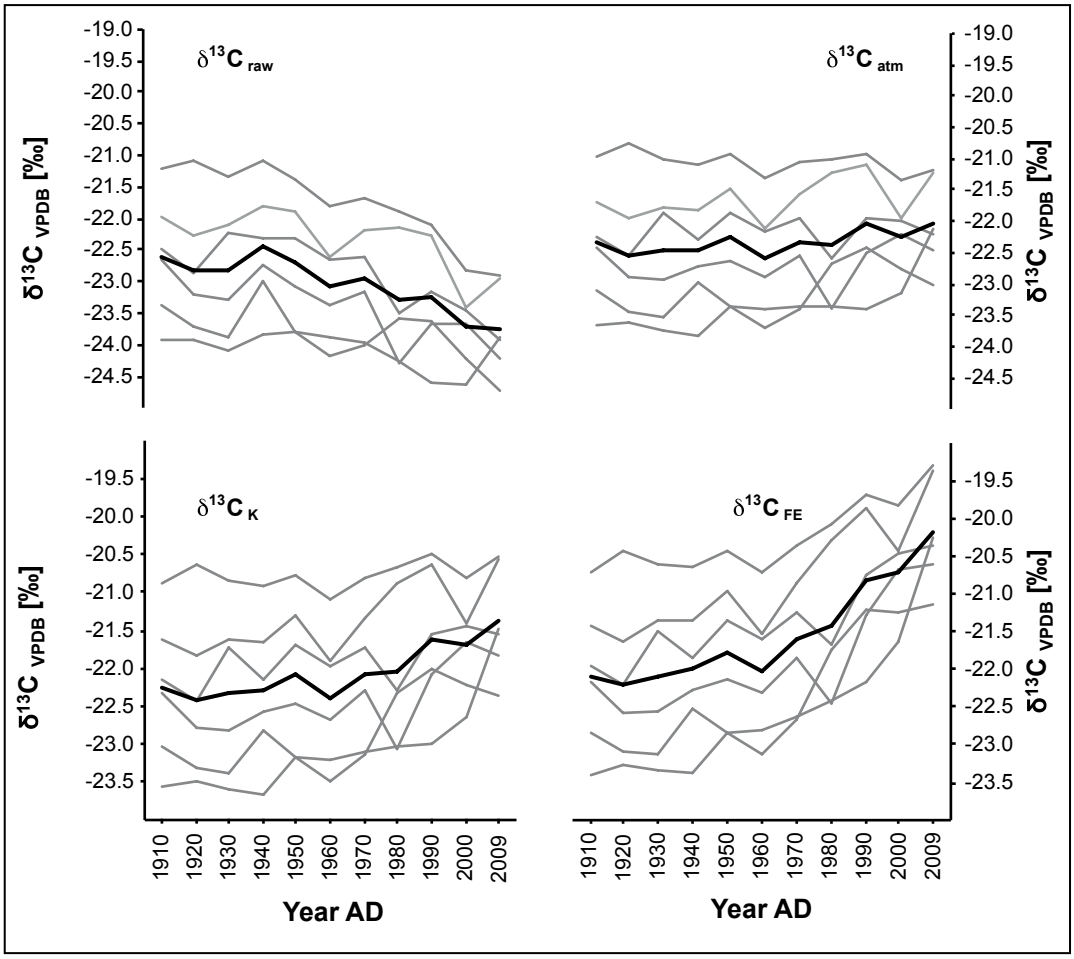

Figure 5-2 Decadally resolved carbon isotope data. Grey lines indicate individual trees, black lines their arithmetic means, for the $\delta^{13}C_{raw}$, $\delta^{13}C_{atm}$, $\delta^{13}C_K$, and $\delta^{13}C_{FE}$ data.

5.2.4 Physiological fractionation and correction

Anthropogenic fossil fuel burning since the beginning of industrialization has lead to a declining trend of $\delta^{13}C$ in atmospheric CO_2 and is also reflected in tree ring $\delta^{13}C_{raw}$ values (Farquhar et al. 1982, McCarroll & Loader 2004, Treydte et al. 2007). This non-climatic decreasing trend inherent in the tree ring data is corrected by applying a procedure detailed in McCarroll and Loader (2004); the dataset is referred to as $\delta^{13}C_{atm}$ hereinafter. As the increased atmospheric CO_2 concentration also influences plant metabolism – through stronger discrimination against the heavier ^{13}C isotope – we additionally corrected the $\delta^{13}C_{raw}$ values following suggestions by Kürschner (1996, hereinafter $\delta^{13}C_K$) and Feng & Epstein et al. (1995, hereinafter $\delta^{13}C_{FE}$).

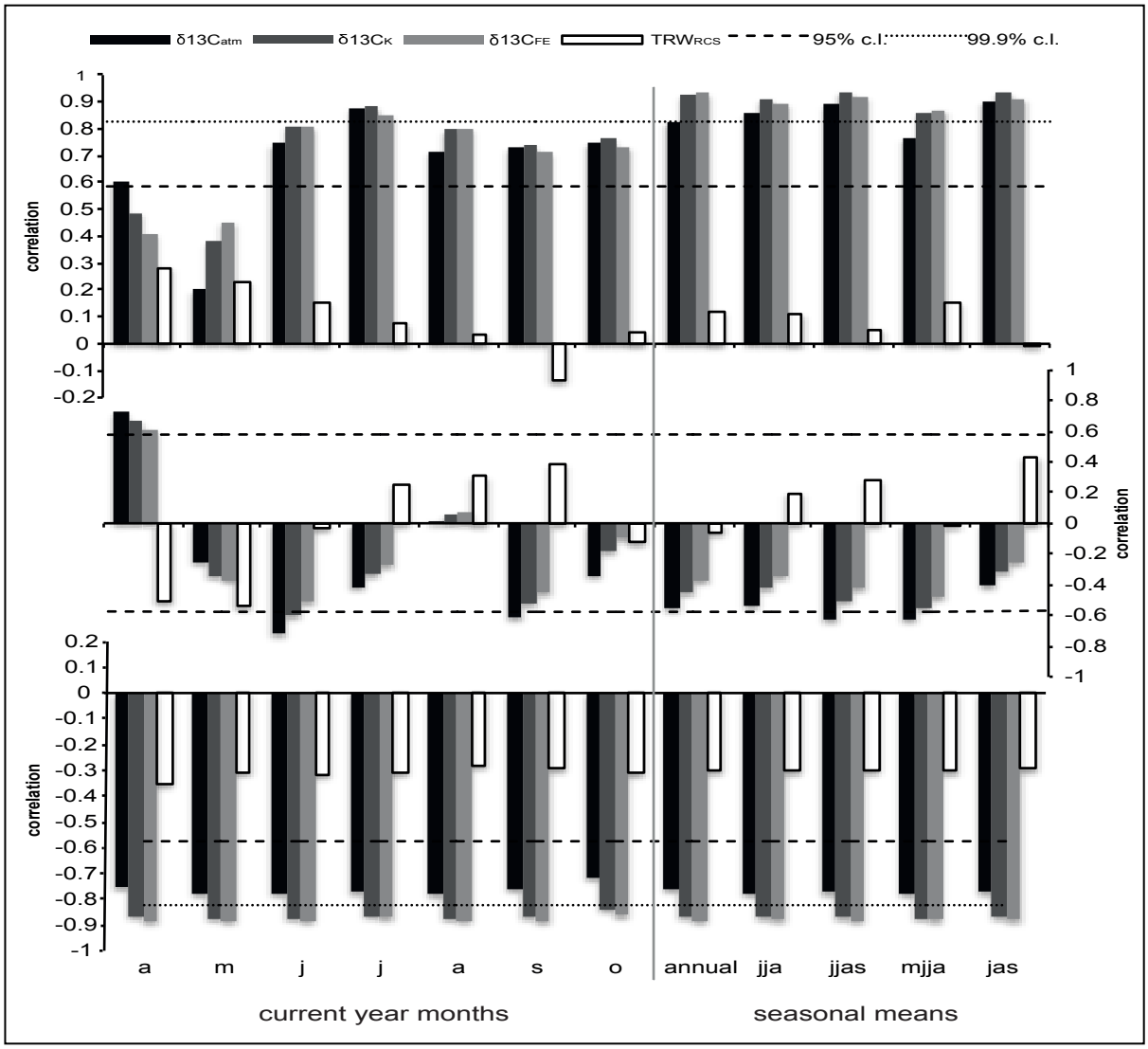

Figure 5-3 Growth-climate relationships. Monthly and seasonal correlation coefficients between $\delta^{13}C_{atm}$ (black), $\delta^{13}C_K$ (grey), and $\delta^{13}C_{FE}$ (light grey) versus temperature (top panel), precipitation (middle), and PDSI (bottom) over the 1901-2009 period. Dashed curves indicate the 95% (bold) and 99% significance levels. These are not corrected for lag-1 autocorrelation effects; for corrected values, see text.

5.2.5 Climate data and calibration

Climate signals of the TRW, $\delta^{13}C_{atm}$, $\delta^{13}C_K$, and, $\delta^{13}C_{FE}$ were assessed using Pearson product-moment correlation coefficients calculated over the 1901-2009 period, including 11 decadal values. Temperature data from the Pic du Midi station (2,862m asl, 43°04'N, 0°09'E), and gridded precipitation (CRU TS 3.1, Mitchell & Jones 2005) and PDSI data (Dai et al. 2004) are considered. To calibrate climate data against the decadally resolved isotope data, decadal arithmetic means were calculated for all climate variables. Since the availability of climate data of the most recent decade varies (temperature 1901-2005, precipitation 1901-2009, PDSI

1901-2005), the period from 2001-2009 represents varying number of values (temperature: 5 values, precipitation: 9 values, PDSI: 5 values).

5.3 Results and discussion

5.3.1 Stable isotope data

The individual stable isotope time series show a remarkable offset among single trees (Fig. 5-2). Mean values of single trees range from -21.75 ‰ to -23.90 ‰ ($\delta^{13}C_{raw}$) and offsets increase up to >3 ‰ during several periods. Whereas these differences do not alter substantially in the different corrections, interseries correlations increase from 0.23 for $\delta^{13}C_{atm}$ to 0.69 for $\delta^{13}C_K$ and 0.93 for $\delta^{13}C_{FE}$. These changes are associated with the common and most important increasing trends added throughout the corrections. The common declining trend inherent in $\delta^{13}C_{raw}$ is removed in the $\delta^{13}C_{atm}$ data. The additional correction for physiological fractionations caused an overall positive low-frequency trend in $\delta^{13}C_K$ – and even more so in $\delta^{13}C_{FE}$, altering the correlations to eventually > 0.9.

5.3.2 Climate signals

Since the $\delta^{13}C_{raw}$ data contain a well-known non-climatic trend, climate/growth relationships are estimated between $\delta^{13}C_{atm}$, $\delta^{13}C_K$, $\delta^{13}C_{FE}$ and monthly temperature anomalies, precipitation sums, and mean PDSI values (Fig. 3-5). Most significant results are revealed among the carbon isotope data and summer temperatures, particularly during July ($p < 0.001$). The strongest association is detected between $\delta^{13}C_K$ and July-September mean temperatures ($r=0.94$, 1901-2009 period). Whereas the influence of precipitation seems overall negligible (except for a 95% significant signal in April), PDSI shows coherent negative correlations up to $r=-0.88$ ($p < 0.001$) likely driven by the longer-term temperature variations.

The strong coherence between $\delta^{13}C_{FE}$ and (summer) temperatures points to the low-frequency trends, inherent in temperature and largely absent from precipitation, as the key variable influencing the correlation results. The relationships between carbon isotope and climate data vary according to their low-frequency loadings: $\delta^{13}C_{FE}$ (in contrast to $\delta^{13}C_{atm}$) correlates significantly with PDSI due to the common low-frequency trends inherent in both datasets. Consequently, $\delta^{13}C_{atm}$ correlates better with precipitation, compared to $\delta^{13}C_K$ and $\delta^{13}C_{FE}$. All significance levels mentioned in the text are not corrected for lag-1 autocorrelation, which are 0.23 for $\delta^{13}C_{atm}$, 0.76 for $\delta^{13}C_K$, 0.93 for $\delta^{13}C_{FE}$, and 0.47 for July-September mean

temperature, for example. After reduction of the degrees of freedom due to lag-1 autocorrelation, $\delta^{13}C_{atm}$ values still exceed the 99.9 % confidence level when correlated with July-September temperatures (r=0.90), in contrast to $\delta^{13}C_K$ and $\delta^{13}C_{FE}$ data.

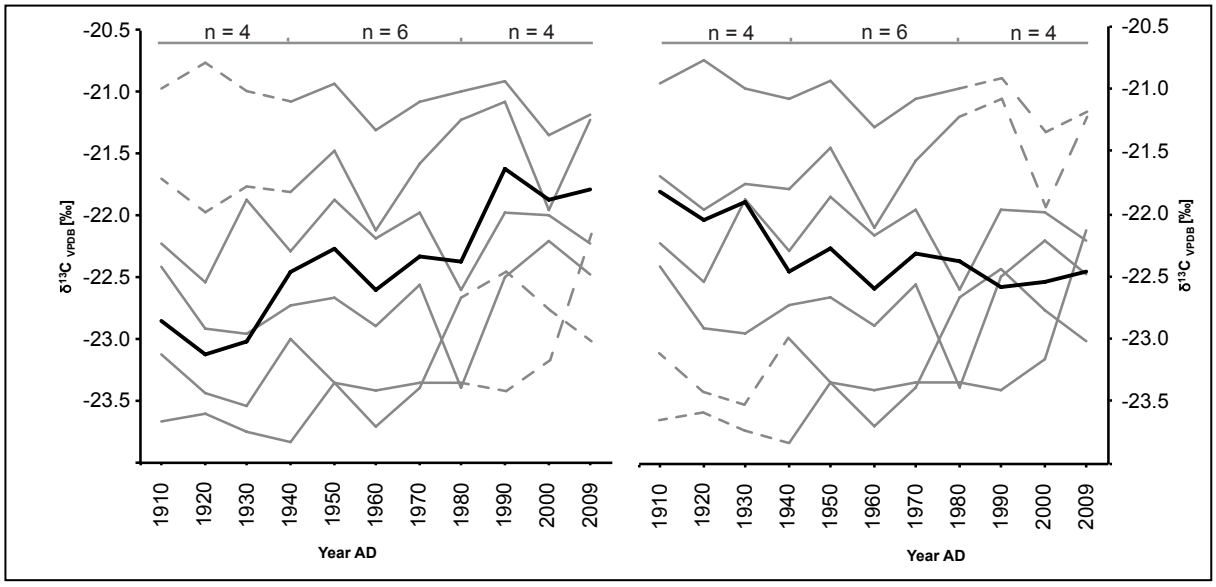

Figure 5-4 Changing $\delta^{13}C_{atm}$ mean curves (black) as a consequence of removing decadal sets of individual trees (grey, see main text). Dashed lines indicate omitted data; left panel: early high and late low decadal values of two individual time series omitted; right panel: early low and late high decadal values of two individual time series omitted.

5.3.3 Spurious trends

The inter-tree offsets shown in this study do not alter the mean values functions (the chronologies), since replication (n=6) does not change throughout the calibration period (1901-2009). However, an inter-tree range of 2-3 ‰ can cause spurious trends within carbon isotope datasets, if replication changes over time – which is a typical feature of longer term tree ring records (Esper et al. 2002). To illustrate this effect, we omitted the first three decadal sets of two individual time series and additionally the last three decadal sets of two different time series, as if the dataset would contain two individuals covering the 1901-1980 period and two individuals covering the 1940-2009 period (as well as two trees covering the full 1901-2009 period) (Fig. 5-4). The replication of this new data is consequently reduced from six to four trees at the beginning (1901-1930) and the end (1980-2009) of the calibration period, which still is considered to be an adequate and representative amount of individuals for isotope based climate evaluations (Leavitt and Long 1984). During the period represented by all individuals (1940-1980) the original data and mean remain unaltered. This setup mirrors tree core composition and age structure changes typical to long-term chronologies (Treydte et

al. 2009, Seftigen et al. 2011, Gagen et al. 2011). The resulting mean chronologies (see the black curves in Fig. 5-4), however, indicate entirely different low-frequency trends as a result of our data treatment. These spurious trends are the consequence of the substantial level differences of individual stable carbon isotope time series that do not cover the exact same period. The cause for these differing trends would remain unknown – and the trends perhaps interpreted as environmental signals – if the wood samples would have been pooled before isotope measurement. Removing the substantial level differences of individual time series by calculating anomalies to the individual mean values prior to producing a chronology could contribute to verify trends inherent in the data and, thus, could help to avoid discarding data of low-replicated periods.

5.4 Conclusions

Decadally resolved carbon isotope measurements capture climate signals in the 20th century, enabling a calibration setup for reconstruction purposes. Especially summer temperature variations are reflected in tree ring stable carbon isotopes, displayed in correlation values of $r=0.90$ ($p<0.001$) between July-September temperature anomalies and $\delta^{13}C_{atm}$ values. Stomata aperture and subsequent isotopic fractionation in the leaves are driven by temperature, while precipitation is of a minor importance to the pine trees from the high-elevation Gerber site.

Commonly applied corrections of the carbon isotope data increase the low-frequency trends of $\delta^{13}C$ time series. The increased trends alter the relationship to climate indices: $\delta^{13}C_K$ and $\delta^{13}C_{FE}$ show higher correlations to climate indices that also incorporate low-frequency trends. The increasing autocorrelation affect the degrees of freedom, however, a feature that is particularly significant with decadally resolved data.

More analyses of the physiological processes are needed to clarify which correction is indeed recommended. In the Spanish Pyrenees, the Kürschner approach ($\delta^{13}C_K$) results in the closest association with temperature data, while the Feng & Epstein approach ($\delta^{13}C_{FE}$) seems to overestimate the low-frequency trend compared to temperature.

Low-frequency trends within carbon isotope data can also be caused by changes in replication and need careful analyses. In this study, tree replication is stable ($n = 6$) over the entire 1901-2009 calibration period. It is concluded that the displayed low-frequency stable carbon isotope trends reflect the increasing temperatures since the beginning of the 20th century.

5.5 References

Andreu, L., Planells, O., Gutierrez, E., Helle, G., Schleser, G.H., 2008. Climatic significance of tree ring width and $\delta^{13}C$ in a Spanish pine forest network. Tellus B 60, 771-781.

Büntgen, U., Frank, D., Grudd, H., Esper, J., 2008. Long-term summer temperature variations in the Pyrenees. Climate Dynamics 31, 615-631.

Büntgen, U., Frank, D.C., Trouet, V., Esper, J., 2010. Diverse climate sensitivity of Mediterranean tree ring width and density. Trees 24, 261-273.

Briffa, K.R., Jones, P.D., Bartholin, T.S., Eckstein, D., Schweingruber, F.H., Karlén, W., Zetterberg, P., Eronen, M., 1992. Fennoscandiansummers from AD 500: temperature changes on short and long timescales. Climate Dynamics 7, 111–119.

Cook, E. R., 1985. A time series analysis approach to tree ring standardization, Ph.D. dissertation, 171 pp., Univ. of Ariz., Tucson.

Dai, A., Trenberth, K. E, Qian, T., 2004. A global dataset of Palmer Drought Severity Index for 1870–2002: Relationship with soil moistureand effects of surface warming. Journal of Hydrometeorolgy 5, 1117-1130.

Dorado Liñán, I., Gutiérrez, E., Heinrich, I., Andreu-Hayles, A., Muntán, E., Campelo, F., Helle, G., 2011. Age effects and climate response in trees: a multi-proxy tree ring test in old-growth life stages. European Journal of Forest Research 131, 933-944.

Dorado Liñán, I., Büntgen, U., Gonzalez-Rouco, F., Zorita, E., Montavez, J.P., Gomez-Navarro, J.J., Brunet, M., Heinrich, I., Helle, G., Gutiérrez, E., 2012. Estimating 750 years of temperature variations and uncertainties in the Pyrenees by tree ring reconstructions and climate simulations. Climate of the Past 8, 919-933.

Esper, J., Cook, E.R., Schweingruber, F.H., 2002. Low-frequency signals in long tree ring chronologies and the reconstruction of past temperature variability. Science 295, 2250-2253.

Esper, J., Cook, E.R., Krusic, P.J., Peters, K., Schweingruber, F.H., 2003. Tests of the RCS method for preserving low-frequency variability in long tree ring chronologies. Tree ring Research 59, 81-98.

Esper, J., Frank, D.C., Battipaglia, G., Büntgen, U., Holert, C., Treydte, K., Siegwolf, R., Saurer, M., 2010. Low-frequency noise in $\delta^{13}C$ and $\delta^{18}O$ tree ring data: A case study of Pinus uncinata in the Spanish Pyrenees. Global Biochemical Cycles 24, doi 10.1029/2010GB0037772.

Farquhar, G.D., O'Leary, M.H., Berry, J.A., 1982. On the relationship between carbon isotope discrimination and the intercellular carbon dioxide concentration in leaves. Australian Journal of Plant Physiology 9, 121-137.

Feng, X., Epstein, S., 1995. Carbon isotopes of trees from aridenvironments and implications for reconstructing atmospheric CO2 concentration. Geochimica et Cosmochimica Acta 59, 12, 2599–2608.

Fritts, H.C., 1976. Tree Rings and Climate. Blackburn Press. 567 p.

Gagen, M., Zorita, E., McCarroll, D., Young, G.H.F., Grudd, H., Jalkanen, R., Loader, N., Robertson, I., Kirchhefer, A.J., 2011. Cloud response to summer temperatures in Fennoscandia over the last thousand years. Geophysical Research Letters 38, doi 10.1029/2010GL046216, 2011.

Green, J.W., 1963. Wood Cellulose. In Whistler, R.L. (Ed.), Methods of Carbohydrate Chemistry III. Academic Press. pp. 9-21.

Helle, G., Schleser, G.H., 2004. Interpreting climate proxies from tree rings. In: Fischer, H., Floeser, G., Kumke, T., Lohmann, G., Miller, H., Negendank, J.F.W., von Storch, H. (Eds.), The climate in Historical Times, Towards a synthesis of Holocene proxy data and climate models. Springer Verlag. pp. 129-148.

Holmes, R.L., 1983. Computer-assisted quality control in tree ring dating and measurement. Tree ring Bulletin 43, 69-78.

IPCC, 2007. Climate Change 2007: The Physical Science Basis. Contribution of Working Group I to the Fourth Assessment Report of the Intergovernmental Panel on Climate Change [Solomon, S., D. Qin, M. Manning, Z. Chen, M. Marquis, K.B. Averyt, M.Tignor and H.L. Miller (eds.)]. Cambridge University Press, Cambridge, United Kingdom and New York, NY, USA.

Kürschner, K., 1996. Leaf stomata as biosensors of paleoatmospheric CO_2 levels. Utrecht, 160 p.

Laumer, W., Andreu, L., Helle, G., Schleser, G. H., Wieloch, T., Wissel, H., 2009. A novel approach for the homogenization of cellulose to use micro-amounts for stable isotope analyses. Rapid Communications in Mass Spectrometry 23, 13, 1934-1940.

Leavitt, S.W., Long, A., 1984. Sampling strategy for stable isotope analysis of tree rings in pine. Nature 311, 145-147.

Loader, N.J., Robertson, I., Barker, A.C., Switsur, V.R., Waterhouse, J.S., 1997. An improved technique for the batch processing of small wholewood samples to α-cellulose. Chemical Geology 136, 313-317.

McCarroll, D., Loader, N.J., 2004. Stable isotopes in tree rings. Quaternary Science Reviews 23, 771-801.

Mitchell, T.D., Jones, P.D., 2005. An improved method of constructing a database of monthly climate observations and associated high-resolution grids. Int. J. Climatology 25, 693-712, doi 10.1002/joc.1181.

Rinn, F., 2007. TSAP - WinTM Professional. Zeitreihenanalyse und Präsentation für Dendrochronologie und verwandte Anwendungen. Benutzerhandbuch, Heidelberg, 56 pp.

Seftigen, K., Linderholm, H.W., Loader, N., Liu, Y., Young, G.H.F., 2011. The influence of climate on $^{13}C/^{12}C$ and $^{18}O/^{16}O$ ratios in tree ring cellulose of Pinus sylvestris L. growing in the central Scandinavian Mountains. Chemical Geology 286, 84-93.

Treydte, K., et al. 2007. Signal strength and climate calibration of a European tree ring isotope network, Geophysical Research Letter 34, doi 10.1029/2007GL031106.

Treydte, K., Frank, D.C., Saurer, M., Helle, G., Schleser, G.H., Esper, J., 2009. Impact of climate and CO_2 on a millennium-long tree ring carbon isotope record. Geochimica et Cosmochimica Acta 71, 4635-4647.

6. Long-term summer temperature variations in the Pyrenees from detrended stable carbon isotopes

Jan Esper[1], Oliver Konter[1], Paul J. Krusic[2], Matthias Saurer[3],

Steffen Holzkämper[2] and Ulf Büntgen[4-6]

[1]*Department of Geography, Johannes Gutenberg University, 55099 Mainz, Germany*

[2]*Department of Physical Geography and Quaternary Geology, Stockholm University, 10691 Stockholm, Sweden*

[3]*Paul Scherrer Institut, 5232 Villigen, Switzerland*

[4]*Swiss Federal Research Institute WSL, 8903 Birmensdorf, Switzerland*

[5]*Oeschger Centre for Climate Change Research, University of Bern, 3012 Bern, Switzerland*

[6]*Global Change Research Centre AS CR, v.v.i., Bělidla 986/4a, CZ-60300 Brno, Czech Republic*

published in Geochronometria 42, 2015

6.1 Introduction

Tree-ring $\delta^{13}C$ records have been used to reconstruct various climate parameters including temperature (Treydte et al., 2009), precipitation (Bale et al., 2011), drought (Kress et al., 2010), relative humidity (Edwards et al., 2008), and cloud cover (Gagen et al., 2011). However, the assessment of potential low frequency trends in these climate parameters, using tree-ring stable isotope data, remains challenging as the isotope records are typically based on *(i)* few trees and *(ii)* pooled wood samples (mixed material from different trees prior to mass spectrometer measurement) (Borella et al., 1998). The pooling procedure limits the ability to analyze varying $\delta^{13}C$ levels among individual trees as well as any potential underlying age-trends that might obscure long-term climate signals (Esper et al., 2010; Dorado Liñán et al., 2011; Hangartner et al., 2012). As a result, climate reconstructions derived from detrended tree-ring $\delta^{13}C$ data, in which $\delta^{13}C$ level differences and age-trends have been analyzed and, if detected, removed, are largely missing from the literature.

The investigation of between-tree $\delta^{13}C$ level differences and $\delta^{13}C$ age-trends requires processing single trees individually throughout the time-demanding and expensive procedure of sample preparation and mass spectrometry measurement. This can realistically be achieved by reducing the temporal resolution of $\delta^{13}C$ measurement from annual to decadal or even lower time steps (Edwards et al., 2008). Here we present the first such experiment, comprising 31 individual $\delta^{13}C$ measurement series from living and dead *Pinus uncinata* trees, from a high elevation site in the Spanish Pyrenees. All trees were treated individually, at decadal resolution, to develop a dataset containing 1007 $\delta^{13}C$ measurements spanning the past millennium. The 31 decadally resolved $\delta^{13}C$ timeseries (each representing a single tree) cannot be used to reconstruct annual extremes, but permit the analysis and treatment of $\delta^{13}C$ level differences and age-trends to develop a detrended stable isotope chronology containing long-term climate variations back to the 13th century.

Statistical calibration and verification of such a record, however, requires annually resolved $\delta^{13}C$ measurements during the period of overlap with instrumental data. This objective is addressed by combining the decadally resolved $\delta^{13}C$ data with 545 annually resolved $\delta^{13}C$ measurements from a sub-sample of *Pinus uncinata* trees covering the 20th century (Konter et al., 2014). The high frequency climate signals of $\delta^{13}C$ (and $\delta^{18}O$ from the same trees) have been explored in detail in Konter et al. (2014) including assessments of the effects of differing $\delta^{13}C$ correction procedures, to account for the Suess effect (Suess, 1955), on the calibration schemes. We here build on these results and develop a millennial-scale reconstruction based on decadally resolved, detrended, $\delta^{13}C$ measurements, with the climate signal attributed to the

comparison of annually resolved $\delta^{13}C$ measurements with instrumental data. The reconstruction is compared to extant long-term estimates of warm season temperature variability from the Spanish Pyrenees, based on maximum latewood density (MXD) data.

6.2 $\delta^{13}C$ Data, Detrending and Calibration Methods

Increment cores from living trees and dry-dead wood were collected (Fig. 6-1) to develop a continuous, millennium-length *Pinus uncinata* composite chronology for the Central Pyrenees (Büntgen et al., 2008). The sampling site is located near lake Gerber (42°38'N, 1°06'E) at the upper treeline (2400 m a.s.l.), where traditional tree-ring width (TRW) and MXD data have been shown to contain a summer temperature signal (Büntgen et al., 2010). From a total of several hundred Pinus uncinata sampled during several field campaigns, 31 trees were used to develop a stable carbon isotope ratio chronology spanning the past 700+ years with a fairly stable temporal distribution, ranging from 5 trees in 1300 C.E. to 13 in 2000 C.E. (bottom panel of Fig. 6-2).

Figure 6-1 Increment borers used to sample 5 mm diameter cores from living (left) and dead (right) *Pinus uncinata* near the timberline in the Spanish Pyrenees.

Increment cores were sectioned into decadal blocks (1991-2000, 1981-1990, ...) using a scalpel and processed individually to quantify the $^{13}C/^{12}C$ ratios in the wood samples (Esper et al., 2010). From five of the 31 trees, this procedure was applied at annual resolution over the 1901-2009 period so that the resulting $\delta^{13}C$ timeseries from this sub-sample is decadally

resolved before 1901 and annually resolved thereafter (Konter et al., 2014). We extracted a-cellulose from the wood samples, homogenized and freeze dried the cellulose, and measured the $^{13}C/^{12}C$ ratios using an isotope ratio mass spectrometer, interfaced elemental analyzer, following standard procedures (Boettger et al., 2007; Battipaglia et al., 2008).

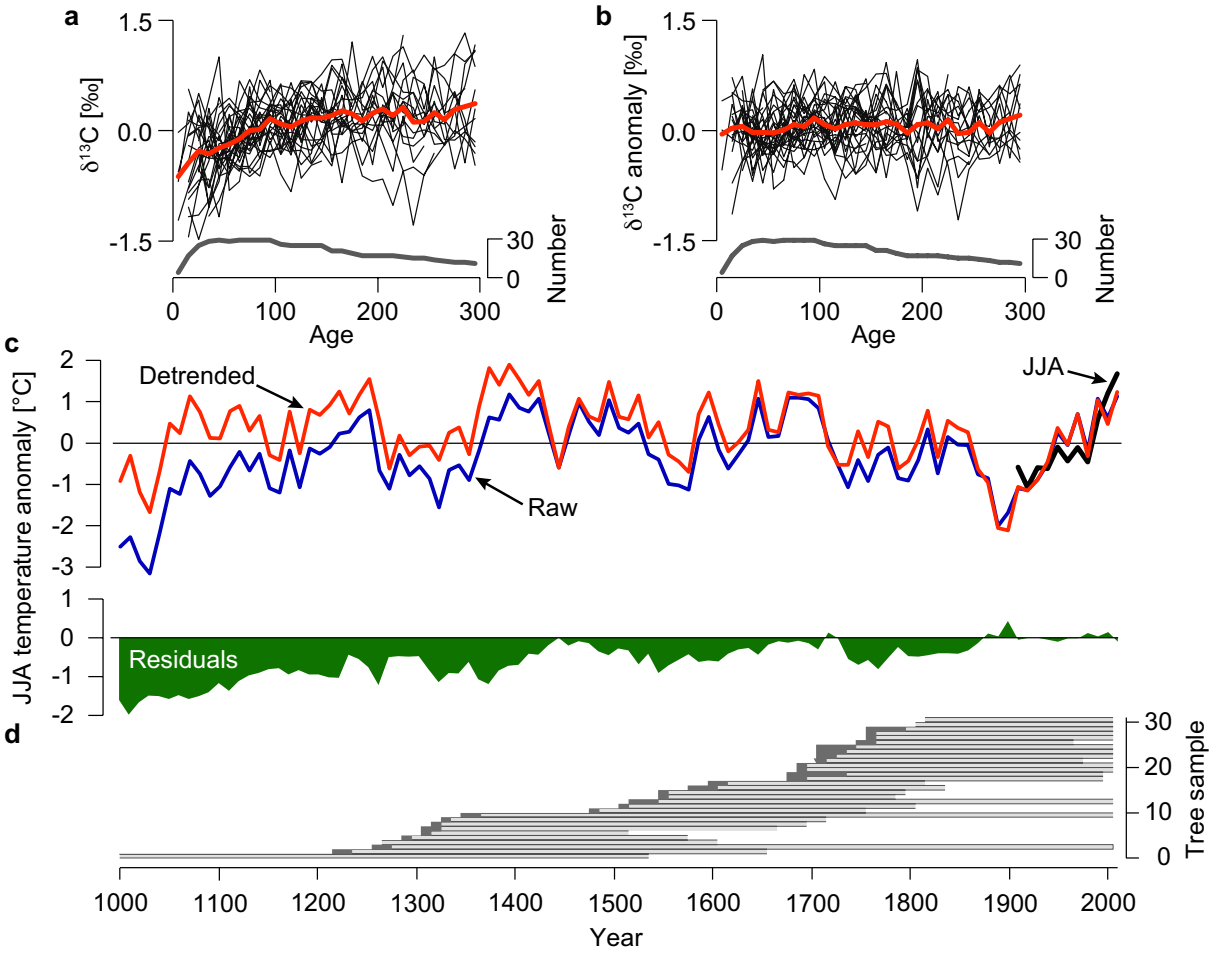

Figure 6-2 $\delta^{13}C$ age-trend detection, correction, and chronology characteristics. (a) The raw $\delta^{13}C$ measurement series of 31 trees (black) and their mean (red) after alignment by cambial age. The data prior to 1850 C.E. are shown to avoid biases due to modern $\delta^{13}C$ correction procedures. Measurement series are expressed as anomalies with respect to the mean values over the years 1-200. Bottom panel shows the replication of the age-aligned data, including an initial increase up to cambial ages of ~30 years due to missing juvenile rings in core samples. (b) Same as in (a), but for the exponential and straight line detrended data. (c) Raw and detrended arithmetic mean chronologies after regression against regional JJA temperatures. Post-1850 data were Kur corrected, and chronology variance changes stabilized to remove effects due to replication changes (see Methods). Bottom panel shows the residual timeseries between the raw and detrended chronologies. (d) Temporal coverage of individual trees throughout the past millennium. Dark grey indicates the number of missing innermost rings on core samples.

The isotope ratios are expressed in the conventional δ notation in parts per thousand (‰) relative to the Vienna Pee Dee Belemnite standard. The resulting $\delta^{13}C$ timeseries were corrected to account for atmospheric changes in $^{13}C/^{12}C$ composition due to combustion of

fossil fuels (~1.8‰ from 1850-2009) and discrimination changes under elevated CO_2 concentrations (0.0073‰/ppmv CO_2) (Kürschner, 1996). In addition to this "Kur" correction we also discuss results based on the $^{13}C/^{12}C$ atmospheric correction (Atm), as well as additional plant physiological responses at the leaf level (0.02‰/ppmv CO_2; Fen) (Feng and Epstein, 1995; overview in Treydte et al., 2009). Detailed assessments of the differently corrected $\delta^{13}C$ timeseries and calibration against instrumental climate data are reported in Konter et al. (2014).

The $\delta^{13}C$ timeseries were detrended using dendrochronological techniques (Cook and Kairiukstis, 1990) to account for level differences among single trees and age-trends inherent to the timeseries (Esper et al., 2010). A detrended $\delta^{13}C$ chronology was developed by (i) aligning the $\delta^{13}C$ measurements prior to 1850 C.E. by biological age (to assess age-trend; Fig. 6-2a), (ii) removing $\delta^{13}C$ age-trends over the first 200 years of the trees' lifespans by calculating residuals from fitted exponential functions (Fig. 6-2b), (iii) removing additional $\delta^{13}C$ level differences of tree-rings older than 200 years by calculating residuals from the mean $\delta^{13}C$ values of these mature rings, and (iv) calculating arithmetic means of the detrended $\delta^{13}C$ timeseries. Temporal variance changes in the resulting chronology, due to replication changes from n = 13 trees in the 20th century to n < 5 trees in the 13th century, were removed by calculating ratios from running, 110-year (11 decadal values) standard deviations, derived from the first-differenced $\delta^{13}C$ chronology (details in Frank et al., 2007).

The final, detrended and variance stabilized, $\delta^{13}C$ chronology was calibrated over the 1901-2009 period against gridded (CRU3.1) June-August (JJA) temperature data averaged over 0-3°E/38-43°N (Mitchell and Jones, 2005; Konter et al., 2014). Calibration was performed using both the annually resolved proxy and instrumental data, as well as the decadally resolved data – with the JJA temperatures averaged to meet the decadal resolution of the $\delta^{13}C$ timeseries. Split calibration/verification trials were performed over the 1951-2009 and 1901-1950 intervals, and the reduction of error (RE) and coefficient of efficiency (CE) calculated to estimate statistical skill of the proxy/climate association (Cook et al., 1994). For temperature reconstruction, the $\delta^{13}C$ chronology was regressed against the decadally resolved JJA temperature data (Esper et al., 2005). Reconstruction uncertainties were estimated by calculating the standard error (SE) from repeated (> 100 times) calibration trials using differently replicated (n = 13, n = 12, ..., n = 3) $\delta^{13}C$ chronologies over the 20th century to account for the replication decline back in time. Finally, the $\delta^{13}C$ based JJA temperature reconstruction is compared to a MXD based reconstruction that was originally calibrated against JJA maximum temperatures (Büntgen et al., 2008) and a multi-site MXD based

reconstruction calibrated against May-September mean temperatures (Dorado Liñán et al., 2012). In this comparison, the temporal resolution of the MXD timeseries was reduced to match the decadally resolved $\delta^{13}C$ record presented here.

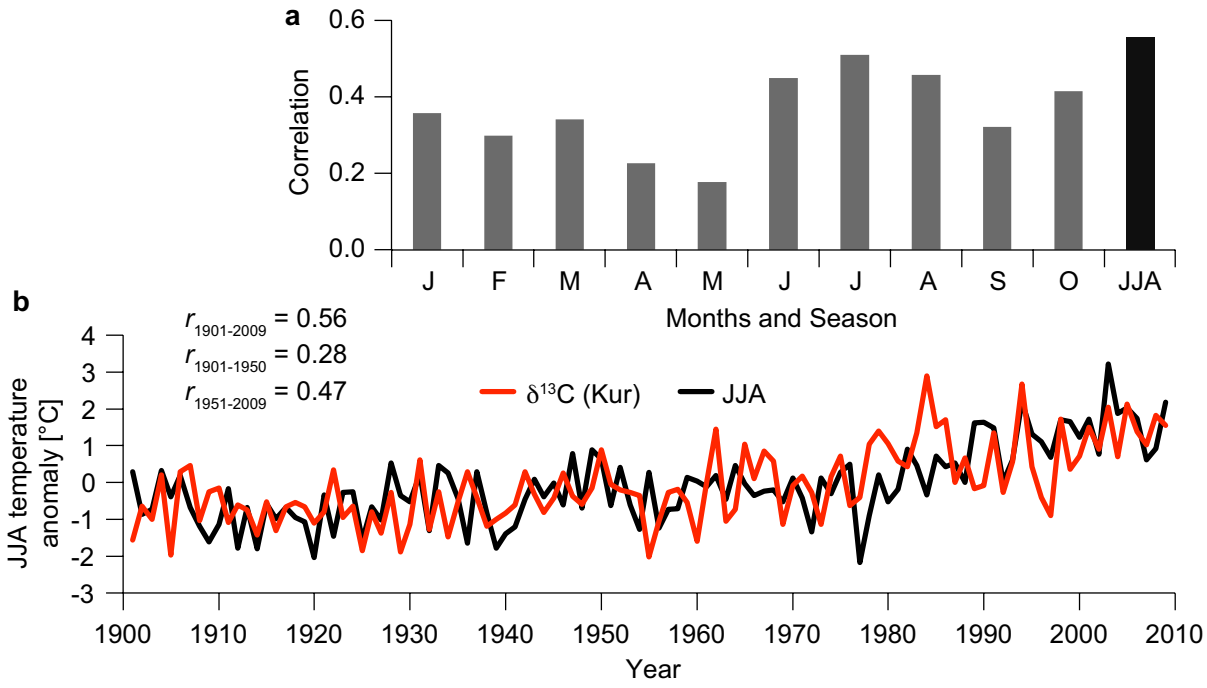

Figure 6-3 Calibration of the annually resolved $\delta^{13}C$ data. (a) Correlation results between the monthly (January to October) and seasonal (JJA) temperature (CRU3.1) and the Kur corrected $\delta^{13}C$ data over the 1901-2009 period. (b) The annually resolved δ13C timeseries (red) scaled to match the mean and variance of the JJA temperature timeseries (black).

6.3 Results and discussion

The removal of $\delta^{13}C$ level differences and age-trends resulted in a millennium-long record indicating higher chronology levels back in time, compared to its non-detrended "raw" counterpart (Fig. 6-2). The detrending procedure corrected the systematically lower $\delta^{13}C$ values of biologically younger rings likely triggered by the (i) uptake of CO_2 enriched ambient air from soil respiration (Francey and Farquhar, 1982), and (ii) decreased hydraulic resistances and higher stomatal conductance of smaller trees (McDowell et al., 2002). As a consequence, the residual timeseries, between the raw and detrended chronologies, increases from -0.26°C in the 17th century to -0.74°C in the 13th century. However, it is important to note, the early periods of the chronology are represented by fewer trees (one before 1230 C.E.). The detrended $\delta^{13}C$ chronology produces higher values during late 15th, late 14th and early 13th centuries, compared to the late 20th century.

Calibration of the annually resolved 20th century $\delta^{13}C$ data against instrumental temperatures revealed a clear seasonal pattern including highest correlations with June, July, and August temperatures (Fig. 6-3a). The correlation against mean JJA temperatures is r = 0.56, though split-period calibration/verification trials indicate a weakening of this association back over the 20th century (Fig. 3b; $r_{1951-2009} = 0.47$ to $r_{1901-1950} = 0.28$), a finding that is likely related to a loss of skill in the meteorological network during the first half of the 20th century (see Konter et al., 2014 for more detail on climate responses and effects of $\delta^{13}C$ correction procedures).

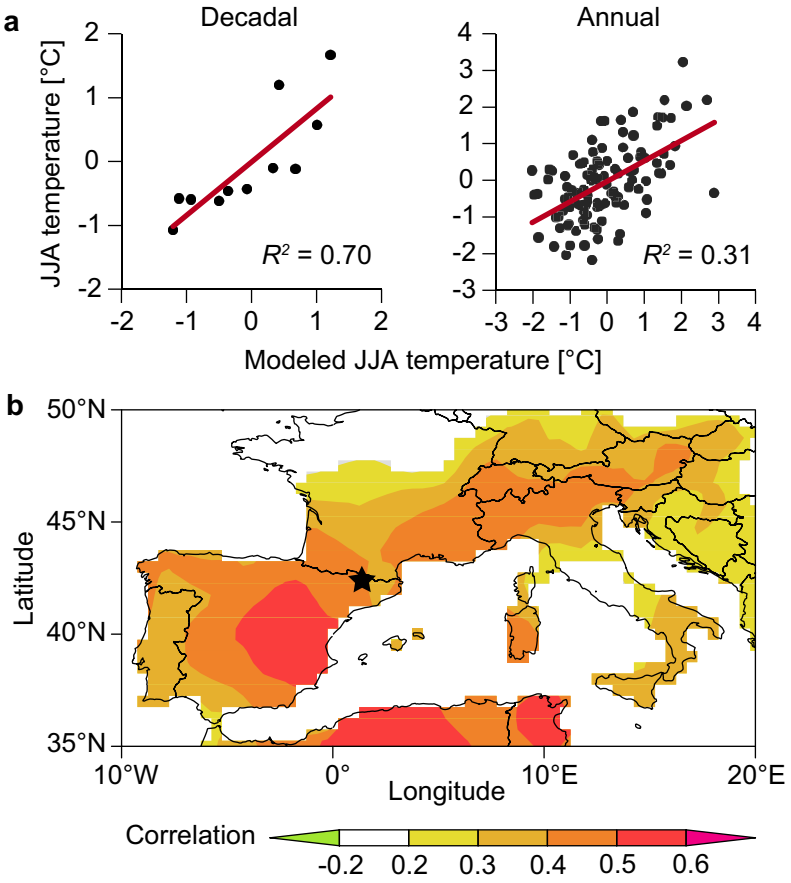

Figure 6-4 $\delta^{13}C$ calibration against regional JJA temperatures. (a) Distribution and linear trends of the decadally (11 values) and annually resolved (109 values) $\delta^{13}C$ and JJA temperature data over the 1901-2009 period. (b) JJA temperature correlation field of the annually resolved $\delta^{13}C$ data. Star indicates the location of the sampling site.

The JJA temperature signal is stronger at the decadal scale ($R^2 = 0.70$; $p < 0.05$), compared to the annual data ($R^2 = 0.32$; $p < 0.001$) (Fig. 4). However, the low-resolution calibration is based on much fewer degrees of freedom (~4) compared to the high-resolution approach (~64), owing to the reduced number of correlation pairs (11 decades compared to 109 annual

values over 1901-2009) and an increased lag-1 autocorrelation (0.56 compared to 0.46). The RE (0.66 for decadal and 0.62 for annual) and CE results (0.64 and 0.28) indicate the $\delta^{13}C$ timeseries match the JJA target data reasonably well, so that a reconstruction based on this proxy would have statistical skill. The spatial pattern of the signal ($r > 0.4$) indicates a predominating influence of Mediterranean synoptic systems on the pine isotopic composition, extending from Northern Africa into the Iberian Peninsula and eastwards over the European Alps (Fig. 6-4b).

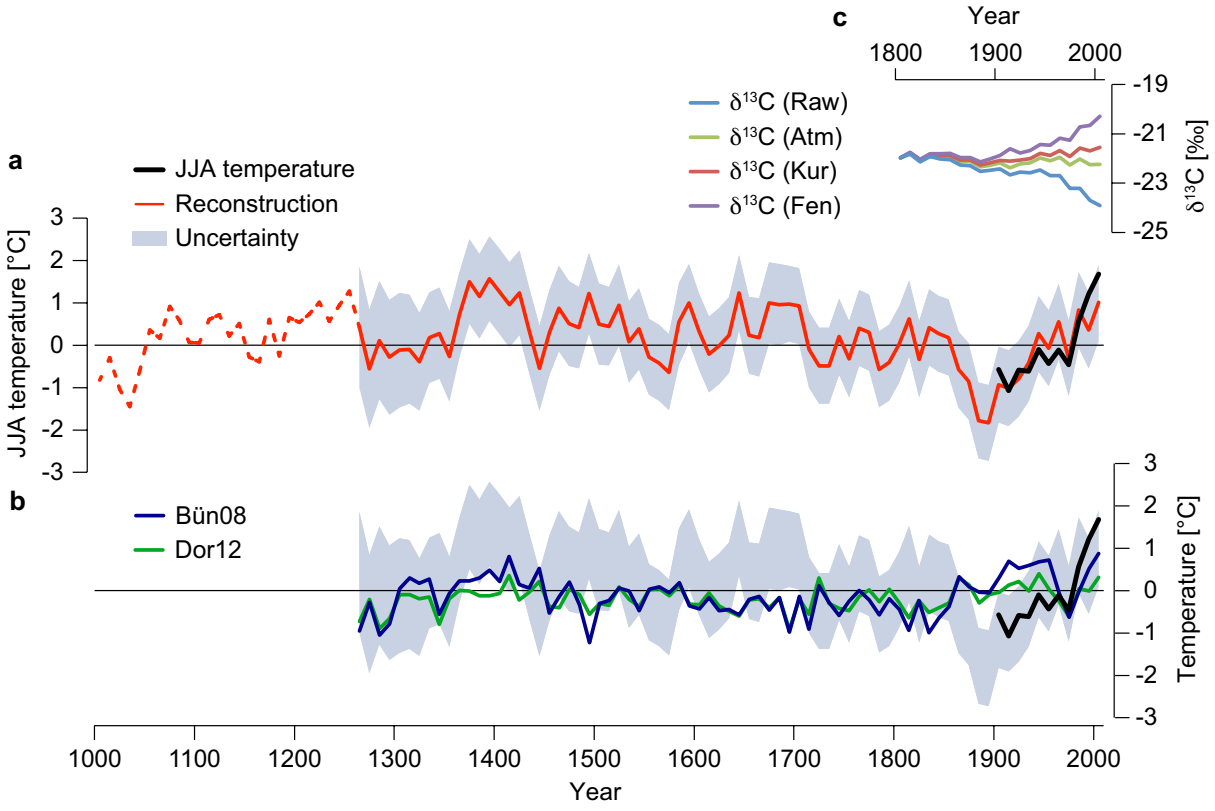

Figure 6-5 $\delta^{13}C$ based JJA temperature reconstruction and comparison with existing estimates. (a) Decadally resolved temperature reconstruction back to the 13th century derived from regression against JJA temperatures. Dashed curve indicates the period prior to 1260 C.E. when sample replication falls below three trees. The SE uncertainty band is derived from calibration trials against JJA temperatures using less-replicated chronologies to assess climate signal strengths during earlier chronology periods (see Methods). (b) MXD based JJA maximum (Büntgen *et al.,* 2008) and May-September mean temperature (Dorado Liñán *et al.,* 2012) reconstructions, plotted together with the regional JJA temperatures and uncertainty band from (a). All timeseries expressed as anomalies with respect to 1961-90. (c) Recent $\delta^{13}C$ chronology tails for the raw data and data after application of the Atm, Kur, and Fen corrections to account for atmospheric $^{13}C/^{12}C$ ratio and tree physiological effects.

The detrended $\delta^{13}C$ reconstruction exhibits decadal scale summer temperature variations ranging from +1.57°C in the 1390s C.E. to -1.83°C in the 1890s C.E. (Fig. 6-5a). The uncertainty band accompanying this reconstruction back to ~1260 C.E., the first decade represented by three trees, shows most of the temperature variations over the past 750 years did not deviate significantly from the 1961-1990 mean, however. The uncertainty band is increasing back in time as a function of the reduced replication of earlier chronology periods. Whereas more recently reconstructed temperatures (+1.01°C from 2001-2009) have been cooler than the late 14th and 15th centuries, the difference between these periods is insignificant.

The new $\delta^{13}C$ based reconstruction shares some characteristics of existing reconstructions derived from MXD data, including a long-term cooling trend from the late 14th to the mid 19th centuries (Fig. 6-5b). However, the high decadal scale summer temperature variance recorded in our $\delta^{13}C$ based record exceeds the variance retained in the MXD reconstructions that were originally calibrated against maximum temperatures (Büntgen et al., 2008) and extended growing season temperatures (Dorado Liñán et al., 2012). The reduced variability of the existing records likely arises from the application of detrending procedures to MXD datasets obtained from predominately living trees (Esper et al., 2003). Consequently, the MXD based reconstructions do not pick up the cool late 19th/early 20th century conditions reflected in the early instrumental record (see black curves in Fig. 6-5b).

Our new $\delta^{13}C$ based reconstruction seems to capture 20th century temperature trends better than the existing MXD records. The performance improvement is largely determined by the applied atmospheric CO_2 correction. We considered the Kur, Fen, and Atm corrections in our reconstruction attempts, choosing the annually resolved reconstruction containing the least trend in residuals after calibration against instrumental summer temperatures (-0.01°C/decade for Kur, +0.06°C/decade for Fen, and -0.10°/decade for Atm; Fig. 6-6). However, the decision to favor one $\delta^{13}C$ correction scheme over another is generally not well justified (Treydte et al., 2009), and perhaps represents the most significant constraint of the new summer temperature reconstruction presented here.

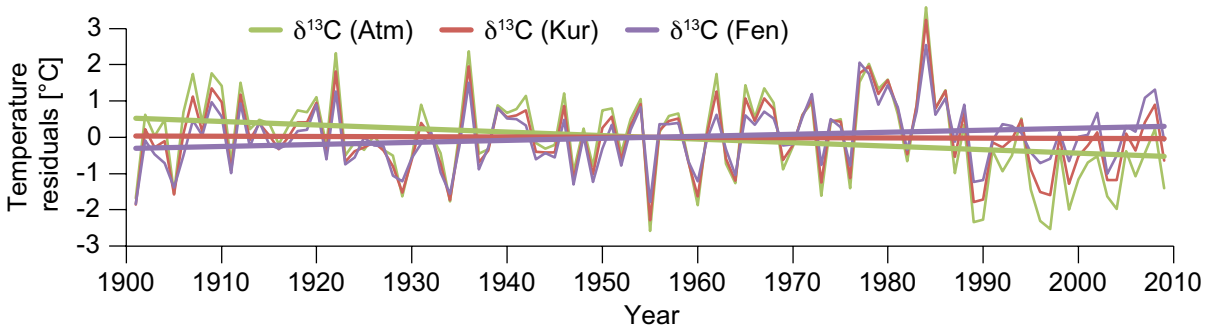

Figure 6-6 Proxy/climate residuals. Annual residuals between the scaled Atm, Kur, and Fen corrected $\delta^{13}C$ timeseries and the target JJA temperature timeseries (thin curves) shown together with the linear regression lines (bold curves) over the 1901-2009 period. Linear trends range from -0.10°/decade for the Atm, +0.06°C/decade for the Fen, to -0.01°C/decade for the Kur corrected data.

6.4 Conclusions

The Spanish Pyrenees $\delta^{13}C$ based reconstruction presented here shows warmer and more variable growing season temperatures during the Little Ice Age than previously described (Büntgen et al., 2008; Dorado Liñán et al., 2012). Developing this reconstruction required systematically removing lower $\delta^{13}C$ values inherent to tree-rings younger than 200 years, that would otherwise lower the mean chronology levels during earlier periods of the past millennium, where these younger rings dominate the reconstruction. As a consequence, earlier warm periods during the late 14th and 15th centuries appear warmer, though not statistically significant, compared to the late 20th century.

A major constraint of the new reconstruction is the substantial difference in recent temperature trends caused by post-1850 $\delta^{13}C$ correction procedures. The correction applied here, accounting for atmospheric $^{13}C/^{12}C$ ratio and plant physiological effects, appeared most suitable as it produced a timeseries without any trend in residuals after regressing against instrumental temperatures. However, developing objective criteria for post-1850 correction, independent of the goodness of fit with instrumental target data, are needed to establish $\delta^{13}C$ based reconstructions as an additional proxy for studying climate variations over past millennia.

6.5 Acknowledgements

Supported by the Mainz Geocycles Research Center. The $\delta^{13}C$-based temperature reconstruction is available at: https://www.blogs.uni-mainz.de/fb09climatology/publications-jan-esper/References

6.6 References

Bale RJ, Robertson I, Salzer MW, Loader NJ, Leavitt SW, Gagen M, Harlan TP and McCarroll D, 2011. An annually resolved bristlecone pine carbon isotope chronology for the last millennium. Quaternary Research Res. 76, 22–29.

Battipaglia G, Jäggi M, Saurer M, Siegwolf RTW and Cotrufo MF, 2008. Climatic sensitivity of $\delta^{18}O$ in the wood and cellulose of tree rings: Results from a mixed stand of Acer pseudoplatanus L. and Fagus sylvatica. Palaeogeogaphy, Palaeoclimatology, Palaeoecology 261, 193–202.

Boettger T, et al., 2007. Wood cellulose preparation methods and mass spectrometric analyses of $\delta^{13}C$, $\delta^{18}O$ and non-exchangeable $\delta^{2}H$ values in cellulose, sugar and starch: an inter-laboratory comparison. Analytical Chemistry 79, 4603–4612.

Borella S, Leuenberger M, Saurer M and Siegwolf R, 1998. Reducing uncertainties in $\delta^{13}C$ analysis of tree rings: Pooling, milling, and cellulose extraction. Journal of Geophysical Research 103, 19519–19526.

Büntgen U, Frank DC, Grudd H, and Esper J, 2008. Long-term summer temperature variations in the Pyrenees. Climate Dynamics 31, 615–631.

Büntgen U, Frank DC, Trouet V, and Esper J, 2010. Diverse climate sensitivity of Mediterranean tree-ring width and density. Trees 24, 261–273.

Cook ER and Kairiukstis LA, 1990. Methods of dendrochronology: applications in environmental science. Dordrecht, Kluwer, 394 pp.

Cook ER, Briffa KR and Jones PD, 1994: Spatial regression methods in dendroclimatology: A review and comparison of two techniques. International Journal of Climatology 14, 379–402.

Dorado Liñán I, et al., 2011. Pooled versus separate measurements of tree-ring stable isotopes. Science of the Total Environment 409, 2244–2251.

Dorado Liñán I, et al., 2012. Estimating 750 years of temperature variations and uncertainties in the Pyrenees by tree-ring reconstructions and climate simulations. Climate of the Past 8, 919–933.

Edwards, TWD, Birks SJ, Luckman BH and MacDonald GM, 2008. Climatic and hydrologic variability during the past millennium in the eastern Rocky Mountains and northern Great Plains of western Canada. Quaternary Research 70, 188–197.

Esper J, Cook ER, Krusic PJ, Peters K and Schweingruber FH, 2003. Tests of the RCS method for preserving low-frequency variability in long tree-ring chronologies. Tree-Ring Research 59, 81–98.

Esper J, Frank DC, Wilson RJS, Briffa KR, 2005. Effect of scaling and regression on reconstructed temperature amplitude for the past millennium. Geophysical Research Letters 32, doi 10.1029/2004GL021236.

Esper J, Frank DC, Battipaglia G, Büntgen U, Holert C, Treydte K, Siegwolf R and Saurer M, 2010. Low-frequency noise in ð^{13}C and ð^{18}O tree ring data: A case study of Pinus uncinata in the Spanish Pyrenees. Global Biogeochemical Cycles 24, doi 10.1029/2010GB0037772.

Feng X and Epstein S, 1995. Carbon isotopes of trees from arid environments and implications for reconstructing atmospheric CO_2 concentration. Geochimica et Cosmochimica Acta 59, 2599–2608.

Francey RJ and Farquhar GD, 1982. An explanation of $^{13}C/^{12}C$ variations in tree rings. Nature 297, 28–31.

Frank D, Esper J and Cook ER, 2007. Adjustment for proxy number and coherence in a large-scale temperature reconstruction. Geophysical Research Letters 34, doi 10.1029/2007GL030571.

Gagen M, et al., 2011. Cloud response to summer temperatures in Fennoscandia over the last thousand years. Geophysical Research Letters 38, doi 10.1029/2010GL046216.

Hangartner S, Kress A, Saurer M, Frank DC and Leuenberger M, 2012. Methods to merge overlapping tree-ring isotope series to generate multi-centennial chronologies. Chemical Geology 294, 127–134.

Konter O, Holzkämper S, Helle G, Büntgen U and Esper J, 2014. Climate sensitivity and parameter coherency in annually resolved δ^{13}C and δ^{18}O from Pinus uncinata tree-ring data in the Spanish Pyrenees. Chemical Geology 377, 12-19.

Kürschner K, 1996. Leaf stomata as biosensors of paleoatmospheric CO_2 levels. LPP Contributions Series 5, 1–153.

Kress A, Saurer M, Siegwolf RTW, Frank DC, Esper J and Bugmann H, 2010. A 350 year drought reconstruction from Alpine tree ring stable isotopes. Global Biochemical Cycles 24, doi 10.1029/2009GB003613.

McDowell NG, Phillips N, Lunch C, Bond B J and Ryan MG, 2002. An investigation of hydraulic limitation and compensation in large, old Douglas-fir trees. Tree Physiology 22, 763–774.

Mitchell TM and Jones PD, 2005. An improved method of constructing a database of monthly climate observations and associated high-resolution grids. Internatinal Journal of Climatology 25, 693–712.

Suess, H. E., 1955. Radiocarbon concentration in modern wood. Science 122, 415–417.

Treydte K, Frank DC, Saurer M, Helle G, Schleser G and Esper J, 2009. Impact of climate and CO_2 on a millennium-long tree-ring carbon isotope record Geochimica et Cosmochimica Acta 73, 4635–4647.

7. Conclusions and perspectives

Paleoclimate research is providing a growing number of tree-ring based centennial and millennial climate reconstructions, which supply extensive information on past natural climate variations and external forcings (Büntgen et al., 2011b; D'Arrigo et al., 2006; Esper et al., 2012; Schneider et al., 2015; Trouet et al., 2009). Understanding past climate variations creates the prerequisites to predict future temperature changes using statistical models, which become increasingly important in the ongoing debate about global change and the late 20th century temperature warming. Methods and results presented in this dissertation contribute to estimate temporally robust climate signals incorporated in various tree-ring parameters, and identify and evaluate biasing factors, thereby minimizing uncertainties associated with climate reconstructions. In particular, effects of age-related climate sensitivity trends in growth and density data, insect-induced disturbances in interannual growth patterns, and effects of elevated atmospheric CO_2 concentrations on stable isotopic compositions were analyzed and evaluated.

The growth and density data of *Pinus sylvestris* L. trees from Northern Fennoscandia used in this thesis were previously utilized for reconstruction purposes (Büntgen et al., 2011a; Esper et al., 2012; Schneider et al., 2015). This dataset yields unique characteristics associated with an evenly age distribution of individual samples as a function of time. Significant age-related trends in climate sensitivity were detected for both parameters in different calibration setups (section 2). Age-related chronologies exhibited decreasing climate sensitivity with increasing age, which exceeded site-related variations. Uncertainties due to replication changes in age-related chronologies were excluded by fitting linear regression models to the growth-climate relationships of individual series. In periods of consecutive summer temperature warming, CSAE trends were particularly enhanced, while cooling periods seemed to remove the bias. Resilient meanderings and a more complex expression of CSAE trends in TRW data considering high- and low-frequency peculiarities make TRW data more prone to age-related effects relative to MXD data. However, datasets including all age-class categories revealed

only minor differences to the best-responding age-class category. The impact of CSAE on previously published reconstructions from Northern Fennoscandia derived from MXD data is likely negligible, as the underlying data structure comprises all age-class categories in both calibration and reconstruction periods (Büntgen et al., 2011a; Esper et al., 2012; Schneider et al., 2015).

Tree growth of both *Larix decidua* Mill. and *Pinus sylvestris* L. trees at high-elevation stands in the Slovakian High Tatra Mountains are distinctly controlled by early-summer temperatures (section 3). In this region, cyclic population mass outbreaks of *Zeiraphera diniana* Gn. (LBM) and associated defoliation patterns in the tree-ring data could not be detected, although residuals between both TRW chronologies indicated interannual growth depressions in the larch (host) data. In contrast to the environmental conditions in the European Alps, low proportions of larch trees in the mixed forests of the High Tatra Mountains, thus scarcity of available food resources for the budmoth specimen, presumably inhibited LBM population cycles from peaking at mass outbreak levels. The distinct May-June temperature signal, the robust chronology statistics, and the detected absence of cyclic biological disruptions indicate high paleoclimatic potential of larch tree-ring data from this region. The absence of recurrent LBM mass outbreaks in the High Tatra Mountains also indicate that the millennium-long reconstruction of early-summer temperatures (Büntgen et al., 2013) may outperform similar approaches from the European Alps where pulsed disruptions are common.

Annually resolved stable oxygen isotope data from *Pinus uncinata* Ramond ex DC individuals from the Spanish Pyrenees exhibited a spring (January-June) precipitation signal, although oxygen isotopic composition seems to be influenced by a variety of factors, including processes related to snow melt and the isotopic composition of the source water (section 4). A significant summer (June-August) temperature signal was detected in annually resolved stable carbon isotope data, with slight seasonal changes (June-September) in the decadally resolved record (section 5). The applied correction procedures for elevated atmospheric CO_2 added various amounts of low-frequency information to the carbon isotopic data and altered the climate signal strength.

The natural adaptation of the trees to varying CO_2 concentrations remains unclear, aggravating the selection of a certain correction method. As summer temperatures mainly control the carbon isotopic composition in tree-rings, the most adequate correction for elevated atmospheric CO_2 was assumed to neither over- nor underestimate the low-frequency

trends of the summer temperature data. For this Mediterranean high altitude environment, the $\delta^{13}C$ values were finally corrected by a factor of 0.0073‰ per ppm CO_2 change (section 6). Additional to this correction, the extended $\delta^{13}C$ chronology from this environment was detrended, due to systematic incorporation of lower $\delta^{13}C$ values in trees younger than 200 years - a novel approach in tree-ring stable isotope chronology development. A 750-year long decadal summer temperature reconstruction was established and revealed higher amplitudes compared to previously reported reconstructions using the more traditional TRW and MXD data from the same sampling sites. Particularly in the Little Ice Age and during the late 14th and 15th century, reconstructed summer temperatures indicated warmer conditions. Still, correction methods for elevated atmospheric CO_2 concentration applied to post-1850 $\delta^{13}C$ data remain crucial to calibration results and subsequent reconstruction approaches.

Uncertainties and biasing factors associated with calibration setups and climate reconstructions can be reduced by carefully executed analyses – from the sampling design and sites to the applied statistical methods. Age-related trends in calibration setups can be mitigated by an elaborate selection of sampled trees, considering cambial age and an evenly distribution of differently aged trees throughout time. Furthermore, analyses of biotic factors, such as insect populations, and the environmental properties of the habitat impacting tree growth at the sampling sites are crucial for bias reduction. Accurately removing the bias in $\delta^{13}C$ records caused by elevated atmospheric CO_2 requires further research and development of objective criteria for post-1850 correction methods independent of the low-frequency trends of the climate target data. Sampling strategies, statistical methods and results presented in this dissertation provide a conceptual basis for evaluating biased calibration approaches, and contribute to improve future paleoclimate reconstructions.

Bibliography

Baltensweiler, W., 1993. A contribution to the explanation of the larch bud moth cycle, the polymorphic fitness hypothesis. Oecologia 93, 251-255.

Baltensweiler, W., Benz, G., Bovey, P., Delucchi, V., 1977. Dynamics Of Larch Bud Moth Populations. Annual Review of Entomology 22, 79-100.

Büntgen, U., Frank, D., Grudd, H., Esper, J., 2008. Long-term summer temperature variations in the Pyrenees. Clim Dynam 31, 615-631.

Büntgen, U., Kyncl, T., Ginzler, C., Jacks, D.S., Esper, J., Tegel, W., Heussner, K.U., Kyncl, J., 2013. Filling the Eastern European gap in millennium-long temperature reconstructions. Proceedings of the National Academy of Science USA 110, 1773-1778.

Büntgen, U., Raible, C.C., Frank, D., Helama, S., Cunningham, L., Hofer, D., Nievergelt, D., Verstege, A., Timonen, M., Stenseth, N.C., Esper, J., 2011a. Causes and Consequences of Past and Projected Scandinavian Summer Temperatures, 500-2100 AD. PLoS ONE 6, e25133.

Büntgen, U., Tegel, W., Nicolussi, K., McCormick, M., Frank, D., Trouet, V., Kaplan, J.O., Heussner, K.-U., Wanner, H., Luterbacher, J., Esper, J., 2011b. 2500 Years of European Climate Variability and Human Susceptibility. Science 331, 578-582.

Carrer, M., Urbinati, C., 2004. Age-Dependent Tree-Ring Growth Responses To Climate In Larix Decidua And Pinus Uncinata. Ecology 85, 730-740.

D'Arrigo, R., Wilson, R., Jacoby, G., 2006. On the long-term context for late twentieth century warming. Journal of Geophysical Research 111.

Dai, A., Trenberth, K.E., Qian, T., 2004. A Global Dataset of Palmer Drought Severity Index for 1870-2002: Relationship with Soil Moisture and Effects of Surface Warming. Journal of Hydrometeorology 5, 1117-1130.

Deslauriers, A., Rossi, S., Anfodillo, T., Saracino, A., 2008. Cambial phenology, wood formation and temperature thresholds in two contrasting years at high altitude in southern Italy. Tree Physiol 28, 863-871.

Dorado Liñán, I., Büntgen, U., González-Rouco, F., Zorita, E., Montávez, J.P., Gómez-Navarro, J.J., Brunet, M., Heinrich, I., Helle, G., Gutiérrez, E., 2012. Estimating 750 years of temperature variations and uncertainties in the Pyrenees by tree-ring reconstructions and climate simulations. Climate of the Past 8, 919-933.

Dorado Liñán, I., Gutiérrez, E., Heinrich, I., Andreu-Hayles, L., Muntán, E., Campelo, F., Helle, G., 2011. Age effects and climate response in trees: a multi-proxy tree-ring test in old-growth life stages. Eur J Forest Res 131, 933-944.

Esper, J., Buntgen, U., Frank, D.C., Nievergelt, D., Liebhold, A., 2007. 1200 years of regular outbreaks in alpine insects. Proceedings. Biological sciences / The Royal Society 274, 671-679.

Esper, J., Frank, D.C., Battipaglia, G., Buntgen, U., Holert, C., Treydte, K., Siegwolf, R., Saurer, M., 2010. Low-frequency noise in delta C-13 and delta O-18 tree ring data: A case study of Pinus uncinata in the Spanish Pyrenees. Global Biogeochem Cy 24.

Esper, J., Frank, D.C., Timonen, M., Zorita, E., Wilson, R.J.S., Luterbacher, J., Holzkämper, S., Fischer, N., Wagner, S., Nievergelt, D., Verstege, A., Büntgen, U., 2012. Orbital Forcing of Tree-Ring Data. Nature Climate Change 2, 862-866.

Esper, J., Gärtner, H., 2001. Interpretation of tree-ring chronologies. Erdkunde 55, 277-288.

Esper, J., Niederer, R., Bebi, P., Frank, D., 2008. Climate signal age effects—Evidence from young and old trees in the Swiss Engadin. Forest Ecology and Management 255, 3783-3789.

Farquhar, G.D., O'Leary, M.H., Berry, J.A., 1982. On the relationship between carbon isotope discrimination and the intercellular carbon dioxide concentration in leaves. Australian Journal of Plant Physiology 9, 121-137.

Feng, X., S., E., 1995. Carbon isotopes of trees from arid environments and implications for reconstructing atmospheric CO2 concentration. Geochimica et Cosmochimica Acta 59, 2599-2608.

Frank, D.C., Poulter, B., Saurer, M., Esper, J., Huntingford, C., Helle, G., Treydte, K., Zimmermann, N.E., Schleser, G.H., Ahlstrom, A., Ciais, P., Friedlingstein, P., Levis, S., Lomas, M., Sitch, S., Viovy, N., Andreu-Hayles, L., Bednarz, Z., Berninger, F., Boettger, T., D'Alessandro, C.M., Daux, V., Filot, M., Grabner, M., Gutierrez, E., Haupt, M., Hilasvuori, E., Jungner, H., Kalela-Brundin, M., Krapiec, M., Leuenberger, M., Loader, N.J., Marah, H., Masson-Delmotte, V., Pazdur, A., Pawelczyk, S., Pierre, M., Planells, O., Pukiene, R., Reynolds-Henne, C.E., Rinne, K.T., Saracino, A., Sonninen, E., Stievenard, M., Switsur, V.R., Szczepanek, M., Szychowska-Krapiec, E., Todaro, L., Waterhouse, J.S., Weigl, M., 2015. Water-use efficiency and transpiration across European forests during the Anthropocene. Nature Climate Change 5, 579-583.

Fritts, H.C., 1976. Tree Rings and Climate. Academic Press, London.

Helle, G., Schleser, G.H., 2004. Interpreting Climate Proxies from Tree-rings, in: Fischer, H., Floeser, G., Kumke, T., Lohmann, G., Miller, H., Negendank, J.F.W., von Storch, H. (Eds.), The climate in Historical Times, Towards a synthesis of Holocene proxy data and climate models. Springer, Berlin, pp. 129-148.

Kürschner, K., 1996. Leaf stomata as biosensors of paeoatmospheric CO2 levels, LPP Contributions Series, Utrecht, p. 153.

Linares, J.C., Taïqui, L., Sangüesa-Barreda, G., Seco, J.I., Camarero, J.J., 2013. Age-related drought sensitivity of Atlas cedar (Cedrus atlantica) in the Moroccan Middle Atlas forests. Dendrochronologia 31, 88-96.

Linderholm, H.W., Linderholm, K., 2004. Age-dependent climate sensitivity of Pinus sylvestris L. in the central Scandinavian Mountains. Boreal Environment Research 9, 307-317.

McCarroll, D., Gagen, M.H., Loader, N.J., Robertson, I., Anchukaitis, K.J., Los, S., Young, G.H.F., Jalkanen, R., Kirchhefer, A., Waterhouse, J.S., 2009. Correction of tree ring stable carbon isotope chronologies for changes in the carbon dioxide content of the atmosphere. Geochimica et Cosmochimica Acta 73, 1539-1547.

McCarroll, D., Loader, N.J., 2004. Stable isotopes in tree rings. Quaternary Sci Rev 23, 771-801.

Meinzer, F.C., Lachenbruch, B., Dawson, T.E., 2011. Size- and Age-Related Changes in Tree Structure and Function Springer Science+Business Media, Dordrecht, Heidelberg, London, New York.

Rossi, S., Deslauriers, A., Anfodillo, T., Carrer, M., 2008. Age-dependent xylogenesis in timberline conifers. New Phytologist 177, 199-208.

Rozas, V., DeSoto, L., Olano, J.M., 2009. Sex-specific, age-dependent sensitivity of tree-ring growth to climate in the dioecious tree Juniperus thurifera. The New phytologist 182, 687-697.

Schneider, L., Smerdon, J.E., Büntgen, U., Wilson, R.J.S., Myglan, V.S., Kirdyanov, A.V., Esper, J., 2015. Revising midlatitude summer temperatures back to A.D. 600 based on a wood density network. Geophys Res Lett, doi: 10.1002/2015GL063956.

Schubert, B.A., Jahren, A.H., 2012. The effect of atmospheric CO2 concentration on carbon isotope fractionation in C3 land plants. Geochimica et Cosmochimica Acta 96, 29-43.

Schweingruber, F.H., 1996. Tree Rings and Environment. Dendroecology. Swiss Federal Institute for Forest, Snow andLandscape Research, Berne, Stuttgart, Vienna, Haupt.

Schweingruber, F.H., 2007. Wood Structure and Environment. Springer Verlag, Berlin, Heidelberg.

Speer, J.H., 2010. Fundamentals of Tree-Ring Research. The University of Arizona Press, Tucson.

Szeicz, J.M., MacDonald, G.M., 1994. Age-dependent tree-ring responses of subarctic white spruce to climate. Canadian Journal of Forest Research 24, 120-132.

Treydte, K., Esper, J., Gärtner, H., 2004. Stabile Isotope in der Dendroklimatologie. Schweizerische Zeitschrift für Forstwesen 155, 222-232.

Treydte, K., Frank, D., Esper, J., Andreu, L., Bednarz, Z., Berninger, F., Boettger, T., D'Alessandro, C.M., Etien, N., Filot, M., Grabner, M., Guillemin, M.T., Gutierrez, E., Haupt, M., Helle, G., Hilasvuori, E., Jungner, H., Kalela-Brundin, M., Krapiec, M., Leuenberger, M., Loader, N.J., Masson-Delmotte, V., Pazdur, A., Pawelczyk, S., Pierre, M., Planells, O., Pukiene, R., Reynolds-Henne, C.E., Rinne, K.T., Saracino, A., Saurer, M., Sonninen, E., Stievenard, M., Switsur, V.R., Szczepanek, M., Szychowska-Krapiec, E., Todaro, L., Waterhouse, J.S., Weigl, M., Schleser, G.H., 2007. Signal strength and climate calibration of a European tree-ring isotope network. Geophys Res Lett 34.

Treydte, K.S., Frank, D.C., Saurer, M., Helle, G., Schleser, G.H., Esper, J., 2009. Impact of climate and CO2 on a millennium-long tree-ring carbon isotope record. Geochimica et Cosmochimica Acta 73, 4635-4647.

Trouet, V., Esper, J., Graham, N.E., Baker, A., Scourse, J.D., Frank, D.C., 2009. Persistent Positive North Atlantic Oscilaation Mode Dominated the Medieval Climate Anomaly. Science 324, 78-80.

van der Schrier, G., Briffa, K.R., Jones, P.D., Osborne, T.J., 2006. Summer Moisture Variability across Europe. Journal of Climate 19, 2818-2834.

Vicente-Serrano, S.M., Beguería, S., López-Moreno, J.I., 2010. A multi-scalar drought index sensitive to global warming: The Standardized Precipitation Evapotranspiration Index - SPEI. Journal of Climate 23, 1696-1718.

Yu, G., Liu, Y., Wang, X., Ma, K., 2008. Age-dependent tree-ring growth responses to climate in Qilian juniper (Sabina przewalskii Kom.). Trees 22, 197-204.

List of figures

List of tables

Curriculum vitae

Not available online.